Excitation-Secretion Coupling of Dense-Core Vesicle Release

DISSERTATION

for the award of the degree

“Doctor rerum naturalium” (Dr. rer. nat)

of the Georg-August-Universität Göttingen

within the doctoral program

Cellular and Molecular Physiology of the Brain

of the Göttingen Graduate Center for Neurosciences, Biophysics

and Molecular Biosciences (GGNB)

submitted by

VALENTINA ĆIRKOVIĆ

born in Jagodina, Serbia

May 2023, Göttingen

Members of the Examination Board

Thesis Committee

Dr. Sonja Wojcik
Department of Molecular Neurobiology
Max Planck Institute for Multidisciplinary Sciences Göttingen

Prof. Dr. Thomas Dresbach
Department of Anatomy and Embryology
University Medical Center Göttingen

Prof. Dr. Tobias Moser
Institute for Auditory Neuroscience & Inner Ear Laboratory
University Medical Center Göttingen

Members of the Examination Board

1st Reviewer: Dr. Sonja Wojcik
Department of Molecular Neurobiology
Max Planck Institute for Multidisciplinary Sciences Göttingen

2nd Reviewer: Prof. Dr. Thomas Dresbach
Department of Anatomy and Embryology
University Medical Center Göttingen

Further members of the Examination Board

Prof. Dr. Tobias Moser
Institute for Auditory Neuroscience & Inner Ear Laboratory
University Medical Center Göttingen

Prof. Dr. Tiago Fleming Outeiro
Experimental Neurodegeneration
University Medical Center Göttingen

Dr. Brett Carter
Synaptic Physiology and Plasticity
European Neuroscience Institute Göttingen

Prof. Dr. Rubén Fernández-Busnadiego
Institute for Neuropathology
University Medical Center Göttingen

Date of oral examination: 19.06.2023

Declaration

I hereby declare that this thesis was written independently and with no other sources and aids than quoted.

Valentina Ćirković

Göttingen, 1st of May 2023

Contents

List of tables

List of figures

Chapter 1:

Chapter 2:

Chapter 3:

Abbreviations

2D-EM - Two-dimensional electron microscopy

3D-EM - Three-dimensional electron microscopy

ABDE - Activity-dependent bulk endocytosis

AFS - Automated freeze substitution

AP - Action potential

AP180 - Adaptor protein 180

AP2 - Adaptor protein 2

ATP - Adenosine 5′-triphosphate

BAIAP3 - Brain-specific angiogenesis inhibitor-1 associated protein 3

BiNT/D - Botulinum neurotoxin D

BK - Voltage-dependent BK-type K+ channels

BME - Basement membrane extract

BSA - Bovine serum albumin

Ca^{2+} - Calcium ion

$CaCl_2$ – Calcium chloride

CAPS - Calcium activator protein for secretion

Cav - Voltage-gated Ca^{2+} channels

CCV - Clathrin-coated endocytic vesicle

CHC - Clathrin heavy chain

ChR - Channelrhodopsin

CICR - Calcium-induced calcium release

CIE - Clathrin-independent fast endocytosis

CIFE - Clathrin-independent fast endocytosis

CLC - Clathrin light chain

Cm - Membrane Capacitance

CME - Clathrin-mediated endocytosis

CNS - Central nervous system

CO_2 - Carbon dioxide

Cs - Cesium

DBH - Dopamine beta-hydroxylase

DCV - Dense-core vesicle

DDSA - Dodecenylsuccinic acid anhydrid

DKO - Double knockout

DMEM - Dulbecco's Modified Eagle's Medium

DMP-30 - 2,4,6-Tris (dimethylaminomethyl) phenol

DMSO - Dimethyl sulfoxide

EDTA - Ethylenediaminetetraacetic acid

EGTA – Egtazic acid

EM - Electron microscopy

EPS15 - Epidermal Growth Factor Receptor Pathway Substrate 15

ER - Endoplasmic reticulum

EYFP - Enhanced Yellow Fluorescent Protein

FCHo1/2 - The F-BAR domain only protein 1 and 2 complex

FEME - Fast-endophilin-mediated endocytosis

FF - Full fusion

GED - GTPase effector domain

GTP - Guanosine-5' triphosphate

$G_{\beta\gamma}$ - G beta-gamma complex

H_2O - water

HEPES - N-2-hydroxyethylpiperazine-N'-2-ethane sulfonic acid

HPF - High-pressure freezing

Hsc70 - Heat-shock cognate 70

ICS - Intracellular solution

IRP – Immediately releasable pool

ITSX - Insulin transferrin selenium

K^+ - Potassium ion

KCl - Potassium chloride

kDa - Kilo dalton

KI - Knock-in

KO - Knockout

KR - Kiss-and-run mode

Kv - Voltage-gated K+ channels

Mg^{2+} - Magnesium

$MgCl_2$ – Magnesium chloride

MNA - Methylnadic anhydride

Munc13 - Mammalian uncoordinated 13

Munc18 - Mammalian uncoordinated 18

N_2O_6Pb - Lead (II) nitrate

Na^+ - Sodium ion

Na_2HPO_4 - Sodium hydrogen phosphate

NaCl - Sodium chloride

NaH_2PO_4 - Sodium dihydrogen phosphate

NaOH - Sodium hydroxide

Nav - Voltage-gated Na+ channels

ns - non-significant

NT-4 - Neurotrophin 4

OsO_4 - Osmium tetroxide

PC12 - Pheochromocytoma Cell Line 12

PCR - Polymerase chain reaction

PH - Pleckstrin homology domain

Pi (3,4) P2 - Phosphatidylinositol (3,4)-bisphosphate

Pi (3,4,5) P3 - Phosphatidylinositol (3,4,5)-trisphosphate

Pi (4,5) P2 - Phosphatidylinositol (4,5)-bisphosphate

PKC - Protein kinase C

PMA - Phorbol 12-myristat 13-acetat

PRD - Proline/arginine-rich domain

ProA - Protein A

PWCPC - Perforated whole-cell patch-clamp

Rab3 - Ras-associated binding protein 3

RRP - Readily releasable pool

RT - Room temperature

SEM - Standard error of the mean

SNAP25 - Synaptosomal-associated protein, 25kDa

SNARE - Soluble N-ethylmaleimide-sensitive-factor attachment protein receptor proteins

SRP - Slowly releasable pool

STED - Stimulated emission depletion microscopy

STEM - Scanning transmission electron microscopy tomography

SV - Synaptic vesicle

Syt1 - Synaptotagmin 1

Syt7 - Synaptotagmin 7

TBE - Tris/Borate/EDTA

TEM - Transmission electron microscopy

TGN - Trans-Golgi network

TH - Tyrosine hydroxylase

TrkA - Tropomyosin receptor kinase A

TTX - Tetrodotoxin

U/ml - Units/milliliter

UFE - Ultrafast endocytosis

UPP - Unprimed pool

VMAT2 - Vesicular monoamine transporter 2

WCPC - Whole-cell patch clamp

WT- Wild-type

0. Abstract

Dense-core vesicles (DCVs) are membrane-bound organelles present in many secretory cells. Depending on cell type, DCVs package and release various types of cargo, such as neuronal peptides, proteins, neurotrophins, ATP, and catecholamines, greatly influencing cellular signalling.

Chromaffin cells from the adrenal medulla are enriched with DCVs, which secrete the catecholamines adrenaline and noradrenaline into the circulation. DCV release can be efficiently monitored by capacitance and amperometry recordings, making these cells a long-established model system for the extensive study of DCV biology. Membrane depolarization of the chromaffin cell causes the opening of voltage-dependent calcium channels and a subsequent increase in intracellular calcium, which initiates SNARE-mediated exocytosis of DCVs. It has been shown that neuroendocrine chromaffin cells perform full-collapse and kiss-and-run modes of exocytosis/endocytosis based on electrophysiological techniques. However, there are dissimilarities in the literature on which mode predominates based on distinct stimulation patterns. When determining the mode of vesicle exocytosis/endocytosis, these discrepancies may result from using different experimental approaches that lead to various interpretations. Nonetheless, this could also mean that the link between the stimulus and the various DCV exocytosis/endocytosis modes must still be adequately determined. Furthermore, the ultrastructural analysis of chromaffin cells prepared with aldehyde fixation or high-pressure freezing (HPF) has resulted in divergent findings. These inconsistencies mean that functional and ultrastructural data analyses of cultured chromaffin cells may require an optimized, applicable, and flexible experimental system.

The present study aimed to investigate DCV exocytosis and subsequent membrane retrieval in response to defined stimuli by combining electrophysiological and ultrastructural analyses. We planned to analyse which mode of DCV fusion predominates after specific stimulation, whether compound fusion or hemifusion intermediates and different modes of endocytosis can be detected. To address these questions, we tested both optogenetic stimulation and field stimulation of cultured chromaffin cells. Field stimulation patterns established by electrophysiological methods were implemented prior to HPF and subsequent analysis by 2D electron microscopy.

The cellular effect of exposure to light and electric field stimulation showed that our optimized methods could be used in cultured chromaffin cells to induce DCV release. Additionally, our voltage ramp stimulation paradigm enabled us to trigger and monitor DCV release with precise temporal resolution. Further, employing HPF, we captured large Ω-shaped profiles and prominent vesicle release during which the vesicle collapses entirely into the plasma

membrane. Most cells also showed distinct coated endocytic structures that were well-preserved with our experimental approach. Our study demonstrates that our improved experimental procedure was able to visualize DCV exocytosis events, including vesicle content release, in cultured neuroendocrine chromaffin cells.

1. Introduction

In times of stress, mammals release adrenaline, preparing the body for a physical response. Adrenaline binds to receptors on heart cells, causing an increase in heart rate and blood pressure, and prompts the liver to release additional sugar to stimulate muscular activity. (Carmichael & Winkler, 1985). This response is called the "fight-or-flight" response, which prepares one to fight an enemy or run away from danger. The body's "fight-or-flight" response occurs due to the release of hormones from the inner section of the two adrenal glands, known as the adrenal medulla, located above the kidneys. The adrenal medulla consists of chromaffin cells that store and secrete catecholamines: adrenaline, noradrenaline, and dopamine. Neuroscientists find chromaffin cells interesting because they not only trigger the "fight-or-flight" response but also provide valuable knowledge on the functioning of other cells, particularly neurons and nerve cells. The adrenal medulla is an inner part of the adrenal endocrine gland, capsuled with the adrenal cortex, which secretes steroid hormones. The medulla is controlled by nerves originating in the spinal cord and discharges hormones into the bloodstream, which helps regulate involuntary functions such as heart rate, intestinal movements, pupil dilation, vasodilation in the skeletal muscles, vasoconstriction in the skin and bronchodilation. Thus, metabolic activity is augmented in almost all organism cells, ensuring a coordinated response for survival (Carmichael & Winkler, 1985; de Diego et al., 2020).

1.1. Origin of adrenal chromaffin cells

In mammals, during embryonic development, the neural crest, a multipotent migratory population, emerges from the lateral edges of the neural plate. Neural crest cells go through an epithelial-mesenchymal transition forming a neural tube. Subsequently, neural crest cells migrate from their dorsal position along different pathways resulting in the development of a range of cell types such as sensory and autonomic neurons, Schwann and satellite cells of peripheral nerves and ganglia, adrenal chromaffin cells, and melanocytes (Vogel, K.S.,1996). Neural crest cells corresponding to the sympathoadrenal neural crest migrate ventrally, and reaching the dorsal aorta, go through linage segregation: the dorsal group of cells yields sympathetic neurons, while the ventral group yields chromaffin cells of the medulla (Takahashi et al., 2013; Kastriti et al., 2020).

1.2. Chromaffin cell characteristics

Chromaffin cells in the adrenal medulla represent modified post-ganglionic sympathetic neurons responsible for releasing catecholamines: adrenaline, noradrenaline, and dopamine. Catecholamines are packaged into compartments called dense-core vesicles (DCVs). In DCVs, catecholamines form a complex with chromogranins, neuropeptides, adenine

nucleotides and Ca^{2+}. The adrenal chromaffin cells are innervated by preganglionic sympathetic nerves that release acetylcholine. In response to acetylcholine stimulation, chromaffin cells secrete their contents through process called exocytosis into the bloodstream (Kobayashi & Coupland., 1993).

1.2.1. Biogenesis and traffic of DCV in adrenal chromaffin cells

DCVs are the prominent organelles of secretory cells that contain and secrete hormones and neuropeptides. The first step in the secretory pathway is the endoplasmic reticulum (ER), where protein synthesis and folding, lipid synthesis and Ca^{2+} storage occur. From the ER, proteins are transported to the Golgi apparatus, where processing and sorting occur. Proteins are packaged into secretory vesicles at the trans-Golgi network (TGN), where the choice of secretory pathways widens. One pathway in all cells is the constitutive pathway in which secretion does not depend on extracellular stimuli and is crucial for cell growth. This type of secretion engages the budding of constitutive vesicles or tubular profiles from the TGN and their transport to and subsequent fusion with the plasma membrane (Gu et al., 2001).

Additionally, many cells maintain another secretory pathway coupled with extracellular stimuli. This highly regulated secretory pathway is present in endocrine, neuronal, and exocrine cells. Such regulated secretion involves DCVs formed either by active budding from TGN, which requires lipids and proteins, or through poly-nodular tubular structures that eventually generate DCVs. The steps involved in DCV biogenesis are shown in Figure 1.1 (Kim et al., 2006).

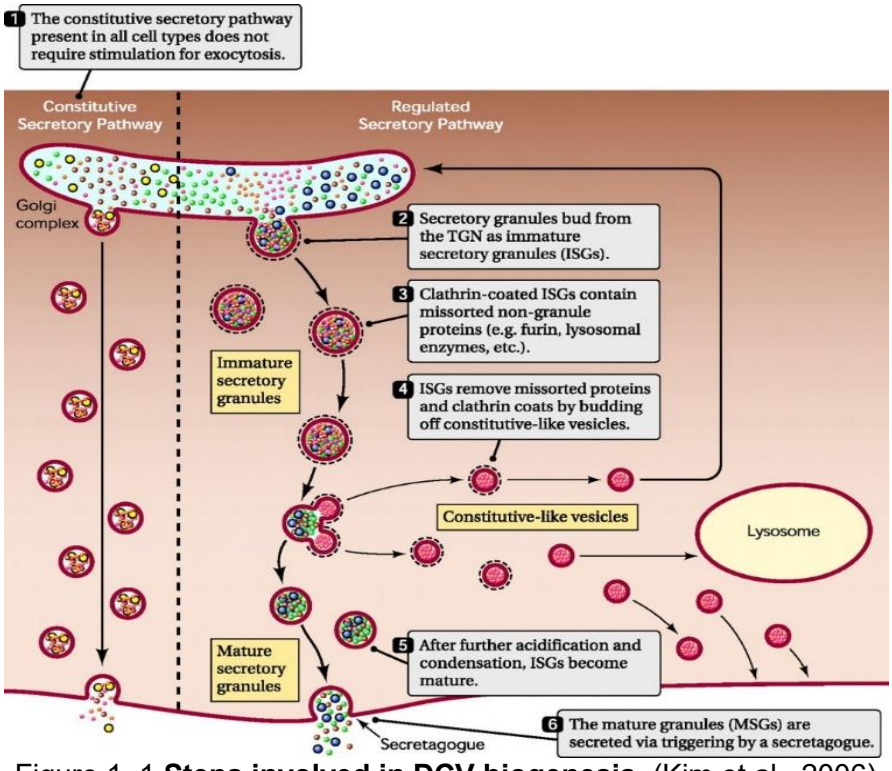

Figure 1. 1 **Steps involved in DCV biogenesis.** (Kim et al., 2006).

The lumen of these vesicles is highly condensed. Thus, a large amount of protein and other molecular cargo is efficiently stored and released on demand. In the regulated secretory pathway, DCVs accumulate in the cytoplasm, located in the reserve pool compartment, until an external signal triggers their fusion with the plasma membrane following the release of vesicle contents.

1.3. Exocytosis of DCVs

1.3.1. Identification of different vesicle pools

The process of exocytosis in both neurons and neuroendocrine cells is dependent on the presence of Ca^{2+} ions. It is regulated by the entry of Ca^{2+} ions through voltage-gated Ca^{2+} channels and other mechanisms, such as Ca^{2+} pumps, exchangers, and intracellular organelles (Carbone et al., 2019). In addition, the photorelease of Ca^{2+} in flash photolysis experiments is useful for the investigation of cellular Ca^{2+} buffering and cellular Ca^{2+} homeostasis (Chow et al., 1996). Capacitance traces acquired with the flash experiments helped discover different pools of vesicle release and their release kinetics. Elevated Ca^{2+} levels triggered the release, leading to an exocytic burst followed by a sustained secretion phase (Voets et al., 1999). The burst release component represents two distinct pools with different kinetics, the readily releasable pool (RRP) and a slowly releasable pool (SRP) (Voets, 2000). Four functionally separate vesicle pools are recognized by studies (Rettig & Neher, 2002) (Fig. 1.2). First is a depot or reserve vesicle pool, and second is an unprimed pool (UPP) that comes from a depot and moves toward the plasma membrane. The UPP undergoes a process of maturation and transitions into both the SRP and RRP, ultimately releasing cargo with different time constants (Ashery et al., 2000; Voets, 2000). The transition rate between the vesicle pool, and vesicle pool size, is regulated by molecules involved in exocytosis and intracellular Ca^{2+} (Sørensen, 2004). Vesicular density decreases as the plasma membrane approaches and of the 22,000 DCVs in chromaffin cells, 1-2% constitute the RRP that can be mobilized for release within seconds, which mediate the "fight-or-flight" response upon stress (Díaz-Flores et al., 2008). Studies showed (Parsons et al., 1995; Steyer et al., 1997) that the docked pool of DCVs is larger than the RRP. Therefore, most docked vesicles are not ready for release and need to undergo a maturation process known as priming in order to become releasable (Stevens et al., 2011).

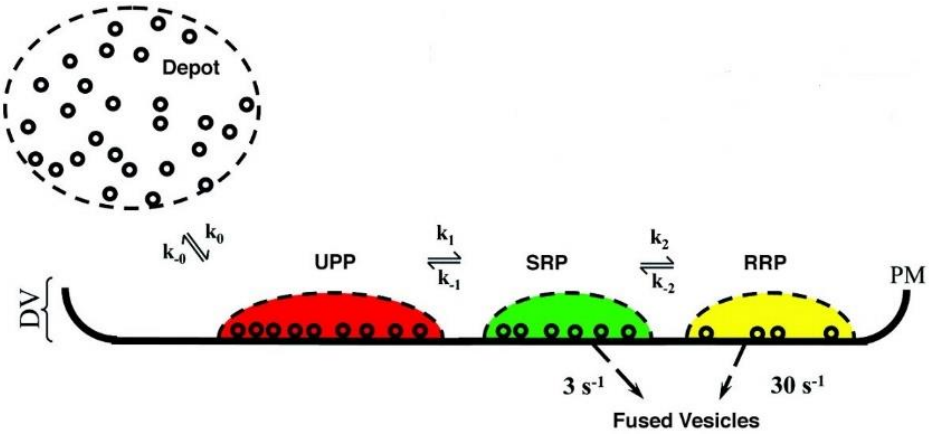

Figure 1. 2 **Identification of different vesicle pools in chromaffin cell using flash photolysis of caged Ca^{2+}**. (Modified from Rettig & Neher, 2002).

DCV exocytosis from adrenal chromaffin cells differs from neurotransmitter release from synaptic vesicles in CNS synapses but also shares many features. The difference between synaptic transmission and catecholamine secretion from chromaffin cells are reflected in different release kinetics between SVs and DCVs. The areas of synapses that are rich in proteins and are involved in neurotransmitter release, commonly known as active zones, are not detectable in chromaffin cells. Additionally, the diameter of SVs is ~50 nm compared to ~100-300 nm big DCVs. SVs contain neurotransmitters, while DCVs are filled with mainly neuropeptides and hormones. As mentioned, exocytosis is a Ca^{2+}-dependent process in both cases, and release occurs from an RRP. Moreover, this release is carried out by similar protein machinery in synapses and chromaffin cells (Stevens et al., 2011; Man et al., 2015). Therefore, DCV exocytosis from adrenal chromaffin cells is a well-known model system for studying the process of exocytosis.

1.3.2. The docked and primed vesicle pool

1.3.2.1. Vesicle docking

Various studies show different criteria for vesicle docking depending on the techniques and biological systems utilized. There are different views among authors concerning the definition of "docked" vesicles. While some consider vesicles located within a specific range (such as ~30 nm) from the plasma membrane to be docked, others only suppose vesicles in visible contact with the plasma membrane as docked (Verhage & Sorensen, 2008). A depot of vesicles is formed by those not near the membrane, and can be utilized when required (Stevens et al., 2011).

It also has been shown that the size of the docked pool exceeds that of the releasable pool, meaning that the majority of docked vesicles are not releasable and require a maturation process called priming to attain releasability. Experiments with increasing intracellular Ca^{2+}

showed that although all docked vesicles could be released, only some were readily releasable (Parsons et al., 1995).

The application of the high-pressure freezing (HPF) method to prepare the sample for electron microscopy (EM) limits freeze artifacts and offers better preservation of the samples compared to chemical fixation (Rostaing et al., 2006; Hammarlund et al., 2007). In addition, the unique structural conservation of HPF samples provides more precise calculations of docked vesicles and could potentially enable the visualization of different subclasses of morphologically docked vesicles (Fig. 1.3) (Stevens et al., 2011).

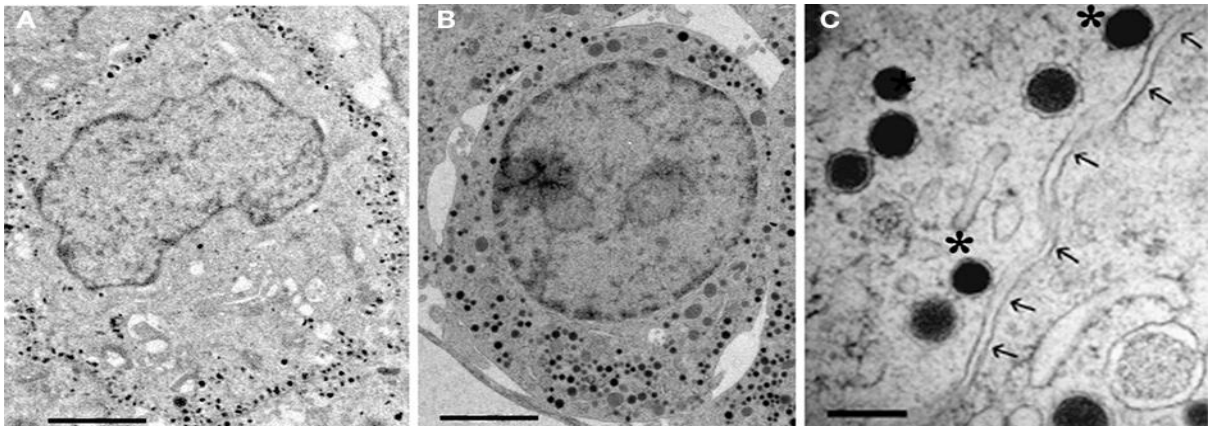

Figure 1. 3 **Ultrastructural organization of chromaffin cells fixed with chemical fixation and HPF.** (A) Chemically fixed chromaffin cell. (B) High-pressure frozen chromaffin cell. (C) Two DCVs ranked as docked (*) based on contact with the cell membrane (arrows) in high-pressure frozen chromaffin cell. (Stevens et al., 2011).

Various proteins have been shown to modulate docking and priming. A group of proteins that play a central role in exocytosis, and are essential for docking and priming, are soluble N-ethylmaleimide-sensitive-factor attachment protein receptor (SNARE) proteins. SNARE proteins form complexes bridging the vesicle and plasma membranes. A ternary complex made of synaptobrevin, a vesicle-membrane associated SNARE protein, syntaxin, and SNAP-25 enables the fusion of plasma and vesicle membrane, permitting exocytosis of vesicle contents (Südhof, 2004; Südhof & Rothman, 2009).

Rab3 proteins, which are small GTPases, and their partners Rabphilins, are proposed to have a role in tethering the vesicles near the plasma membrane, enabling the vesicle docking in chromaffin cells (Chung et al., 1995). Additionally, it has been shown that Rab3 stimulates docking upstream of Munc18-1 (van Weering et al., 2007). Chromaffin cells from knockout (KO) of Munc18-1 show a reduction in secretion and morphologically docked vesicles (Voets et al., 2001; Weimer et al., 2003). Furthermore, in Munc18 null mutant mice, syntaxin levels are reduced, which correlates with the ability of Munc18-1 to bind to closed syntaxin1 and promote docking (Gulyás-Kovács et al., 2007). Genetic approaches with syntaxin, SNAP-25, and synaptotagmin-1(Syt-1) deletion also showed reduced morphologically docked vesicles in

mouse chromaffin cells (de Wit et al., 2006; de Wit et al., 2009). However, the deletion of synaptobrevin (Borisovska et al., 2005) did not result in a docking deficit.

Moreover, the deletion of the mammalian uncoordinated homology-13 (Munc13) proteins, which are crucial for docking and priming in SVs, showed no DCVs docking deficit in mouse chromaffin cells, emphasizing that SV and DCV docking mechanisms are distinct (Man et al., 2015).

Assays on docking and priming showed that some vesicles could be nonfunctionally docked (" ‘dead-end’ docking") (Verhage & Sorensen, 2008). Furthermore, a significant docking deficit is associated with a release deficit, meaning that the priming pool of vesicles is yielded from docked vesicle pool (Stevens et al., 2011).

1.3.2.2. Vesicle priming

In the electrophysiological meaning, priming is the process that permits vesicles to enter a readily releasable pool (Verhage & Sorensen, 2008). SNARE complex, consisting of synaptobrevin, syntaxin, and SNAP-25, is a central component of exocytosis in neurosecretory cells. It has been demonstrated that the deletion of synaptobrevin-1 and -2 in chromaffin cells shows a deficit in release without abolishing the docking of vesicles (Borisovska et al., 2005). In SNAP-25 KO mice, the calcium-triggered release was also abolished, although vesicle docking persisted (Sorensen et al., 2003). In syntaxin-deficient chromaffin cells, catecholamine release was also absent (de Wit et al., 2006).

Manipulations of proteins responsible for secretion can affect the release rate, meaning that RRP release can be blocked while SRP is still functional. For example, the deletion of Syt-1, a Ca^{2+} sensor for regulated exocytosis (Koh & Bellen, 2003; Nagy et al., 2006), abolishes rapid release while the SRP remains unaffected (Voets et al., 2001). Synaptotagmin-7 (Syt-7) can also be found in chromaffin cells and is most likely responsible for slower release (Schonn et al., 2008; Araç et al., 2006). It has been shown that Syt-7 mediates vesicle priming and fusion through interaction with Munc13 and Syt-1, positioning the vesicles close to the plasma membrane (Tawfik et al., 2021).

Loss of Snapin, a protein that binds to SNAP-25 and fortifies the linkage of the SNARE complex with Syt, leads to a substantial reduction in RRP with with no impact on SRP. Snapin appears to be critical in modulating neurosecretion by enhancing the interaction of Syt-1 and SNAP-25 (Tian et al., 2005).

In complexin-2 KO mice, exocytosis is reduced, but fusion kinetics and the dilation of fusion pore and morphological vesicle docking are not affected. Thus, complexin-2 promotes priming by stabilizing the SNARE complex (Cai et al., 2008).

Recently, endophilin's role in exocytosis in the adrenal chromaffin cell has been demonstrated. With its SH3 domain, endophilin binds to intersectin-1 and mediates the priming through its interaction with SNARE proteins and the actin cytoskeleton (Gowrisankaran et al., 2020).

Calcium activator protein for secretion (CAPS) is a priming factor of the RRP and sustained secretion in the presence of Ca^{2+}(Stevens & Rettig, 2009; Liu et al., 2008, 2010). In CAPS1-2 KO mice, secretion in chromaffin cells is reduced (Liu et al., 2008) with morphological vesicle docking intact (Speidel et al., 2005; Liu et al., 2008). Expression of wild-type CAPS1 or CAPS2 in CAPS1-2 KO led to enhancement of RRP and SRP compared to KO mice. Overexpression of CAPS1 or CAPS2 in wild-type chromaffin cells showed increased RRP, indicating that CAPS proteins promote priming. It has been reported that the expression of open syntaxin can rescue the CAPS DKO phenotype. CAPS proteins function downstream of Munc13 but interact functionally with Munc13 facilitating the second step of the priming process (Liu et al., 2010).

Munc13 is a protein family that consists of Munc13-1, Munc13-2, Munc13-3, Munc13-4 and brain-specific angiogenesis inhibitor-1 associated protein 3 (Baiap3) (Koch et al., 2000). Munc13s are crucial for neurotransmitter release and have a role in priming synaptic vesicles at various synapses (Brose et al., 2000). It has been shown that Munc13s induce the release of DCVs but show no effect on DCV morphological docking in chromaffin cells (Ashery et al., 2000). Additional experiments reveal that the ability to facilitate the exocytosis of DCVs varies among the various Munc13 proteins. In adrenal glands, isoforms Munc13-1, Munc13-2 and Baiap3 were detected (Man et al., 2015). In Baiap3 KO mice, exocytosis was intact, and overexpression of Baiap3 in wild-type cells did not induce enhancement in DCV release. Deletion of Munc13-1, which is the essential Munc13 isoform in SV exocytosis (Augustin et al., 1999; Varoqueaux et al., 2002), did not cause a drastic reduction in secretion in adrenal chromaffin cells. However, in Munc13 ½ DKO, DCV release was dramatically reduced without affecting DCV docking. Therefore, Munc13-2 is an essential isoform in the chromaffin cell that plays a role in the physiological priming of DCVs (Man et al., 2015).

1.3.3. Proposed model for exocytosis from docking step to vesicle fusion

Adrenal chromaffin cells were the first model system where it was shown that exocytosis depends on Ca^{2+} (Bittner & Holz, 1992; Rüden & Neher, 1993), which was later demonstrated in neurons (Dittman & Regehr, 1998; Stevens & Wesseling, 1998; Gomis et al., 1999). Experiments in the adrenal chromaffin cells have revealed the existence of different vesicle pools. Using stepwise increases in Ca^{2+}, three releasable pools with different release rates can be triggered. There is also a large depot pool of vesicles where hundreds of vesicles were observed to be morphologically docked (Rettig & Neher, 2002). The status of vesicles relies on the presence and activity of diverse docking and priming factors.

Figure 1.4 (modified from de Wit et al., 2009) showcases the proposed minimal working model for exocytosis where SNARE complex, synaptotagmin, complexin, and Munc18-1 are considered (de Wit et al., 2009). This model consists of four steps: First, Munc 18-1 binds to the Habc domain and the N-terminal domain of syntaxin-1 in its closed conformation (Dulubova et al., 1999; Dulubova et al., 2007; Khvotchev et al., 2007). In the second step, binding of the syntaxin-1/Munc18-1 heterodimer and SNAP-25 occurs (Burkhardt et al., 2008; Zilly et al., 2006). Third, the vesicles make their way to the plasma membrane where Syt-1, through its C_2B domain, interacts with syntaxin-1/Munc18-1/SNAP-25 complex (Gaffaney et al., 2008; Lynch et al., 2007; Tang et al., 2006; Xue et al., 2008), which enables vesicle docking. Syt-7 has an additional role in positioning the vesicles close to Ca^{2+} channels (Neher & Penner, 1994). During the fourth step, the synaptobrevin-2 attaches to the synaptotagmin-1/syntaxin-1/Munc18-1/SNAP-25 complex, resulting in the formation of a four helical SNARE bundle, permitting complexins to unite, which leads to the fusion of the vesicle.

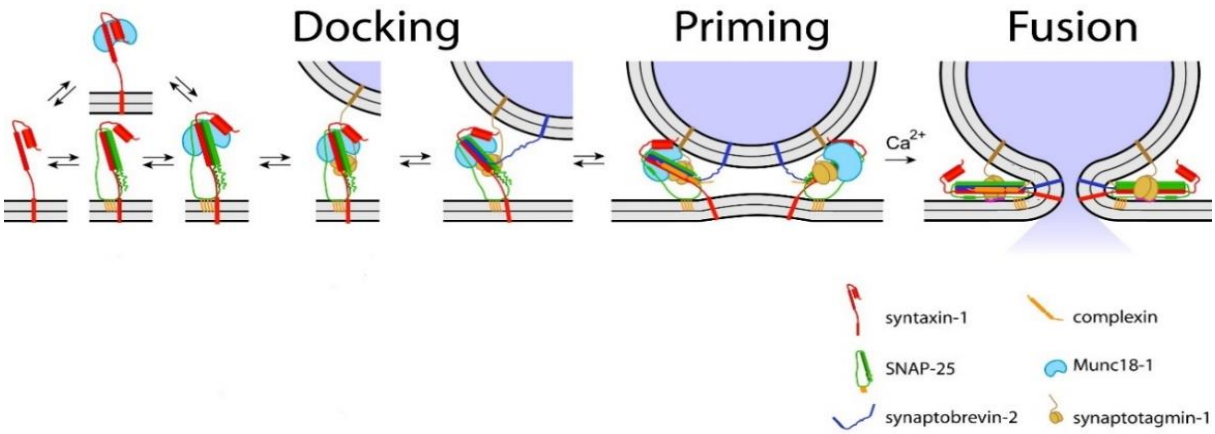

Figure 1. 4 **The proposed working model for the exocytosis illustrates the following steps in the exocytic pathway.** (modified from de Wit et al., 2009).

1.4. Different modes of endocytosis

In neurons and neuroendocrine cells, exocytosis of neurotransmitters, hormones, and peptides through the fusion of the vesicles is followed by specific endocytosis of vesicle membrane components. Specialized endocytic mechanisms lead to the internalization of the plasma membrane components into the vesicles that bud into the cell's cytoplasm and connect with the endosomes. Endosomal processes lead some internalized molecules to the lysosome for degradation, while others are recycled back to the cell surface or aimed at other intracellular compartments (Conibear & Tam, 2009).

Endocytosis is a crucial mechanism for the overall physiology and homeostasis of the cell. There are different modes of endocytosis which can be classified into two gropus: phagocytosis, which takes in large particles, and pinocytosis which takes fluid. Phagocytosis occurs in some mammalian cells, while pinocytosis happens in all mammalian cells. Figure 1.5

shows four primary mechanisms of pinocytosis: “macropinocytosis, clathrin-mediated endocytosis (CME), caveolae-mediated endocytosis, and clathrin- and caveolae-independent endocytosis” (Conner & Schmid, 2003).

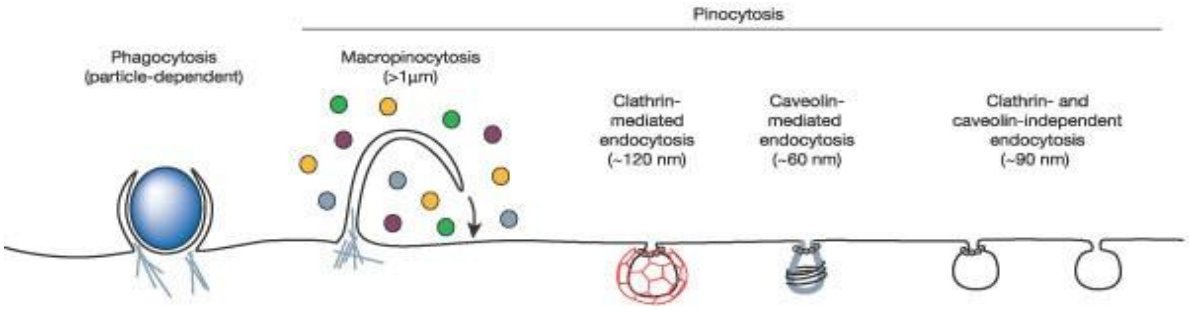

Figure 1. 5 **Different endocytic pathways of the mammalian cell.** (Conner & Schmid, 2003).

CME is a major endocytic pathway (Saheki & De Camilli, 2012; Milosevic, 2018). However, since the coat mediates the formation of vesicles, CME is considered a slow process. Therefore, after intense stimulus, particular systems, such as ribbon synapses (Paillart et al., 2003), utilize bulk endocytosis to remove excessive plasma membrane. It was also proposed that parallel to CME, an alternative endocytosis model, such as kiss-and-run (KR) occurs in the cell under moderate stimulation conditions (Fesce et al. 1994). In situations where the quick responses of the cell are needed, fast endocytic mechanisms like clathrin-independent fast endocytosis (CIFE) and ultrafast endocytosis (UFE) mechanisms have been demonstrated (Watanabe & Boucrot, 2017). The slow and fast endocytic pathways have been investigated and demonstrated in neurons and chromaffin cells (Gersdorff & Matthews, 1994; Artalejo et al., 1995).

1.4.1. Phagocytosis

Phagocytosis is viewed as ingesting mechanism of large (≥0.5 μm) particles. Macrophages and other professional phagocytes eliminate foreign bodies from the cell (Flannagan et al., 2012; Uribe-Querol & Rosales, 2020). Different phagocytic receptors for detecting foreign particles are expressed on professional phagocytes that activate phagocytosis. Phagocytosis consists of four phases: particle detection, internalization process, formation of the phagosome, and maturation of phagosome to phagolysosome (Uribe-Querol & Rosales, 2020). For example, macrophages play a significant role in phagocytosis, and cytokines derived from macrophages have been indicated to regulate adrenal gland functions (González-Hernández et al., 1994). The presence of adrenal medulla macrophages was investigated in rat adrenal medulla. It has been shown that adrenal chromaffin cells express the neurotrophin receptor TrkA and respond to NT-4 in vitro by induction of c-fos-ir. These data indicate an

apparent role of NT-4 in regulating the functions of adrenal medullary cells (Schober et al., 1998).

1.4.2. Macropinocytosis

Macropinocytosis is a unique endocytic process important for antigen presentation, recycling of plasma proteins, migration and signaling. In many cell types, upon stimulation, macropinocytosis is started by the polymerization of actin at the plasma membrane to induce “membrane ruffles” (Lin et al., 2020). Ruffles then form irregularly shaped vesicles called macropinosomes that can be routed to other organelles in the endolysosomal system (Jack Wang et al., 2014). It has been shown that in human dendritic cells, macropinocytosis increases in a regulated fashion and depends on intracellular Ca^{2+} concentration rise that precedes the PI3 kinase-dependent step, and it is accompanied by the formation of enlarged endosomes (Falcone et al., 2006). In addition, it was investigated that macropinocytosis induces membrane internalization at growth cones (Kabayama et al., 2009). Various kinases and phosphatases also play significant roles by regulating Pi(3,4,5)P3 and Pi(3,4)P2 or by modulating the activity of proteins essential for the pathways to control macropinocytosis formation (Mercer & Helenius, 2012; Watanabe & Boucrot, 2017).

1.4.3. Caveolin-mediated endocytosis

Flask-shaped and nonclathrin-coated plasmalemmal invagination, named caveolae, were first observed on the surface of endothelial cells (Yamada, 1955). Experiments with immunogold EM have demonstrated the association of a 22-kDa protein with caveolae, which is called caveolin (Rothberg et al., 1992). This dimeric protein forms a caveolin coat on the the membrane invaginations and has structural importance (Pelkmans & Helenius, 2002). Additionally, caveolae, which are cholesterol-rich microdomains, contain a GTPase dynamin localized to the neck of the flask-shaped caveolar structure (Hinshaw, 2000; Henley et al., 1998; Oh et al., 1998). In caveolar endocytosis, caveolae are not static but bud off from the plasma membrane, and the budding of caveolae is mediated by dynamin (Pelkmans et al., 2001; Henley et al., 1998; Echarri et al., 2012). Various signaling molecules are joined with caveolae, highlighting their role in the managing of specific signaling pathways (Anderson, 1998; Razani et al., 2002). The presence and relevance of caveolae-mediated endocytosis in physiological homeostasis have been demonstrated in different cell types (Razani et al., 2002; Shajahan et al., 2004).

1.4.4. Clathrin-independent fast endocytosis (CIE)

As mentioned previously, macropinocytosis and caveolin endocytosis are types of CIE. Moreover, it has been investigated that several other processes belong to CIE and are present

at synapses, such as activity-dependent bulk endocytosis (ABDE), fast-endophilin-mediated endocytosis (FEME), KR, and UFE (Watanabe & Boucrot, 2017). Different CIEs do not exhibit continuous activity and may employ alternative molecular pathways to efficiently recycle excess membranes. Knowledge of the exact mechanism of CIE is lacking mainly because it is activated upon certain stimuli or is too rapid, which makes it challenging to observe (Watanabe & Boucrot, 2017).

1.4.4.1. Fast endophilin-mediated endocytosis (FEME)

Fast endophilin-mediated endocytosis (FEME) belongs to CIE that involves protein endophilin to form endocytic vesicles fast upon specific stimulations (Wu et al., 2014; Watanabe & Boucrot, 2017). FEME is not a continuously occurring endocytic pathway and requires the activation of certain receptors, such as G-protein coupled receptors to initiate (Boucrot et al., 2015). Through its C-terminal SH3 domain, endophilin binds to the activated receptors and additional proteins such as dynamin and synaptojanin. Membrane curvature is induced and stabilized through endophilin's BAR domain. Endophilin's SH3 and BAR domains facilitate dynamin's scission from the cell surface (Renard et al., 2015; Boucrot et al., 2012). After forming, vesicles bud off from the plasma membrane and, together with endophilin, travel inside the cell (Watanabe & Boucrot, 2017).

1.4.4.2. Ultra-fast endocytosis (UFE)

The utilization of a novel EM technique can assist in resolving compensatory membrane recycling events. For example, the use of optogenetic stimulation-coupled cryofixation ("Flash-and-freeze") and EM enabled capturing of rare exocytotic and endocytotic events at hippocampal mossy fiber synapses (Imig et al., 2020). In addition, earlier studies have presented an alternative rapid pathway for vesicle recovery in neurons (Watanabe, 2013). In the "Flash-and-freeze" method, neurons are stimulated using optogenetics, and synaptic transmission is induced. Capturing membrane dynamics involves the precise freezing of neurons at a specific moment (Watanabe, 2016). Findings from this study indicated that the plasma membrane underwent rapid recovery after a single stimulus and that this ultrafast endocytic pathway did not show the presence of clathrin (Watanabe, 2013). Instead, clathrin operates in the formation of SVs from endosomal intermediates when the internalized membrane merges with the endosome (Watanabe et al., 2014).

It has been investigated whether the increase in Ca^{2+} may trigger UFE, but the rate of endocytosis was unaltered with elevating Ca^{2+}. In addition, F-actin has been shown to play a role in UFE. However, it remains to be resolved whether actin plays an active role via its polymerization or a passive role in preserving surface tension around the endocytic site. Moreover, another critical factor in UFE is dynamin, which has a role in the fission process

upon which vesicle is internalized (Watanabe, 2013). UFE is necessary because fusion sites must be restored fast by rapidly removing the excess membrane. It is also possible that UFE mediated the recovery of vesicle proteins, which needs more examination (Watanabe & Boucrot, 2017).

Furthermore, recent findings in chromaffin cells showed that endocytic vesicles are formed from the closure of Ω-shaped profiles that already created before stimulation. It has also been shown that varying Ca^{+2} influxes lead to speed-specific slow, fast, or ultrafast (< 0.6 s) endocytosis (Shin et al., 2021). These studies in adrenal chromaffin cell reveal significant mechanisms that underly endocytosis.

1.4.4.3. Bulk endocytosis

Bulk endocytosis is mainly activated with high-intensity stimulation and elevated Ca^{2+} in the cell (Hayashi et al., 2008). During this process, endosomal intermediates are formed at the plasma membrane but disappear ultimately as new vesicles are created (Clayton et al., 2008; Wu et al., 2014). In activity-dependent bulk endocytosis (ABDE), the fission of endosomal structures depends on endocytic proteins such as syndapin-1 and dynamin (Cheung & Cousin, 2013). However, there is the case where bulk endocytosis may also occur independently of dynamin (Wu et al., 2014; Ferguson et al., 2007), suggesting the existence of multiple pathways for the fission of the large structures from the plasma membrane. Structural studies show that the BAR superfamily of proteins has a role in endocytosis, actin regulation, and signaling (Itoh & De Camilli, 2006). Various models for transforming endosomal intermediates into vesicles have been suggested, but the precise process by which this occurs remains unclear (Saheki & De Camilli, 2012).

Additionally, recent studies in chromaffin cells showed that large plasma membrane invaginations thought to be precursors of bulk endocytosis are sites for clathrin-coated pits after stimulation, suggesting an association between two endocytic pathways (Arpino et al., 2022).

1.4.4.4. Kiss-and-run mechanism (KR)

The endocytic mechanism where the vesicle does not entirely collapse with the plasma membrane after the fusion is called kiss-and-run (KR) fusion (also called cavicapture) (Fesce et al., 1994). During KR, the vesicle releases its contents through a transient fusion pore while maintaining its morphological shape (Alabi & Tsien, 2013). It has been shown that at synapses of cultured hippocampal neurons, during KR, the vesicle interior is exposed shortly (< 6 ms) and that this endocytotic pathway includes about 20% of the release events during standard synaptic transmission (Stevens & Williams, 2000). In addition, evidence for the KR mechanism

was obtained for peptide- and amine-containing vesicles of neuroendocrine and other cells (Albillos et al. 1997; Holroyd et al. 2002; Taraska et al. 2003).

Some studies demonstrated that pore stability is related to the function of SNARE proteins and that SNARE-mediated generated force tilts the balance between KR and full fusion (FF) (Alabi & Tsien, 2013). For example, weakening the mechanical coupling between SNARE complex formation and auxiliary proteins at the plasma membrane leads to FF (Kesavan et al., 2007; Bretou et al., 2008). In reconstituted systems (Shi et al., 2012), it has been suggested that one SNARE complex suffices for membrane fusion (during KR), and three such complexes are required to prevent the developing fusion pore from reclosing (during FF). Additionally, the fusion pore stability can be altered by synaptotagmin (Wang et al., 2001; Segovia et al., 2010), complexin (Archer et al., 2002) and $G_{\beta\gamma}$ (Gerachshenko et al., 2005; Blackmer et al., 2005).

In metastable-narrow-pore theory (Alabi & Tsien, 2013; Wu et al., 2014), it has been described that a narrow pore with a diameter of less than 5 nm either closes (KR) to restrict or expands until flattened (FF) to facilitate the content release. However, recent experiments on chromaffin cells proposed a dynamic-pore theory (Shin et al., 2018) that demonstrates refinements over the narrow-pore theory. In dynamic-pore theory, the pore size can vary. The extensive range of pores can expand, constrict, or close at different rates from 0 to more than 8.9 nm/s. The study displays that dynamic pore behavior results from the competition between expansion and constriction (Shin et al., 2018). In addition, it has been shown that F-actin facilitates (Berberian et al., 2009) and dynamin limits content release (Tsuboi et al., 2004; Trexler et al., 2016). Furthermore, Ca^{2+} may likely facilitate expansion and constriction depending on its low or high levels. Thus, it has been demonstrated that substantial Ca^{2+} influx facilitates pore constriction (Shin et al., 2018). Therefore, according to the new study, the release rate depends not merely on narrow pore closure or FF, but on the interplay between expansion, constriction and specific proteins (Shin et al., 2018).

1.4.5. Clathrin-mediated endocytosis (CME)

CME is a crucial endocytic pathway for intracellular communication throughout the organism's life (Seto et al., 2002). Furthermore, nerve terminals are rich with clathrin and clathrin complementary proteins, and the main cargo of clathrin-coated vesicles are SV proteins (Maycox et al., 1992). Thus, after neurotransmission, recycling of SV membrane proteins is necessary and is achieved through CME (De Camilli & Takei 1996).

During CME, by the assembly of cytosolic coat proteins, mainly clathrin, "coated pits" are formed on the plasma membrane (Conner & Schmid, 2003). Coated membrane invaginations bud from the membrane to form clathrin-coated endocytic vesicles (CCVs). Clathrin represents a formation called "triskelion", made of three heavy chains (CHC) and three firmly connected

light chains (CLC) (Brodsky et al., 2001; Kirchhausen, 2000). In addition, adaptor protein complex 2 (AP2) is involved in CME, having a role in clathrin assembly and vesicle formation (Brodsky et al., 2001; Collins et al., 2002; Marsh et al., 1999). Furthermore, the GTPase dynamin is essential and best represented in the context of CME. Dynamin's pleckstrin homology (PH) domain enables this protein phosphatidylinositol-4,5-bisphosphate (Pi (4,5) P2) binding; the GTPase effector domain (GED), GTPase, and middle domains enable self-assembly, where the proline/arginine-rich domain (PRD) enables interaction with other endocytic components (Conner & Schmid, 2003). For its activity, dynamin must go through GTP-hydrolysis-driven conformational changes (Song et al., 2003). Besides mentioned crucial proteins, various additional molecules have been described to have a role in regulating CME, such as AP-180, amphiphysin, Eps15, and epsin (Brodsky et al., 2001; Slepnev & De Camilli, 2000; Saheki & De Camilli, 2012), which emphasizes the fact that CME is a highly dynamic process.

Through the interaction of proteins with other proteins and lipids, CME is a highly temporally and spatially regulated process (Saheki & De Camilli, 2012; Milosevic, 2018, Fig. 1.6.). Interaction of the clathrin adaptor proteins and cargo proteins leads to formation of the pit (Edeling et al., 2006; Owen et al., 2004). FCHo1/2, intersectin, and Eps15 interactions at the plasma membrane lead to the recruitment of adaptor proteins such as AP-2, AP180 and others to the formation pit's site (Henne et al., 2010), which form the adaptor protein complex that selects cargo (Diril et al., 2006; Ford et al., 2001, 2002). The adaptor protein complex recruits clathrin triskelion, leading to coat assembly (Kirchhausen, 2000). A set of proteins, including clathrin, induce curvature of the plasma membrane. Clathrin-coated membrane buds are formed from which coated vesicles are generated that ultimately bud off by a dynamin that oligomerizes at bud necks and leads to a fission reaction (Ferguson & Camilli, 2012). Synaptojanin-1 allows the displacement of adaptor proteins, promoting vesicle uncoating. (Cremona et al., 1999; Schuske et al., 2003; Verstreken et al., 2003). ATPase Hsc70 and its cofactor auxilin promote clathrin disassembly, producing coat-free vesicles (Guan et al., 2010; Xing et al., 2010).

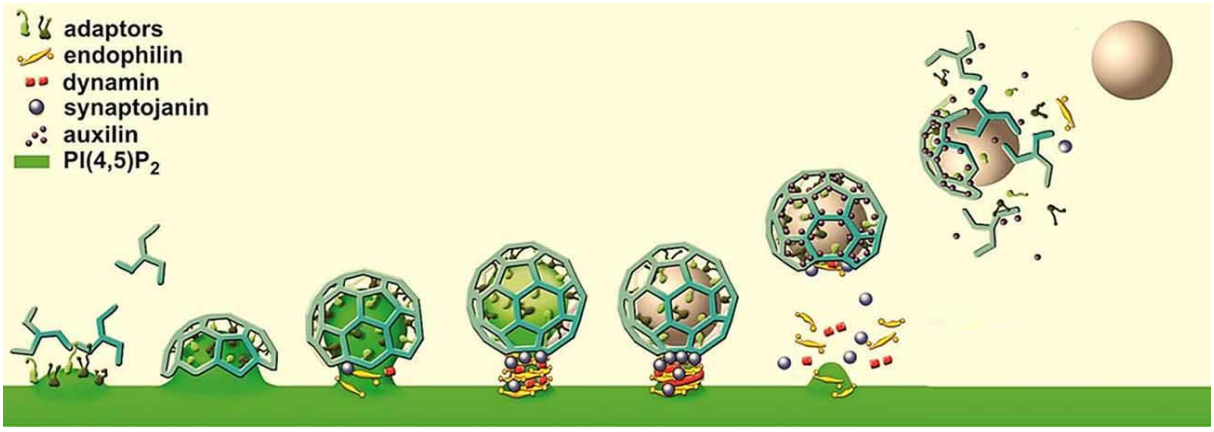

Figure 1. 6 **A working model illustrating protein-protein and protein-lipid dynamic interaction for clathrin-mediated endocytosis.** (Milosevic, 2018).

Clathrin- and dynamin-mediated endocytosis in adrenal chromaffin cells also represents a crucial endocytic pathway. In addition, experiments on a bovine chromaffin cell demonstrated a nibbling mechanism for clathrin-mediated membrane retrieval after strong stimulation (Bittner et al., 2013). They suggest that clathrin, dynamin, and other vesicular endogenous proteins, such as DBH, VMAT2, and Syt, begin to accumulate within seconds at the fusion sites and remain there for several minutes after endocytosis. The fused vesicular membrane is slowly removed from the cell surface through multiple rounds of CME.

CME is thought to be induced primarily from relatively flat plasma membrane portions. However, it has been demonstrated that CCVs may occur at flat portion and membrane invagination in primary neuroendocrine chromaffin cells after the KCl-induced depolarizations (Arpino et al., 2022). Furthermore, the study suggests membrane invaginations are precursors for bulk endocytosis, representing sites for clathrin-coated pits and generation of vesicles in secretory cells, emphasizing collaboration between CME and bulk endocytosis.

1.5. Chromaffin cell as a model system to investigate exo- and endocytosis

Neurons and neuroendocrine cells contain secretory vesicles filled with neurotransmitters, hormones, and peptides, which secret their content via exocytosis. Since chromaffin cells are postganglionic sympathetic neurons, they and neurons have similar molecular machinery that orchestrates exocytosis (De Camilli & Jahn, 1990). Therefore, adrenal chromaffin cells became a prominent model system for studying exocytosis (Bader et al., 2002).

In adrenal chromaffin cells, catecholamines (adrenaline and noradrenaline) are packaged into compartments called DCVs. DCVs originate from the Golgi apparatus, where the production of cargo peptides is processed. DCVs then undergo a maturation process under controlled conditions and subsequently translocate the plasma membrane, fusing and releasing their contents into the circulation. After DCVs fusion and content release, the excess membrane is removed, and DCVs proteins are recycled via endocytosis (Dembla & Becherer, 2021).

Vesicle fusion with the plasma membrane leads to a transient increase in the plasma membrane area. This increase can be monitored electrically as surface membrane capacitance increases (Jaffe et al., 1978; Gillespie, 1979; Neher & Marty, 1982). Capacitance measurements provide high temporal resolution to detect the exocytosis of a single secretory vesicle. However, capacitance is challenging to measure accurately in small single compartments, such as nerve terminals with attached axons. Thus, important information on exocytosis has been acquired with this method, mainly in neuroendocrine cells (Parsons et al., 1995; Seward et al., 1996; Gingrich & Byrne, 1985). This technique has provided knowledge about the fusion process (Almers & Tse, 1990) and the process of endocytosis (Smith & Neher, 1997; Artalejo et al., 1995).

Catecholamines are oxidizable molecules that can be detected electrochemically using carbon fiber microelectrodes (Gonon et al., 1993). Therefore, amperometric measurements have been used to explore the kinetics of exocytotic events (Neher, 1998). Spike-like waveforms of amperometric current represent the release from single vesicles. An amperometric spike, usually, is preceded by the so-called "foot". A foot is described as a slow release from a narrow fusion pore in the first milliseconds of its formation (Chow et al., 1992). Due to their round shape, chromaffin cells are suitable for combining capacitance and amperometry measurements to resolve the underlying mechanism and time course of vesicle release in neuroendocrine cells (Chow et al., 1996). For example, capacitance and amperometry measurements demonstrated the role of the Munc13 protein family in the priming step in exocytosis in adrenal chromaffin cells (Man et al., 2015).

Chromaffin cells are also suitable for morphological analysis by EM (Lever, 1955; Sjostrand & Wetzstein, 1956; De Robertis & Sabatini, 1960). In EM pictures, DCVs are identified by a vesicular membrane containing an electron-dense core (Plattner et al., 1997; Koval et al., 2001; Unsicker et al., 2005). Many EM studies have been performed to explain the molecular mechanism of vesicle transport, docking, and fusion (Ashery et al., 2000; Voets et al., 2001; Sørensen et al., 2003; de Wit et al., 2006). Combining specific mouse lines, electrophysiology and EM can give insights into vesicular or plasma membrane proteins included in vesicle docking and priming. For example, it has been demonstrated that Munc13-1 and Munc13-2, essential for SV docking and priming, also have a significant role in vesicle priming but not in vesicle docking in chromaffin cells (Man et al., 2015). This study emphasizes that vesicle docking is a unique process that can be resolved using the EM technique. Furthermore, the EM findings apart from DCVs confirm the existence of mitochondria, endoplasmic reticulum, Golgi membranes, multi-vesicular bodies, cilia, centrioles, and intracellular fibrils or tubules (Coupland, 1965). Therefore, chromaffin cells are an excellent model system for studying morphological aspects of the cell using EM.

Super-resolution stimulated emission depletion (STED) microscopy experiments demonstrated fusion pore dynamics of DCVs in chromaffin cells (Zhao et al., 2016; Shin et al., 2018, 2020, 2021), leading the way for visualization of endocytic membrane dynamics. In a recent study in chromaffin cells (Shin et al., 2021), capacitance induced by 1-s depolarization stimulation showed no endocytosis, slow, fast, ultrafast, or overshoot endocytosis. Moreover, EM images from high-pressure frozen chromaffin cells exposed to 70 mM KCl displayed the different sizes of Ω-shaped profiles. Additionally, in the resting condition, flat, Λ-, Ω-, and O-shaped profiles (Shin et al., 2021) have been visualized at the plasma membrane, which may indicate endocytic intermediates (Fig. 1.7). Therefore, it has been demonstrated that endocytosis is not generated explicitly from the flat-to-round transformation upon stimulation but from preformed Ω profiles and fusion pore closure (KR), processes induced by calcium influx and dynamin-mediated (Shin et al., 2021). Using electrophysiological techniques, STED microscopy, and EM in chromaffin cells, a new membrane transformation theory underlying endocytosis has been established (Shin et al., 2021).

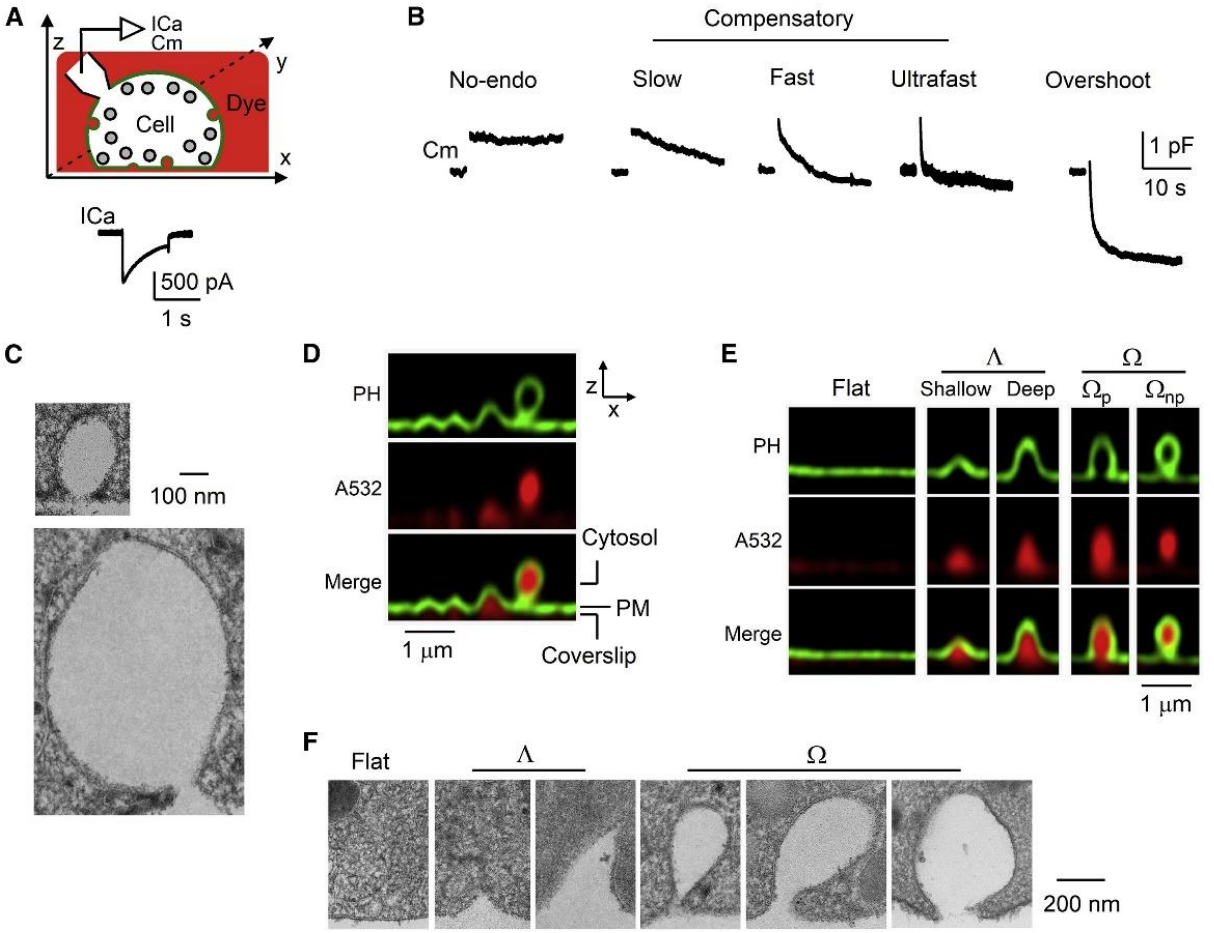

Figure 1. 7 **Membrane dynamics and different endocytic modes in adrenal chromaffin cells**. (A) Top: whole-cell patch-clamp drawing. Bottom: Ca^{2+} current induced by the stimulation. (B) Capacitance induced by stimulation shows different modes of endocytosis. (C) Electron microscopic images depicting different sizes of Ω profiles. (D) STED images of a cell in resting conditions. (E) Flat, Λ-, Ω-shaped profiles chromaffin cells in resting conditions. (F)

Electron microscopic images showing flat, Λ-, Ω-shaped profiles in resting cells. (Shin et al., 2021).

Therefore, the use of adrenal chromaffin cells as a model system has been shown to have a profound impact on studies and discoveries involving the processes of exo- and endocytosis.

1.6. Aims and experimental approach of this project

SV exocytosis is one of the best-regulated processes in cell biology (Wojcik & Brose, 2007). Molecular machinery maintaining the various steps of exocytosis has been investigated (Jahn & Fasshauer, 2012; Südhof, 2013). Additionally, membrane retrieval after exocytosis and critical factors included in the process of endocytosis have also been examined (Milosevic, 2018; Saheki & De Camilli, 2012). Despite extensive investigation, the exact mechanism and the intermediate steps involved in the transition from exocytosis to endocytosis in SV have not been fully captured in response to a specific stimulus.

For this project, adrenal chromaffin cells have been used to examine how a specific stimulus triggers the vesicle release. Chromaffin cells are an excellent model system for stimulation-secretion coupling of DCV release because they are full of these vesicles, and it is relatively easy to monitor their release. In addition, DCVs also exist in nerve terminals (Merighi, 2018). However, it is much more challenging to observe the release of these vesicles. Therefore, we employ chromaffin cell as a model system for DCV release.

The release of SV and DCV is thought to be analogous. In the past, the function of the Munc13 family, which is already known to play a role in SV release (Chen et al., 2013; Breustedt et al., 2010), was analyzed in DCV release in chromaffin cells (Man et al., 2015). Now we know that Munc13s are also crucial for DCVs. Furthermore, we know that docking and priming are not two separate steps in synapses (Wojcik & Brose, 2007). Docking is a morphological term, and priming comes from physiological experiments. Moreover, Munc13s regulate docking and priming in SVs. It is known that physiologically Munc13s also regulate DCV release, but apparently, the docking in chromaffin cells happens differently (Man et al., 2015).

The SNARE proteins synaptobrevin-2, SNAP-25, and syntaxin-1 are critical regulators of exocytosis in neurons and neuroendocrine cells. Studies on SNAP-25 and syntaxin-1 KO have demonstrated docking deficit in chromaffin cells (de Wit et al., 2009). However, in synaptobrevin-2 null mice with conventional fixation, docking deficit in chromaffin cells has not been shown (Gerber et al., 2008). In contrast, another study where PC12 cells were fixed with HPF prior to EM revealed that DCV docking is impaired when synaptobrevin cleavage is caused by botulinum neurotoxin D (BiNT/D) (Wu et al., 2012), implicating synaptobrevin in docking.

Excitation-secretion coupling of DCV release was assessed electrophysiologically using an optogenetic, electric field, and voltage ramp stimulation. Optogenetics has proven to be an ideal tool in neuroscience, enabling precise induction of action potentials with short light pulses (Berndt et al., 2011; Madisen et al., 2012; Imig et al., 2020). In addition, exposing excitable cells to electrical stimulation and voltage ramp stimulation has also been demonstrated (Bagalkot et al., 2019; Lynch et al., 2018; Duan et al., 2003).

Previous HPF experiments were done in unstimulated chromaffin cells (Plattner et al., 1997; Koval et al., 2001). To investigate the morphological characteristics of chromaffin cells upon a specific stimulus, cultured chromaffin cells were stimulated utilizing a "Zap-and-freeze" technique (Kusick et al., 2020) and visualized using EM. HPF happens very promptly, immobilizing cellular structures within the millisecond timescale. Furthermore, during HPF, an increase in atmospheric pressure operates simultaneously with fast liquid nitrogen cooling of the sample to inhibit the volumetric expansion of water, suppressing ice crystal formation (Moor, 1987; Imig & Cooper, 2016).

We investigated exocytosis and subsequent membrane retrieval using cultured chrmaffin cells. In addition, optogenetic, field, and ramp stimulation were tested. Stimulation patterns initially established in cultured cells using whole-cell patch clamp, have been implemented prior to HPF and subsequent analysis by 2D and 3D EM.

Therefore, the main objective of this thesis is to investigate DCV exocytosis and endocytosis in response to defined stimuli by combining electrophysiological and ultrastructural analyses. We are addressing the following questions:

Which mode of DCV fusion predominates (full fusion vs. kiss-and-run)?

Whether compound fusion or hemifusion intermediates can be detected?

Which modes of endocytosis can be detected?

2. Materials and Methods

2.1. Animals

Experiments were performed on chromaffin cells cultured from C57BL/6N wild-type mice and transgenic mice. Transgenic mice expressing channelrhodopsin-2(H134R)-EYFP (ChR2(H134R)-EYFP) (Madisen et al., 2012) and Cre - recombinase driven by the tyrosine hydroxylase promoter (Jackson Laboratory B6. Cg-$^{7630403G23RikTg\ (Th\text{-}cre)1Tmd/J}$) were used for optogenetic experiments.

2.2. Mouse chromaffin cell culture

2.2.1. Media and chemicals

Cell medium: 30 ml DMEM (Dulbecco's Modified Eagle's Medium) Linaris 4.5/2.2 (GMF2143KYA), 300 µl ITS-X (100x) (Gibco; LOT: 2415099),120 µl Penicillin/Streptomycin (100x) (Thermo Fischer Scientific).

10x Locke's solution: 1540 mM NaCl (Merck), 56 mM KCl (Merck), 8.4 mM NaH_2PO_4 (Merck), 21.4 mM Na_2HPO_4 (Merck) and 100 mM D-glucose (Sigma Aldrich), pH 7.0 with NaOH.

Solution for Papain digest: 200 mg/L L-cysteine (Thermo Fischer Scientific), 1 mM $CaCl_2$, 0.5 mM EDTA in DMEM (Gibco).

STOP solution: 10% fetal bovine serum (Gibco), 2.5 g/L trypsin inhibitor (Gibco), 2.5 g/L albumin in DMEM (Gibco).

2.2.2. Cell culture

Cell medium was prepared and equilibrated in the incubator at 37°C and 5 % CO_2. 10x Locke's solution was diluted to 1x and kept on ice. STOP-solution and the solution for the Papain digest were thawed and STOP solution was stored in incubator (loosen cap). The solution for Papain digest was bubbled with carbogen for 10-15 min and filter sterilized. Papain enzyme was added to the solution to a concentration of 16 or 25 U/ml. Prepared Papain solution was stored in the incubator (loosen cap). Next, postnatal (P0 or P1) adrenal glands were dissected from mice and placed in ice-cold 1x Locke's solution. All connective tissue was removed, and glands were kept on ice. Papain solution (500 µl) was aliquoted into Eppendorf tubes (1 tube for 2 glands). Glands were placed in Papain solution under sterile conditions and incubated in Papain solution at 37°C for 35-45 minutes in an Eppendorf Thermocycler (450 rpm), followed by addition of 500 µl pre-warmed STOP solution and incubation for 15 min. Without disturbing the glands, the solution was removed and 60 µl culture medium was added. The adrenal glands were triturated gently through a 200 µl pipette tip. The entire cell

suspension obtained from two glands (one animal) was 150 µl. On three separate sterile coverslips in a 6-well plate, 50 µl cell suspension was plated. The plate was placed in incubator without disturbing the drops and after 30 minutes 2 ml culture medium was added to each well. The cells were incubated at 37 °C and 5 % CO_2 and used within 2-3 days after plating.

2.3. Genotyping

Mouse tails were collected in tubes and stored at -20°C. The day after the cell culture, genotyping was performed. Before starting the genotyping, nexttec™ cleanPlate96 was equilibrated by adding 350 µl of Prep buffer, incubated at room temperature for 5 minutes and then centrifuged at 350 RCF for 1 minute. DNA lysis was done by adding 300 µl Lysis Buffer (265 µl G1, 10 µl G2, 25 µl G3 buffer) per tail. Tubes with tails were placed in a Thermomixer at 62^0C at 1100 rpm and incubated for one hour. DNA purification was done by adding 120µl of the lysates to the equilibrated nexttec™ cleanPlate96, incubated for 3 min at room temperature and then centrifuged at 700 RCF for 1 minute. Purified DNA is used for polymerase chain reaction (PCR). Primer sequences and fragment lengths for PCR are listed in Table 1. Master mix and PCR programs utilized are listed in Table 2. PCR results were analyzed with agarose gel 1.5% in 1x TBE electrophoresis buffer. For visualizing DNA, DNA Red gel Nucleic Acid stain (Sigma) was used. The gels were read with Intas GDS Touch II software and Intas Scientific Grad camera with 5.0 MPixel.

Mice used in the optogenetic experiments were heterozygotes (Ai32 wt/fl/THcre+ and Ai32 wt/fl/THcre-).

Mouse line	Allele	Primer sequence	Fragment length
Ai32xTHCRE	WT	27488: 5'-AAG GGA GCT GCA GTG GAG TA-3' 27489: 5'-CCG AAA ATC TGT GGG AAG TC-3'	297
	KI	17795: 5'-GGC ATT AAA GCA GCG TAT CC-3' 32320: 5'-ACA TGG TCC TGC TGG AGT TC-3'	212
	Cre	4193: 5'-CCTGGAAAATGCTTCTGTCCG -3' 24366: 5'-CCTGGAAAATGCTTCTGTCCG -3	
	R	26512: 5'-CTACAGCTCCTGGGCAACG -3' 30545: 5'-AAGCTGATCCGGAACCCTTAA -3' 33787: 5'-CGGCCGAATTCGATCTAGC -3'	Recombined 215 Not recombined 99

Table 1. **Primer sequences and fragment lengths for the corresponding mouse line.**

Mouse line	Master mix + DNA	PCR program
Ai32xTHCRE	WT: 1µl DNA, 1µl 27488 (5pmol), 1µl 27489 (5pmol), 1µl dNTP's, 2µl 10x Buffer, 1µl Red Taq polymerase (Sigma), 13µl H_2O. KI: 1µl DNA, 1µl 17795 (5pmol), 1µl 32320 (5pmol), 1µl dNTP's, 2µl 10x Buffer, 1µl Red Taq polymerase (Sigma), 13µl H_2O. CRE: 1µl DNA, 1µl 4193 (5pmol), 1µl 24366 (5pmol), 1µl dNTP's, 2µl 10x Buffer, 1µl Red Taq polymerase (Sigma), 13µl H_2O. R:1µl DNA, 1µl 26512 (5pmol), 1µl 30545 (5pmol), 1µl 33787 (5pmol), 1µl dNTP's, 2µl 10x Buffer, 1µl Red Taq polymerase (Sigma), 12µl H_2O.	Ai32 (WT, KI) 94°C 3min **94°C 20sec** **61°C 30sec** **72°C 30sec 34x** 72°C 2min 10°C hold THCRE 94°C 3min **94°C 30sec** **51°C 30sec** **72°C 30sec 31x** 72°C 10min 12°C hold Recombined 94°C 10min **94°C 30sec** **60°C 45sec** **72°C 2min 34x** 72°C 10min 10°C hold

Table 2. **Master mix and PCR program for the respective mouse line.**

2.4. Electrophysiology and data analysis

Conventional whole-cell and perforated whole-cell patch-clamp (PWCPC) recordings were performed at room and under controlled temperature (30-35°C) with 3-5 MΩ pipettes (Lindau and Neher, 1988; Voets et al., 2000). An EPC-10 double patch-clamp amplifier was used together with the Patchmaster software package (HEKA Electronics) and an inverted microscope (Zeiss Axiovert 200). Capacitance measurements were performed using the software lock-in extension of Patchmaster. With a built-in sine wave stimulus, the membrane capacitance (Cm) of the cell was recorded by the lock-in Cm measurement. The holding potential was -70 mV. In the PWCPC technique, an antibiotic, in this case, amphotericin B, is added to the internal recording solution and forms small pores in the cell membrane without mechanically rupturing the cell membrane. Monovalent ions move through these pores allowing access to the cell interior (Rae et al., 1991; Ishibashi et al., 2012). Before an experiment, a stock solution of amphotericin B is prepared at a concentration of 50 mg/ml in

dimethyl sulfoxide (DMSO) and stored at -20°C (may be used for up to a week). On the day of the recording, 3 µl of amphotericin stock solution was added to 497 µl intracellular solution (ICS), giving a final concentration of 0.15 mg/ml. The solution was then vortexed (Bender & Hobein Vortex Genie 2) and sonicated in a water sonicator (Bandelin Sonorex digital 10 P) for 1 minute. Amphotericin B at the tip of the patch pipette may impair the initial GΩ seal formation; therefore, the pipette (GB150-8P) tip was pre-filled with an antibiotic - free solution by immersing the pipette tip for 20-30 s in amphotericin B-free ICS. The pipette was then backfilled with the corresponding ICS containing amphotericin B.

2.4.1. Solutions

Cs-Glutamate-based intracellular solution (Voltage ramp stimulation): H_2O,137 mM Glutamic acid (stock 290 mM) (Sigma), 9.45 mM HEPES (stock 20 mM) (Sigma), 0.1 mM EGTA (stock 4 mM) (Sigma/Millipore), 8 mM NaCl (stock 200 mM) (Merck), 1 mM $MgCl_2$ (stock 20 mM) (Sigma), 0.3 mM GTP-Na (stock 3 mM) (Sigma; CAS:36051317), 2 mM ATP-Mg (stock 20 mM) (Sigma; CAS:74804129).

Cs-Glutamate-based intracellular solution for "high" calcium-infusion and carbon fiber electrode internal solution (Amperometry): H_2O, 137 mM Glutamic acid (stock 290 mM) (Sigma), 9.45 mM HEPES (stock 20 mM) (Sigma), 0.1 mM EGTA (stock 2 mM) (Sigma/Millipore), 8 mM NaCl (stock 200 mM) (Merck), 1 mM $MgCl_2$ (stock 20 mM) (Sigma), 0.1 mM $CaCl_2$ (2 mM), 0.3 mM GTP-Na (stock 3 mM) (Sigma; CAS:36051317), 2 mM ATP-Mg (stock 20 mM) (Sigma; CAS:74804129); 3 M KCl (carbon fiber electrode).

K^+- Gluconate-based intracellular solution (Electric field and light stimulation): H_2O, 119.8 mM K-Gluconate (stock 27 0mM) (Sigma), 35.5 mM HEPES (stock 80 mM) (Sigma), 0.1 mM EGTA (stock 1 mM) (Sigma/Millipore), 8 mM NaCl (stock 200 mM) (Merck), 1 mM $MgCl_2$ (stock 20 mM) (Sigma), 0.3 mM GTP-Na (stock 3 mM) (Sigma; CAS:36051317), 2 mM ATP-Mg (stock 20 mM) (Sigma; CAS:74804129).

Extracellular solution Standard: 147 mM NaCl (Merck; CAS:7647145), 10 mM HEPES (Sigma; CAS:7365459), 10 mM Dextrose (Sigma; CAS:50997), 2.8 mM KCl (1M KCl) (Sigma/Millipore), 2 mM $CaCl_2$ (1 M $CaCl_2$) (Merck), 1 mM $MgCl_2$ (1 M $MgCl_2$) (Sigma) pH = 7.2 using NaOH, Osmolarity: 307-310 mOsm.

Extracellular solution with Ficoll PM70: 132 mM NaCl (Merck; CAS:7647145), 10 mM HEPES (Sigma; CAS:7365459), 10 mM Dextrose (Sigma; CAS:50997), 2.8 mM KCl (1 M KCl) (Sigma/Millipore), 2 mM $CaCl_2$ (1 M $CaCl_2$) (Merck), 1 mM $MgCl_2$ (1 M $MgCl_2$) (Sigma), 5% Ficoll PM70 (Sigma; CAS:72146895), pH = 7.2 using NaOH, Osmolarity: 300-305 mOsm.

Addition to the extracellular solution: In some experiments, 100 nM PMA [1 mM PMA stock solution was dissolved in DMSO (Sigma) 1:50 dilution (working stock solution), then working stock solution was dissolved 1:2000 in extracellular solution to achieve a final 100 nM PMA concentration] was used. Also, 5 mM caffeine (Sigma) in an external standard solution was tested. In voltage ramp experiments, 500 nM tetrodotoxin (TTX) (Sigma) in an extracellular solution was used.

Addition to the internal solution: For perforated patch-clamp 0.15 mg/ml [stock 50 mg/ml, diluted in DMSO (Sigma)] Amphotericin B (Merck/Millipore; CAS: 1397893) added in internal recording solution was utilized.

2.4.2. Amperometry

2.4.2.1. Carbon fiber electrodes

Glass capillaries (GB150-8P without filament) were stored in 80% ethanol. One glass capillary was taken, and a single carbon fiber was sucked into the capillary with an attached tube - the fiber was longer than the capillary. Pipettes were then pulled with a pipette puller, with the carbon fiber inside the glass capillary. The carbon fiber was cut before taking pipettes out of the puller. The carbon fiber inside the pipette should be intact. The electrode tip was then dipped into melted wax (StickyWax, KerrLab, Part No 00625) for 2-3 minutes and pulled out slowly. The electrode was transferred to a metal rack and baked in the oven at 100°C for 2-3h or overnight. One carbon fiber was used for 2-3 cells by cutting the tip between cells. Electrodes were backfilled with 3 M KCl before recording.

2.4.2.2. Amperometric measurements

One way to measure catecholamine release is to record the flux of catecholamines during their discharge through the fusion pore. Catecholamines oxidize at the surface of a carbon fiber electrode placed onto the cell membrane (Chow et al., 1992; Man et al., 2015; de Diego et al., 2020). Amperometric current spikes represent a release of catecholamines from a single vesicle. The formation of the initial fusion pore and subsequent initial release of molecules correspond to a "foot" signal, which often precedes the amperometric spike. In these experiments, we approached a single chromaffin cell with a 5 µm diameter carbon fiber electrode held at a positive potential (+700 mV) and recorded for 30 s to detect oxidized catecholamines. The cell was infused through a patch pipette containing solution with free Ca^{2+} of about 5 µm to trigger the fusion of secretory vesicles with the plasma membrane. In some experiments, the cell was stimulated with a series of depolarization steps [first six short (10ms) and four long depolarizations (100ms)], and simultaneously with amperometry recordings, a change in capacitance was measured (Voets et al., 1999; Man et al., 2015).

2.4.3. Light stimulation

Chromaffin cells expressing ChR2(H134R)-EYFP were recorded in current clamp configuration and stimulated with a blue LED (10 mW/ mm^2) for 5 s, either continuously at 4 Hz or discontinuously at 10 Hz (Fig. 2.1). Capacitance was measured in voltage clamp configuration just before and right after stimulation. The latency time when switching between the current clamp configuration and the voltage clamp configuration was 300-350 ms. Values at 0-0.001 s and 2.530-2.531 s of the membrane potential trace were taken for comparison between responsive and nonresponsive cells.

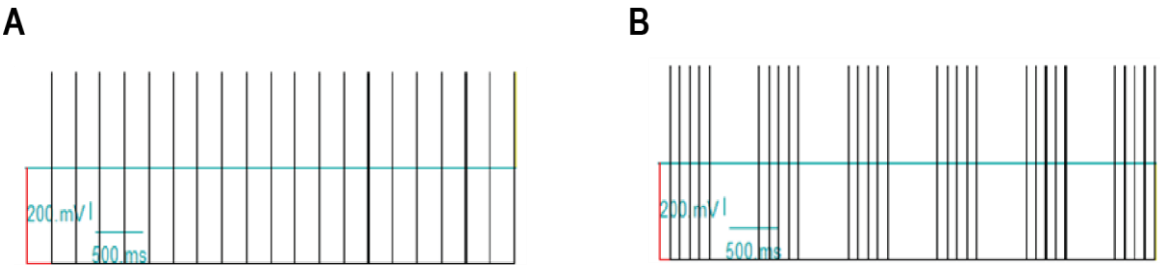

Figure 2. 1 **Stimulation with a blue LED for 5 s at** (A) **4 Hz and** (B) **10 Hz.**

2.4.4. Electric field stimulation

To test electric field stimulation the RC-46SLP bath chamber (Warner Instruments) was used. The cells were recorded in current clamp configuration and stimulated using a battery-operated stimulus isolator (Digitimer DS2A Isolated Voltage Stimulator) with varying stimulus strengths and stimulus lengths (Table 3). Multiple stimuli were used for testing different frequencies (i.e., 4, 10, 20, 30 Hz). A stimulus length of 1 ms and the stimulus strength 40 V, 20 V, and 10 V were applied for optimization of future experiments.

Stimulus length	Stimulus strength	Frequency
0.04 ms 0.08 ms 0.1 ms 0.3 ms 0.5 ms 1 ms 5 ms 10 ms	10 V 20 V 30 V 40 V 50 V 60 V 70 V 80 V 90 V	4 Hz 10 Hz 20 Hz 30 Hz

Table 3. **Different stimulus lengths, strengths and frequencies tested.**

To optimize the number of stimuli to be used, stimulation consisting of 10, 20 and 30 stimuli at 4 Hz or 10 Hz was applied. Recordings were acquired according to protocols (1)-(6).

(1) 5000 ms baseline + 10 stimuli at 4 Hz (i.e., 1 ms + 249 ms interval)
(2) 5000 ms baseline + 20 stimuli at 4 Hz

(3) 5000 ms baseline + 30 stimuli at 4 Hz
(4) 5000 ms baseline + 10 stimuli at 10 Hz (i.e., 1 ms + 99 ms interval)
(5) 5000 ms baseline + 20 stimuli at 10 Hz
(6) 5000 ms baseline + 30 stimuli at 10 Hz

To determine whether electric filed stimulation causes capacitance change I started using similar stimulation patterns as previously applied in the light stimulation. Therefore, capacitance was measured right before and after the stimulation.

In addition, stimulation consisting of four-burst with 5 stimuli at 10 Hz was also tested (Fig. 2.2). Capacitance recordings done right before and after stimulation were taken as a measure of DCV release. Recording protocol applied was 5000 ms baseline + 4 bursts at 10 Hz. The interval between bursts was 300 ms.

Figure 2. 2 **Electric filed stimulation with four-burst at 10 Hz.**

2.4.5. Voltage ramp stimulation

In voltage ramp experiments, voltage ramps were used to simulate action potentials (APs), with an initial rising phase of 12 ms, a second fast rising phase of 2 ms, and the third falling phase of 6 ms (Fig. 2.3 A). To test the AP frequency, 4 Hz, 10 Hz and 20 Hz were used. A series of AP-like waveforms, which were defined as “bursts” were also implemented. Four-burst (Fig. 2.3 B) and five-burst stimulations were tested. The frequency of AP-like waveforms in a burst was 10 Hz. Sequences of AP ramps were linked to the 1000 kHz sine wave, 35 mV (peak-to-peak).

Figure 2. 3 (A) **Single voltage ramp imitated by three ramps and** (B) **four-burst AP-like ramps stimulation.**

2.4.6. Data Analysis

2.4.6.1. Amperometry measurement

Kinetic parameters extracted from a secretory spike were analyzed in a macro (Mosharov and Sulzer, 2005) running under IgorPro software (Wavemetrics). First, currents were filtered using

a Gaussian filter with a cut-off set at 1 kHz. The spike detection threshold was set at 5 pA, and the foot detection threshold was set at 2 pA. Spike parameters analyzed, such as maximal current amplitude (I_{max}) and the spike charge (Q), give information about the amount of transmitter released from a single vesicle. Spike parameters such as half-width ($t_{1/2}$), 50-90% rise time (rise time$_{50-90}$), and 75-25% decay time (decay time$_{75-25}$) provide information on the kinetics of the vesicle fusion with the plasma membrane and were also analyzed. Finally, the "foot" signal corresponds to the diffusion of the vesicular transmitter through a slowly opening fusion pore before the complete fusion of the vesicle with the plasma membrane. Thus, pre-spike "foot" parameters, such as foot amplitude, foot charge, and foot duration, were also analyzed.

2.4.6.2. Capacitance measurement

Capacitance data were analyzed with the software IgorPro (WaveMetrics).

In electric field and optogenetic stimulation experiments, capacitance recordings done right before and after stimulation were taken as a measure of DCV release. Capacitance measurements were taken from the last 500 ms of the trace right before stimulation (Cm1), and of the first 500 ms from the capacitance trace after stimulation (Cm2). The total capacitance change (ΔCm) was calculated as the difference between Cm2 and Cm1.

In voltage ramp experiments, the last 100 ms from Cm1, and the first 100 ms from Cm2 were measured. The total capacitance change (ΔCm) was calculated in the same way, as the difference between Cm2 and Cm1. In burst stimulation (four-burst and five-burst, 4x 5 AP-like ramps and 5x 5 AP-like ramps respectively), the last 100 ms from Cm1, and the first 100 ms from Cm2, Cm3, Cm4, Cm5, Cm6 were measured. The total capacitance was the difference between Cm5 (four-burst) or Cm6 (five-burst) and Cm1. Total capacitance of each burst (ΔCm1,2,3,4,5) was calculated according to equations (7)-(11).

(7) ΔCm1=Cm2-Cm1 (four and five-burst stimulation)

(8) ΔCm2=Cm3-Cm2 (four and five-burst stimulation)

(9) ΔCm3=Cm4-Cm3 (four and five-burst stimulation)

(10) ΔCm4=Cm5-Cm4 (four and five-burst stimulation)

(11) ΔCm5=Cm6-Cm5 (five-burst stimulation)

To detect endocytosis after stimulation, the four-burst protocol was extended for 30 s (Fig. 2.4.). Capacitance (ΔCm5) was calculated as the difference between last 100 ms of the capacitance trace Cm6 and last burst Cm5 (difference between 33.7-33.8 s and 3.53-3.63 s).

Figure 2. 4 **Four-burst stimulation extended for 30 s.**

In experiments where cells were stimulated with six short (10 ms) and four long (100 ms) depolarizations, the last 270 ms from Cm1 were measured, and 270 ms from Cm2-Cm11. The total capacitance change was the difference between Cm11 and Cm1. Total capacitance change of each depolarization step (ΔCm1-10) was calculated according to equations (12)-(21).

(12) ΔCm1=Cm2-Cm1

(13) ΔCm2=Cm3-Cm2

(14) ΔCm3=Cm4-Cm3

(15) ΔCm4=Cm5-Cm4

(16) ΔCm5=Cm6-Cm5

(17) ΔCm6=Cm7-Cm6

(18) ΔCm7=Cm8-Cm7

(19) ΔCm8=Cm9-Cm8

(20) ΔCm9=Cm10-Cm9

(21) ΔCm10=Cm11-Cm10

2.4.6.3. Statistics

Data are expressed as mean ± standard error of the mean (SEM). Statistical analysis of data set was performed with GraphPad Prism software (version 9) (* when $p<0.05$; **when $p<0.01$; ***when $p<0.001$, and ****$p<0.0001$). First, Kolmogorov - Smirnov normality test and D´Agostino & Pearson omnibus normality test were used. For comparison of two conditions and if data were not normally distributed, a Mann-Whitney unpaired t-test was performed. A nonparametric Kruskal-Wallis test was executed to compare three or more conditions if data were not normally distributed. A one-way analysis of variance was used to compare three or more conditions when data were normally distributed.

2.5. High-pressure freezing, sample processing for electron microscopy and data analysis

Collaboration with Dr. Benjamin Cooper, Kirsten Weyand, Valentin Schwarze, and Sabine Beuermann

2.5.1. Chemicals and solutions

High-pressure freezing: Liquid nitrogen; extracellular solution (132 mM NaCl (Merck), 10 mM HEPES (Sigma), 10 mM Dextrose (Sigma), 2.8 mM KCl (1M KCl) (Sigma/Millipore), 2 mM $CaCl_2$ (1 M $CaCl_2$) (Merck), 1 mM $MgCl_2$ (1 M $MgCl_2$) (Sigma) with 5% Ficoll PM70 (Sigma); extracellular solution with 100 nM phorbol 12-myristat 13-acetat (PMA); extracellular solution with dimethyl sulfoxide (DMSO).

Automated freeze substitution (AFS): Liquid nitrogen; Tannic acid: 0.1% tannic acid in acetone; Osmium: 2% osmium tetroxide (OsO4) in acetone.

Plastic embedding: EPON: 2-Dodecenylsuccinic acid anhydride (DDSA), Glycid ether 100, Methylnadic anhydride (MNA), 2,4,6-Tris (dimethylaminomethyl)phenol (DMP-30).

Contrasting and fiducial marker: Uranyl acetate: 1 % uranyl acetate in water; Reynold's Lead Citrate Solution: 80 mM Lead (II) nitrate (N_2O_6Pb), 120 mM Sodium citrate dihydrate in decarbonated water; Protein A (ProtA) coupled to 10 nm gold particles; Lead (II) Nitrate.

2.5.2. High-pressure freezing (HPF)

Prior to the generation of chromaffin cell cultures, sapphire disks (Leica; #16770158) were coated with a carbon-coordinate system, baked for 12 hours at 120° C, and then treated with DMEM - high glucose (Sigma-Aldrich, D6546) containing 2% Cultrex Reduced Growth Factor Basement Membrane Extract (RGF BME). Chromaffin cell cultures from C57BL/6N wild-type P0 or P1 mice were then prepared on coated sapphire disks. Cultures were frozen two days after the culture with a Leica EM ICE high-pressure freezing device equipped with an electrical stimulation ("Zap-and-Freeze") module (Kusick et al., 2020). All steps were completed in the darkroom under dim red illumination provided by a Kindermann dukalux x-Tronic (type 2580; 640 nm) and a KL1500 LCD light source (Schott) supplied with a red insert filter (Schott; #562 44 287 3) (Imig et al., 2020). Experiments were performed at near-physiological temperatures. Thus, the heated EM ICE loading stage was set at 37° C, and the high-pressure freezing chamber was held at 35 °C. In preparation of the experiment, all electrical middleplates (Leica; #16771880) were functionally tested and then discharged via 5 min exposure to blue light (λ 460 nm), thereby preventing unintentional stimulation of chromaffin cells during loading of the HPF freezing assembly. Chromaffin cells were frozen in a sapphire 'sandwich' configuration comprising two sapphire disks (1 x cell-bearing; 1 x lid) separated by a mylar spacer ring (outer diameter, inner diameter, depth = 6 x 5 x 0.1 mm, Leica; #16771883). Sapphire disk sandwiches were loaded into a specialized middleplate (Leica; #16771880) equipped with capacitors and a photo-switch permitting light-evoked discharge of the capacitors via electrodes in contact with the cell-bearing sapphire disk sandwich. The loaded middleplate is itself sandwiched between two specialized half cylinders designed to permit light-evoked

discharge of the middleplate capacitors before channeling pressurized liquid nitrogen across the sapphire disc assembly during cryofixation.

Experimental variables included the stimulation protocol delivered to the cells and the pharmacological composition of the liquid media in which they were frozen. The electrical field (10 V cm^{-1}) stimulation protocol tested comprised the delivery of four 10 Hz trains, where each train comprised 5 x 1 ms light pulses and cells were frozen immediately after delivery of the last light pulse. Liquid media used for HPF was extracellular solution supplemented with 5% ficoll (PM70) and treated with either 100 nM PMA [1 mM PMA stock solution was first dissolved in DMSO 1:50 dilution (working stock solution), then working stock solution was dissolved 1:2000 in extracellular solution to achieve a final 100 nM PMA concentration], or DMSO alone (vehicle control). Final concentration of DMSO in PMA and DMSO only conditions was 0.05 vol/vol %. Four conditions were tested: 1) PMA treatment; PMA treatment with electrical field stimulation; 3) DMSO treatment with electrical field stimulation, and 4) DMSO treatment (vehicle control).

To assemble the sapphire sandwiches, cultured chromaffin cells were transferred from the incubator and submerged in a petri dish containing prewarmed extracellular solution supplemented with 5% Ficoll cryoprotectant. In a submerged state, a mylar spacer ring was positioned on top of the sapphire disk and this assembly was transiently removed from liquid and placed on Whatman filter paper. Promptly, a sapphire disk serving as the “lid” was dipped into the extracellular solution containing 100 nM PMA or DMSO and then placed on top to finalize the sapphire disk sandwich assembly. The sapphire disk assembly was loaded into the electrical stimulation middleplate (Leica; #16771880) to which 1 µl of Ficoll solution had been added to each electrode to promote electrical conductance. The sapphire disk assembly was covered with a rubber cover ring (500 µm; Leica; #16771884), excess liquid was removed with Whatman filter paper, and the electrical middle plate containing the sapphire disk assembly was transferred on top of a half cylinder (Leica; #16771846) on the heated stage of the HPF device.

Precisely 2 min following completion of the sapphire disk assembly and exposure of cells to either DMSO- or PMA-treated extracellular solution, the electrical stimulation-coupled high-pressure freezing was initiated to cryoimmobilize chromaffin cells in defined activity states. During HPF, an increase in atmospheric pressure operates simultaneously with rapid liquid nitrogen cooling of the sample to inhibit the volumetric expansion of water, suppressing ice crystal formation (Moor, 1987). High-pressure frozen samples were stored in liquid nitrogen until further processing by automated freeze-substitution.

2.5.3. Automated freeze substitution (AFS)

Frozen cultures were subjected to automated-freeze substitution (AFS) using a Leica AFS2 as previously described (Imig and Cooper, 2017; Rostaing et al., 2006). Briefly, high-pressure frozen samples were removed from liquid nitrogen storage, and the sapphire disk assembly was carefully separated with custom-made cryo-forceps. Next, the sapphire disk carrying the cells was placed into a sapphire disk revolver submerged in 0.1% tannic acid in anhydrous acetone for four days at −90 °C. The samples were then fixed with 2% osmium tetroxide in anhydrous acetone, with the temperature slowly ramping up over several days to 4°C. Finally, osmium tetroxide was washed from the samples in acetone, and the samples were brought to room temperature for epoxy resin (EPON) infiltration and embedding.

2.5.4. Epon infiltration, polymerization, and sapphire disk removal

For epoxy embedding, EPON resin was prepared following the Luft method (Luft, 1961) using two stock solutions [Stock solution A, 62 ml Glycid ether 100 and 100 ml DDSA; Stock Solution B, 100 ml Glycid ether 100 and 89 ml MNA]. Stock solutions A and B were mixed with a ratio of 3:7 prior to the addition of 1,48% DMP-30 catalyst. Samples were infiltrated in 2 ml Eppendorf tubes through graded concentrations of 30% (3 h), 60% (3 h), and 90% (overnight) dilutions of EPON in anhydrous acetone. The following day samples were incubated in freshly made 100 % EPON. Gelatin capsules were then filled with 100% EPON and a paper label identifying the cells was placed into the capsules. Next, the sapphire disks were transferred sample-up on a silicone mould filled with 100% EPON, and gelatine capsules were inverted on the silicone mould. Finally, samples placed on a silicone mould with gelatin capsules on top were put into the oven for polymerization at 60° C for 48 h. The next day, sapphire disks were removed from the plastic block, then trimmed using a Leica-EM TRIM (Imig & Cooper, 2017; Maus et al., 2020).

2.5.5. Ultramicrotomy and contrasting

For cutting the sections from EPON-embedded samples, a Leica EM UC7 ultramicrotome equipped with a diamond knife (Diatome, jumbo 45°) was utilized. Section series were collected onto formvar-filmed, carbon-coated, copper mesh grids in the following repetitive sequence: 60 nm sections were collected for 2D TEM; and 500 nm-thick sections for light microscopic analysis using histological stains.

For a light microscopic analyses to assess cell density, 500 nm-thick sections were dried on glass slides and contrasted with methylene blue Nissl stain. For 2D TEM, 60 nm-thick sections were post-contrasted in solutions containing 1% aqueous uranyl acetate for 30 minutes and then in 0.3% Reynold’s lead citrate for 2 minutes (Imig and Cooper, 2017; Maus et al., 2020).

2.5.6. Electron microscopy and data analyses

2.5.6.1. Two-dimensional image acquisition

For two-dimensional (2D) ultrastructural analyses of chromaffin cell morphology, electron micrographs were acquired using Talos F200C scanning/transmission electron microscope (Thermo Scientific) equipped with an X-FEG operating at 80 kV acceleration voltage and a CETA 16 MP sCMOS camera (Thermo Scientific). An overview of all visible cells on the grid was obtained at 84 x magnification using MAPS software (Thermo Scientific). After identifying chromaffin cells at low magnification, tiled montages of individual chromaffin cells were acquired 11,000 x magnification (3 x 3 tiles; tile format = 4096 x 4096 pixels; pixel spacing = 0.31 nm). Cells with clear membranes, with a nucleus and a few cells without a nucleus were included for analysis. The number of cells without a nucleus was: electric field stimulation and PMA 16 cells, PMA 17 cells, electric filed stimulation and DMSO 15 cells, no stimulation and DMSO 17 cells.

2.5.6.2. Data Analysis

For 2D ultrastructural analyses, electron micrographs were manually segmented using the IMOD package similar to the method described previously (Kremer et al., 1996; Imig and Cooper, 2017; Imig et al., 2020). Morphological parameters, such as cell perimeter, cell area, nucleus perimeter, nucleus area, cytoplasm area, endocytic event count, and endocytic event length, were quantified from 2D electron micrographs. All parameters were extracted using the imodinfo command and imported into Excel using a custom-written VBA macro. All analyses were performed blindly. When indicated, the number of endocytic events and event length were normalized to the cell perimeter.

2.5.6.3. Statistics

Data are expressed as mean ± standard error of the mean (SEM). Statistical analysis of data was performed with GraphPad Prism software (version 9) (* when $p<0.05$; **when $p<0.01$; *** when $p<0.001$, and ****$p<0.0001$). For the comparison of the two conditions, a Mann-Whitney unpaired t-test was performed. A nonparametric Kruskal-Wallis test was executed to compare three or more conditions.

3. Results

3.1. Testing Ficoll® PM 70 with capacitance and amperometric measurements

During HPF, cryoprotectants are mainly used. Cryoprotectants improve the freezing quality by increasing the sample's overall cooling rate (Dahl & Staehelin, 1989). For freezing experiments with adrenal slices, bovine serum albumin (BSA) cryoprotectant has been used (Man et al., 2015). The present study was planned to execute HPF and whole-cell patch clamp (WCPC) experiments under similar conditions. Therefore, to avoid cryoprotectant BSA, which is unsuitable for electrophysiological recordings, HPF was done without cryoprotectant. However, the first attempt to freeze cultured chromaffin cells without cryoprotectant led to frequent sample loss. Therefore, Ficoll® PM 70 was tested as a matrix to prevent the loss of cells. Ficoll is a polysaccharide polymer, very soluble and well suited for studying the permeability of membranes (Oliver 3rd et al., 1992; Venturoli & Rippe, 2005; Georgalis et al., 2012). Since there is some indication that Ficoll may change the properties of the fusion pore (Furuya et al., 1989), capacitance and amperometric measurements were done to establish whether the presence of Ficoll® PM 70 would affect DCV release kinetics in standard recording solution and solutions containing either 5% or 7,5 % Ficoll® PM 70.

Carbon-fiber amperometry and WCPC on cultured chromaffin cells were combined to assess whether Ficoll® PM 70 affects exocytosis. In these experiments, we approached an individual chromaffin cell with a 5 µm diameter carbon fiber electrode held at a positive potential (+700 mV) for the electrochemical detection of oxidized catecholamines. Additionally, a depolarization train consisting of six 10 ms followed by four 100 ms depolarization to 0 mV was applied to chromaffin cells from P0 or P1 wild-type animals. Stimulation with six short and four long depolarization steps is thought to deplete the IRP and RRP (Schonn et al., 2008; Voets et al., 1999). Capacitance and current traces obtained from chromaffin cells exposed to the standard extracellular solution and extracellular solutions containing 5% or 7,5% Ficoll® PM 70 are shown in Figure 3.1. Capacitance measurements after each depolarization were intact in the presence of Ficoll® PM 70 (Fig. 3.1 B, C). Accordingly, the total capacitance change (ΔCm) after the train was not affected by the presence of Ficoll® PM 70 (Fig. 3.1 A, C). The ionic membrane currents induced by each depolarization were also not affected by the presence of Ficoll® PM 70 (Fig. 3.1 D, E).

Simultaneously with capacitance measurements, amperometric measurements were done. Each current "spike" corresponds to the release of catecholamines from a single exocytotic vesicle fusion event (Fig. 3.2 A, B). Therefore, quantifications of spike parameters such as maximal current amplitude and the spike charge permit an estimation of the amount of transmitter released from a single vesicle. In addition, amperometric spike parameters such as

half-width, rise, and decay time provide information on the fusion event's kinetics and the transmitter's diffusion to the detection electrode. All spike parameters, duration, half-width, maximum amplitude, charge, rise time, and decay time, were unchanged (Fig 3.2 C-H). The amplitude, duration, and charge of the spike foot, which corresponds to the diffusion of the vesicular transmitter through a slowly opening fusion pore prior to full fusion of the vesicle with the plasma membrane, were also unchanged (Fig. 3.2 I-K).

To test further whether Ficoll® PM 70 affects the kinetics of single catecholamine release events, single spike amperometry was performed while infusing the cells with a solution with ~5 µM Ca^{2+} through the patch pipette to trigger vesicle fusion with the plasma membrane, without depolarization stimulation. These data also indicated that Ficoll® PM 70 did not affect kinetics parameters extracted from a secretory spike, nor do kinetics parameters extracted from a foot appear to be altered (Fig. 3.3).

The present study implies that Ficoll® PM 70 can be used for further electrophysiological and HPF experiments. Thus, for the future experiments 5% Ficoll® PM 70 was used.

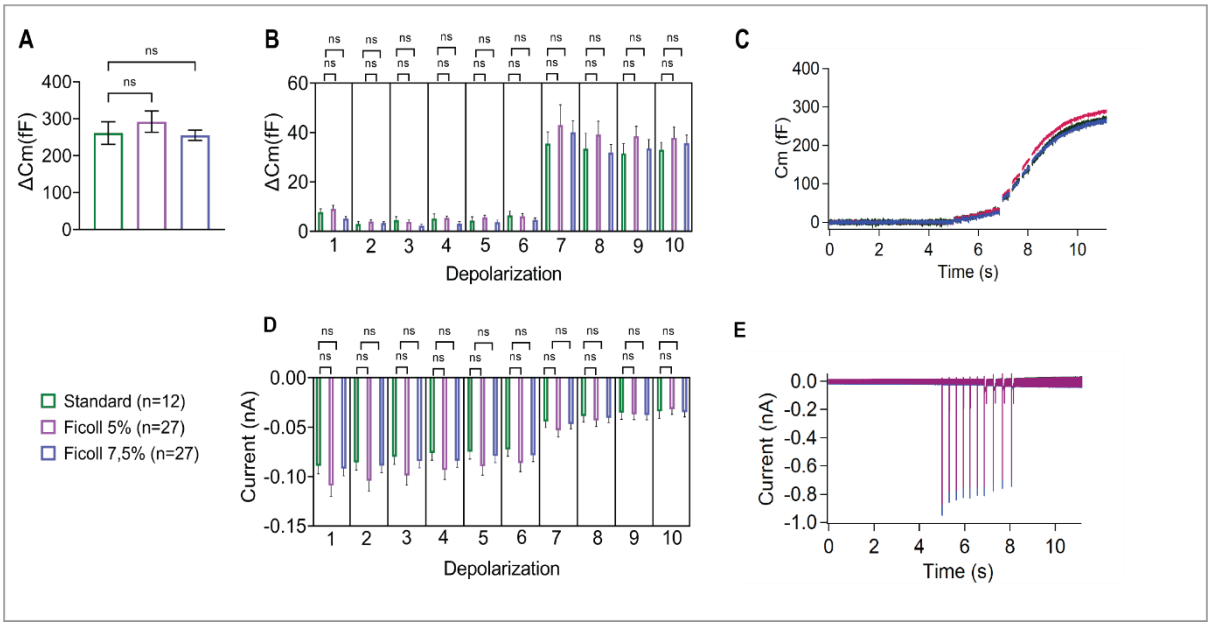

Figure 3. 1 **Ficoll® PM 70 does not impair DCV exocytosis after depolarization.** (A) Total ΔCm in standard (green), 5% Ficoll (purple), and 7,5% (blue) Ficoll® PM 70 solutions after depolarization was unchanged. (B) ΔCm after each depolarization step between solutions was unaltered. (C) Averaged capacitance traces during 6x10 ms and 4x100 ms depolarization to 0 mV. (D) No significant difference was found in the amplitude of the ionic currents after each depolarization step between solutions. (E) Averaged current traces after the depolarization stimulation.

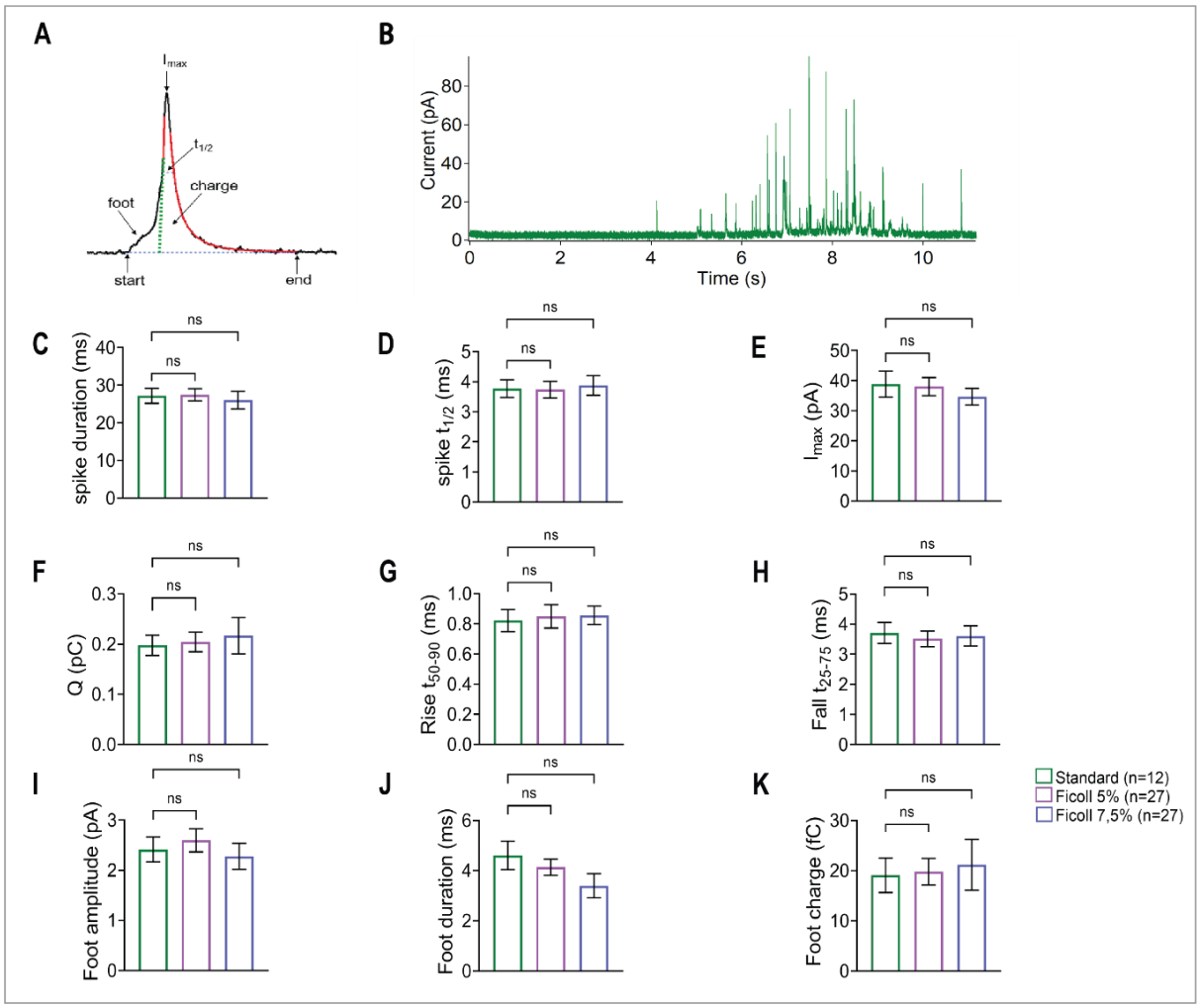

Figure 3. 2 **Ficoll ® PM 70 did not affect kinetics parameters extracted from a secretory spike and foot after depolarization**. (A) Illustration of a single amperometric spike and the parameters analyzed. (B) Amperometric recording of catecholamine-induced currents in standard solution during the stimulation. (C-H) Spike features such as duration, current, charge, half-width, and rise and fall time are not significantly altered by Ficoll ® PM 70. (I-K) Pre-spike (foot) features, which indicate the initial fusion pore opening, are not affected by Ficoll ® PM 70. Standard solution (green); 5% Ficoll (purple), and 7,5% (blue) Ficoll® PM 70 solutions.

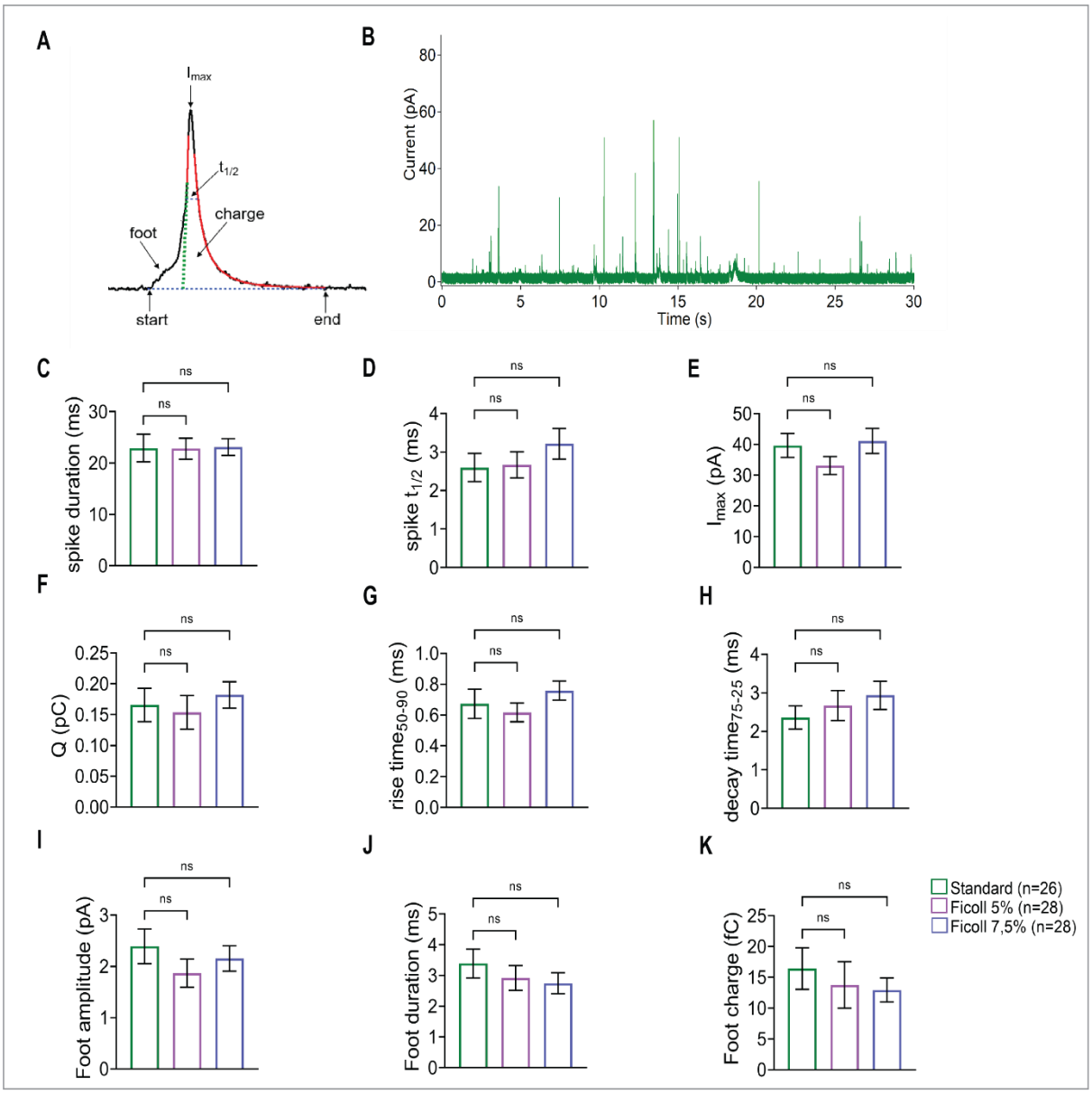

Figure 3. 3 **Ficoll ® PM 70 did not affect kinetics parameters extracted from a secretory spike and foot while infusing the cells with a solution with ~5 µM Ca^{2+} through the patch pipette to trigger vesicle fusion with the plasma membrane, without depolarization stimulation**. (A) Illustration of a single amperometric spike and the parameters analyzed. (B) Amperometric recording of catecholamine-induced currents in standard solution. (C-H) Spike features duration, current, charge, half-width, rise and fall time are not significantly altered by the presence of Ficoll ® PM 70. (I-K) Pre-spike (foot) features are not affected by Ficoll ® PM 70. Standard solution (green); 5% Ficoll (purple), and 7,5% (blue) Ficoll® PM 70 solutions.

3.2. Optogenetic stimulation of chromaffin cells

Next, to test whether chromaffin cells can be stimulated optogenetically, mice expressing a Cre-recombinase (Cre)-inducible version of channelrhodopsin-2-EYFP (ChR2-EYFP) (mouse line: Ai32) (Madisen et al., 2012) were crossed to mice expressing Cre under the control of the tyrosine hydroxylase promoter (TH-Cre; JaxLab B6. Cg-Tg(Th-cre)1Tmd/J). Conventional WCPC and perforated whole-cell patch-clamp (PWCPC) recordings were performed (Lindau & Neher, 1988; Voets et al., 2000; Rae et al., 1991; Ishibashi et al., 2012). Chromaffin cells

expressing ChR2-EYFP were recorded in the current clamp configuration and stimulated with a blue LED (10 mW/ mm^2) for 5 s, either continuously at 4 Hz or discontinuously, to induce bursts of action potentials at 10 Hz. In addition, cell capacitance was recorded in voltage clamp configuration right before and after stimulation (Fig. 3.4). Increasing cell capacitance after stimulation (ΔCm) indicates DCV fusion with the cell membrane. In both cases, using WCPC and PWCPC, action potentials (APs) were induced by optogenetic stimulation at 4 Hz and 10 Hz (Fig. 3.5 and Fig. 3.7). However, not all cells responded to stimulation (66/148). To examine whether the membrane potential of the cell can be the reason for the cell's unresponsiveness to the stimulation, the membrane potential of the cell that fired APs, the cell with AP failure, and of the cell that did not respond to stimulation was measured between 0-0.001 s and between 2.530-2.531 s. In the case of the WCPC, there is a significant difference in membrane potential between the cell that fired APs and the cell that did not respond to the light stimulation with both measurements (i.e., 0-0.001 s and 2.530-2.531 s) (Fig. 3.6). But there is no significant difference between the cells with fired APs and cells with AP failure. In the case of PWCPC, when membrane potential was measured between 0-0.001 s and 2.530 s, a significant difference between cells that fired APs, the cells with AP failure, and the cells that did not respond to the stimulation was shown (Fig. 3.8). These data indicate that optogenetic stimulation can be used to induce DCV release in chromaffin cells, and that cells that did not respond to the stimulation tended to have more positive membrane potentials.

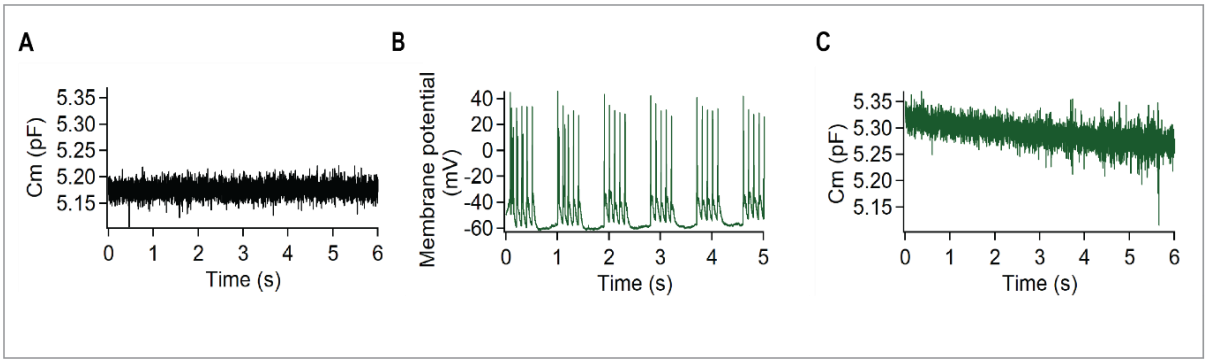

Figure 3. 4 **Exemplary capacitance recordings from chromaffin cell in response to optogenetic stimulation at 10 Hz applied in 6 bursts.** (A) Capacitance trace in voltage clamp configuration before stimulation. (B) Sample trace of action potentials induced by optogenetic stimulation at 10 Hz in current clamp configuration. (C) Capacitance trace in voltage clamp configuration after stimulation.

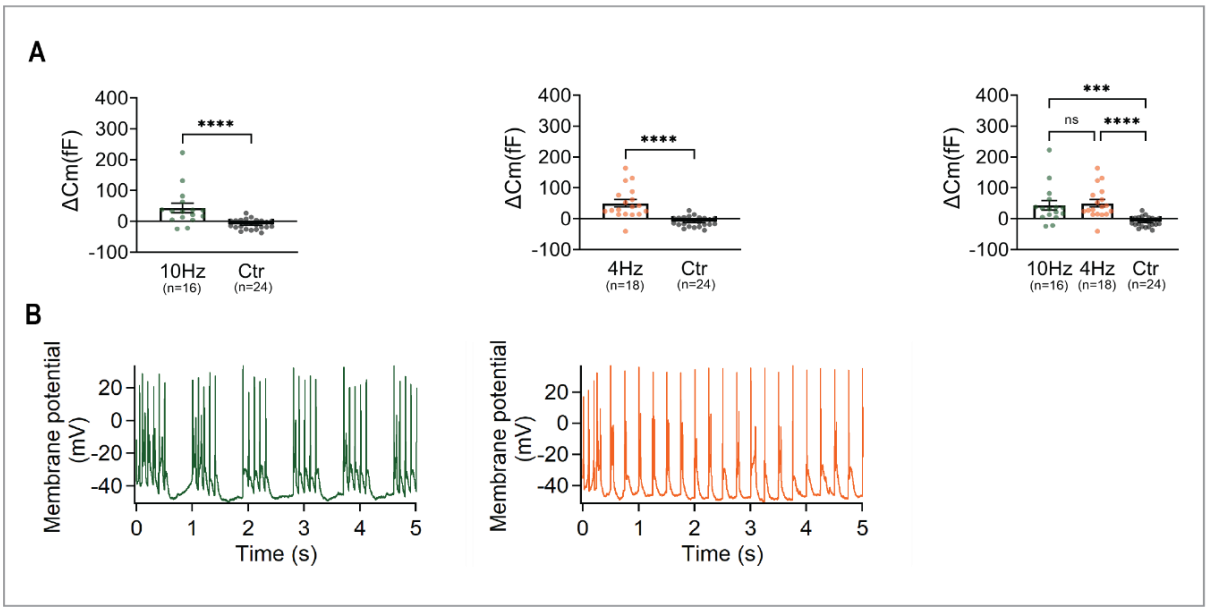

Figure 3. 5 **Increase in cell capacitance after optogenetic stimulation measured with WCPC**. (A) Increase in cell capacitance after stimulation compared to unstimulated cells indicates that DCV release was induced by the optogenetic stimulation. (B) Sample traces of action potentials induced by optogenetic stimulation at 10 Hz (green) and 4 Hz (orange). Stimulation at 10 Hz was applied in 6 bursts.
Error bars indicate mean ± SEM; ***p < 0.001; ****p < 0.0001.

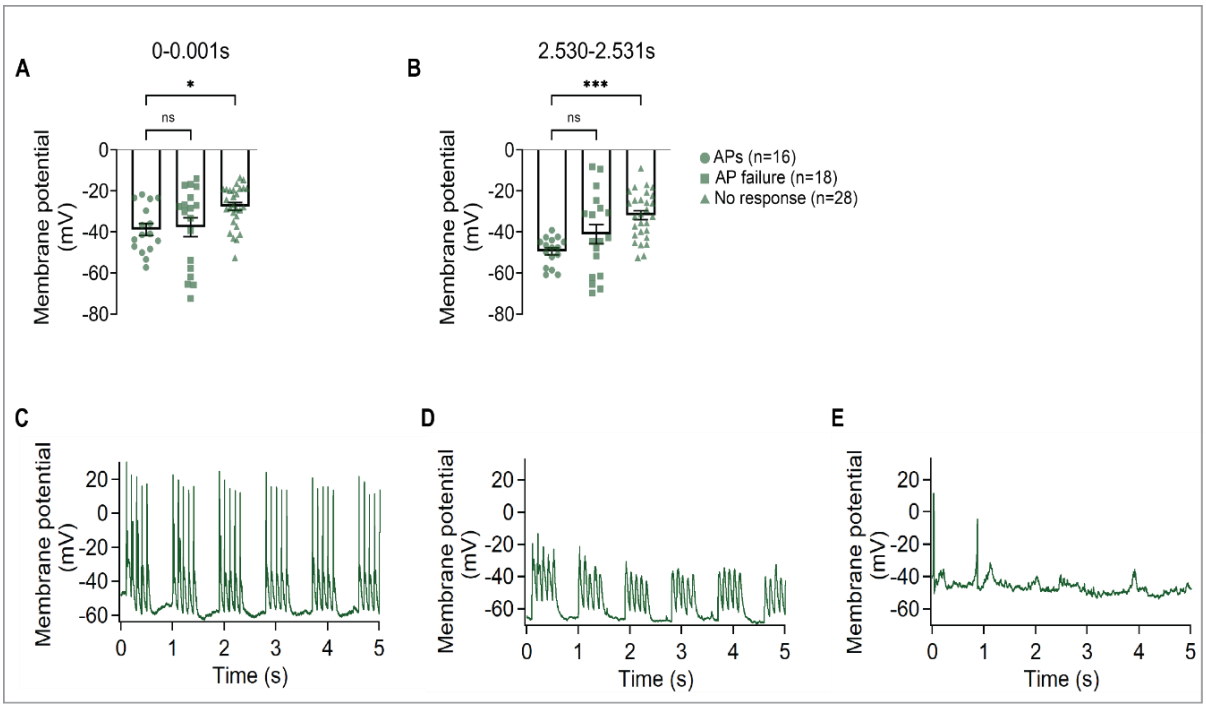

Figure 3. 6 **Membrane potential during the optogenetic stimulation may cause cell unresponsiveness during WCPC.** (A,B) The membrane potential of the cell that fired APs, the cell with AP failure, and the nonresponsive cell measured between (A) 0-0.001 s and (B) 2.530-2.531 s after the stimulation at 10 Hz. (C) Sample trace of action potentials induced by optogenetic stimulation at 10 Hz. (D) Sample trace with AP failure after optogenetic stimulation. (E) Sampe trace with no response after the stimulation.
Error bars indicate mean ± SEM; *p < 0.05; ***p <0.001

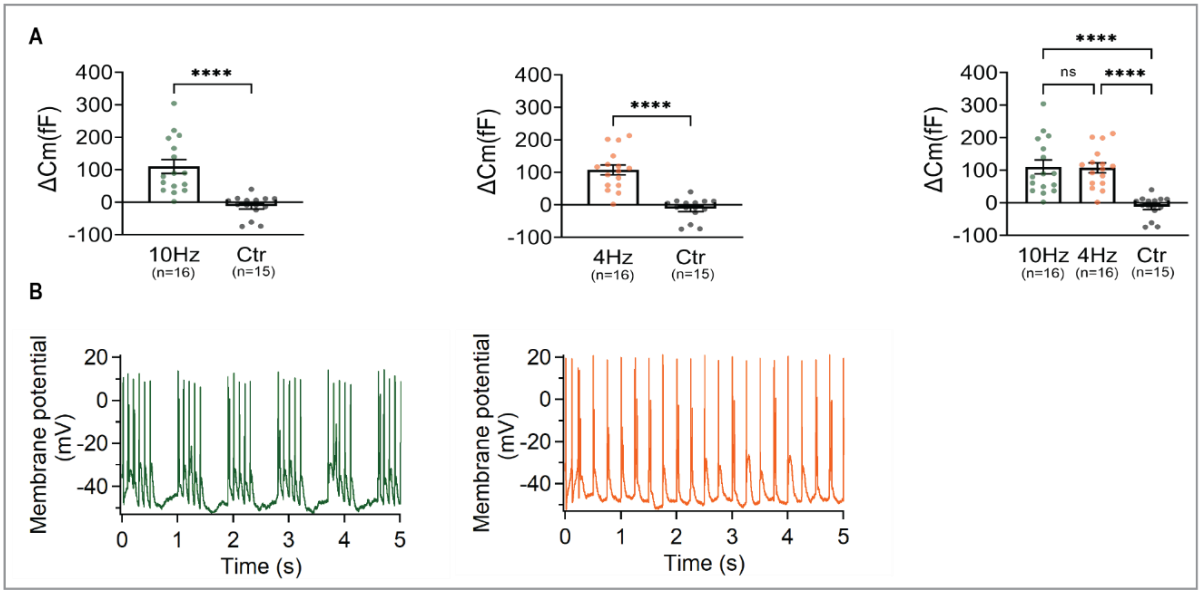

Figure 3. 7 **Increase in cell capacitance after optogenetic stimulation measured with PWCPC.** (A) Increase in cell capacitance after stimulation compared to unstimulated cells demonstrates that DCV release was induced by the optogenetic stimulation performed with perforated patch-clamp. (B) Sample traces of action potentials induced by optogenetic stimulation at 10 Hz (green) and 4 Hz (orange). Stimulation at 10 Hz was applied in 6 bursts. Error bars indicate mean ± SEM; ****p < 0.0001.

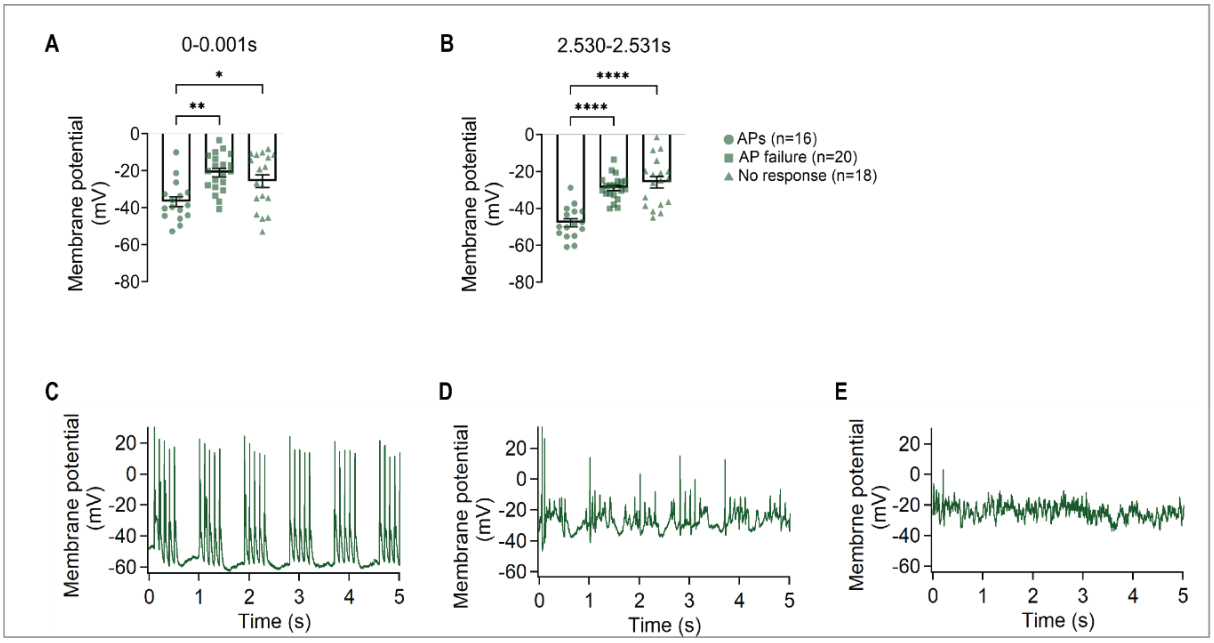

Figure 3. 8 **Membrane potential during the optogenetic stimulation may cause cell unresponsiveness during the PWCPC.** (A,B) The membrane potential of the cell that fired APs, the cell with AP failure, and the nonresponsive cell measured between (A) 0-0.001 s and (B) 2.530-2.531 s after the stimulation at 10 Hz. (C) Sample trace of action potentials induced by optogenetic stimulation at 10 Hz. (D) Sample trace with AP failure, and (E) no response after the stimulation.
Error bars indicate mean ± SEM; *p < 0.05; **p < 0.01; ****p < 0.0001.

3.3. Electric field stimulation of chromaffin cells

Since expression of ChR2-EYFP was only detected in a subset of cells, and not all cells responded to optogenetic stimulation, we tested electric field stimulation. It was assessed how much capacitance change could be detected with a different type of stimulation. In these experiments, minimal and maximum stimulation (in current clamp configuration, Fig. 3.9) was used to determine which electric field stimulation is sufficient for the cell to respond with action potentials and trigger vesicle release. Cell responsiveness was tested with a single stimulus, varying stimulus strength, and length. A stimulus length of 1 ms and the stimulus strength of 40 V, 20 V, and 10 V were applied to optimize future experiments. Then, multiple stimuli were used for testing different frequencies (i.e., 4, 10, 20, 30 Hz). To optimize the number of stimuli to be used, 10, 20, and 30 stimuli at 4 Hz or 10 Hz were applied. Capacitance recordings (in voltage clamp configuration) done right before and after stimulation were taken as a measure of DCV release (Fig. 3.9).

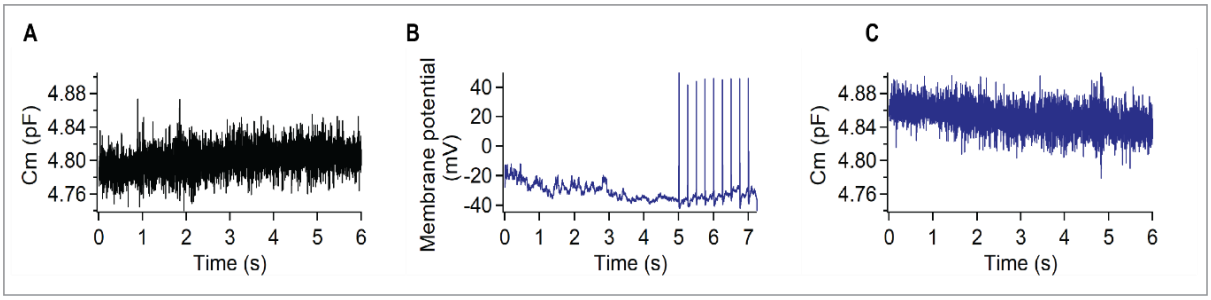

Figure 3. 9 **Exemplary capacitance recordings from chromaffin cell in response to electric field stimulation at 4 Hz**. (A) Capacitance trace in voltage clamp configuration before stimulation. (B) Sample trace of action potentials induced by electric field stimulation at 4 Hz in current clamp configuration. (C) Capacitance trace in voltage clamp configuration after stimulation.

The cellular effect of exposure to an electric field with differing stimulus lengths and stimulation intensities showed that a stimulus of 40 V and a stimulus length of 1 ms was suitable. Therefore, stimulation consisting of 10, 20, and 30 stimuli at 4 Hz or 10 Hz was applied. Cells exposed to, 10, 20, and 30 stimuli at 4 Hz showed greater capacitance change than unstimulated control cells (Fig. 3.10 A, B, C). Thus, field stimulation can be used in chromaffin cells to induce DCV release. There was no statistical difference in the capacitance change induced by the different number of stimuli (Fig. 3.10 D).

In contrast to this, although stimulation with 10, 20, and 30 stimuli at 10 Hz induced action potentials (Fig. 3.11 E, F, G) and a change in capacitance, there was no statistically significant difference compared to the unstimulated group (Fig. 3.11 A, B, C).

Considering that chromaffin cells tend to fire in bursts, the burst protocol was the next stimulation pattern to be examined (Fig. 3.12).

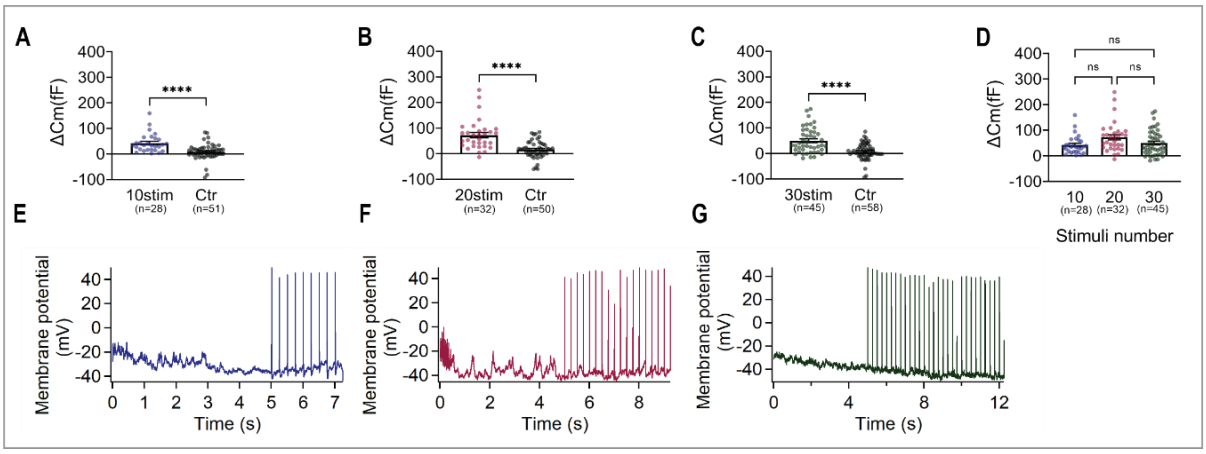

Figure 3. 10 **Establishing field stimulation patterns for chromaffin cells at 4 Hz.** (A-C) Increase in cell capacitance after (A) 10 stimuli, (B) 20 stimuli and (C) 30 stimuli at 4 Hz with 40 V. (D) No significant difference was observed between different number of stimuli. (E-G) Sample traces of action potentials induced by electric field stimulation at 4 Hz with (E) 10, (F) 20 and (G) 30 stimuli.
Error bars indicate mean ± SEM; ****p < 0.0001.

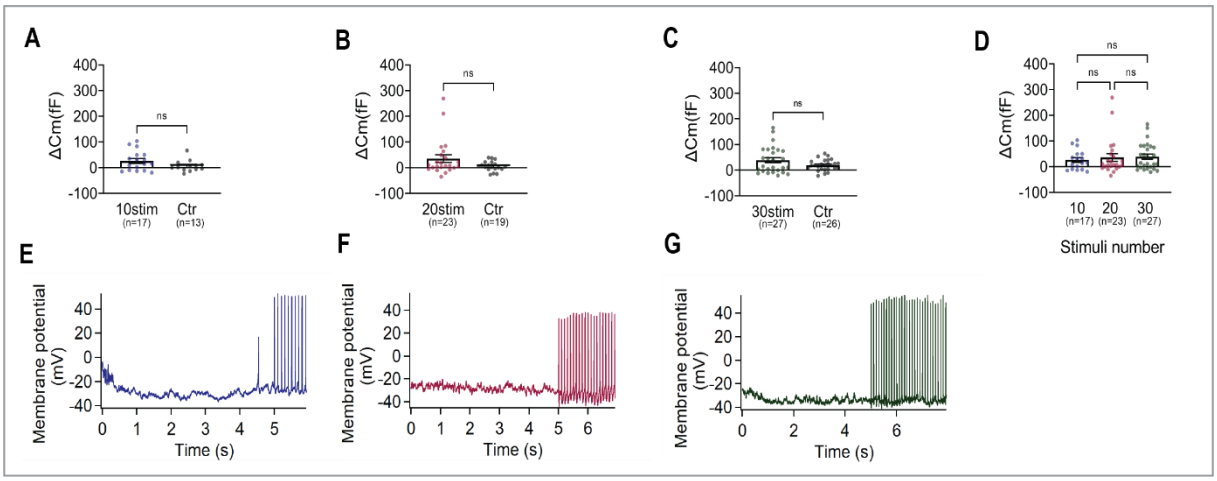

Figure 3. 11 **Establishing field stimulation patterns for chromaffin cells at 10 Hz**. (A-C) Capacitance change after (A) 10 stimuli, (B) 20 stimuli and (C) 30 stimuli at 10 Hz with 40 V. (D) No significant difference was observed between different number of stimuli. (E-G) Sample traces of action potentials induced by electric field stimulation at 10 Hz with (E) 10, (F) 20 and (G) 30 stimuli.

3.4. Electric field stimulation of chromaffin cells with four-burst of five stimuli at 10 Hz

Next, stimulation consisting of four-burst of five stimuli at 10 Hz was tested with electric field stimulation using PWCPC. Since HPF experiments must be done in the presence of Ficoll® PM 70, the stimulation has been tested in a standard extracellular solution and a solution containing 5% Ficoll® PM 70 with 20 V. Data showed that four-burst stimulation caused an increase in capacitance in both cases (Fig. 3.12 A, C). Thus, four-burst of five stimuli at 10 Hz with electric filed stimulation can be used in a chromaffin cell to induce DCV release (Fig. 3.12).

Moreover, to test whether there is a more significant increase in cell capacitance upon electric field stimulation with an additional brief application of phorbol 12-myristate 13-acetate (PMA)

or caffeine, the cells were exposed for the 30 s to 100 nM PMA (Fig. 3.13) or 5 mM caffeine in standard solution (Fig. 3.14). For these experiments, stimulus strength was lowerd to 10 V. No significant difference was observed in treated cells compared to the control condition (Fig. 3.13. and Fig. 3.14). Additionally, there is no correlation between the number of APs and capacitance change between treated (PMA or caffeine) or not treated cells (Fig. 3.13 C and Fig. 3.14 C). Also, no correlation between capacitance change and the number of PMA or caffeine exposures was found (Fig. 3.13 D and Fig. 3.14 D). Although the four-burst protocol with electric field stimulation triggers the release of a sufficient number of vesicles that can be visualized by electron microscopy without additional treatment, PMA was used for HPF experiments since the effect of PMA was seen in the ramp protocols maximizing the DCV release (Fig. 3.17).

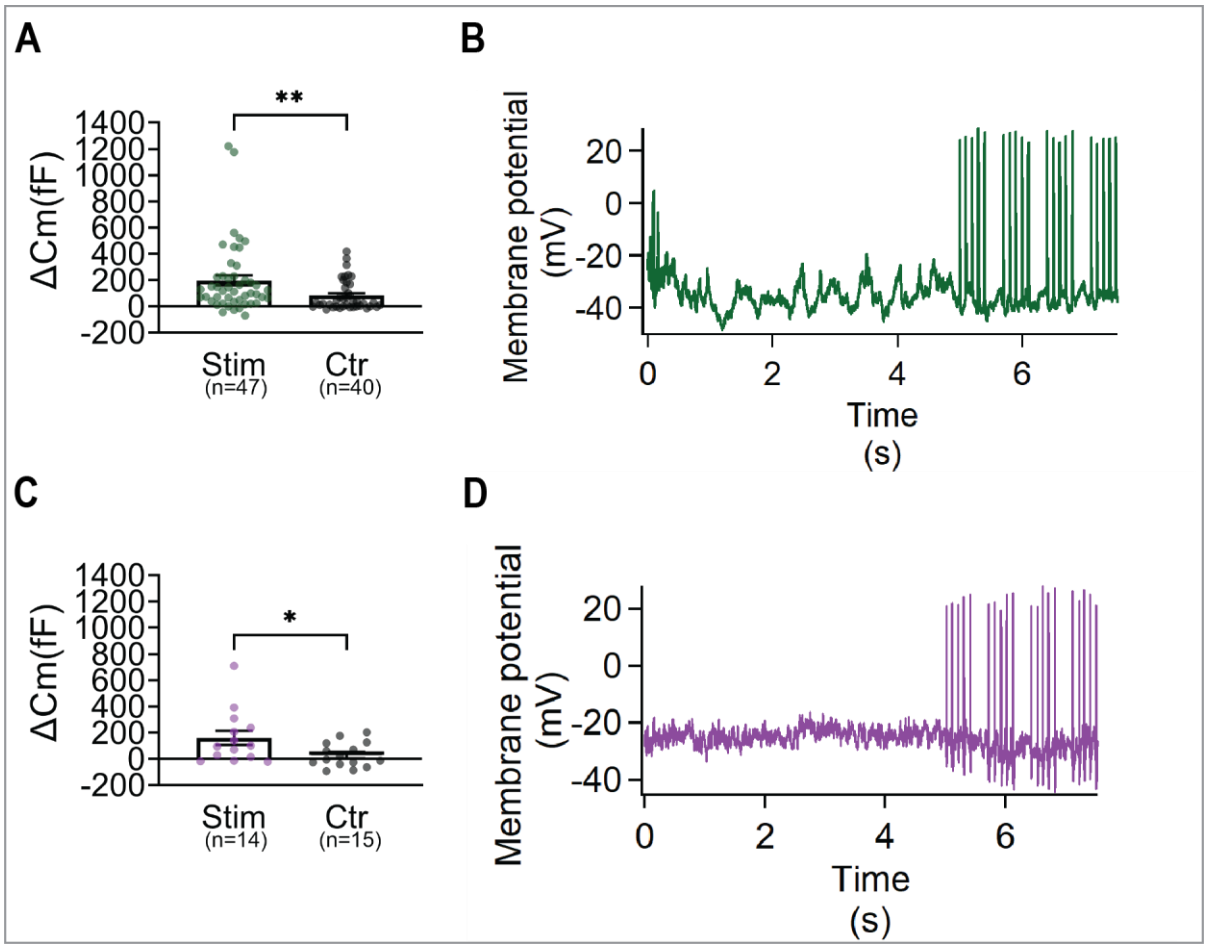

Figure 3. 12 **Increase in cell capacitance after four-burst at 10 Hz with electric field stimulation with 20 V.** (A) Capacitance change after the stimulation in standard solution. (B) Induced action potentials after the stimulation in standard solution. (C) Capacitance change after the stimulation in 5% Ficoll ® PM 70. (D) Induced action potentials after the stimulation in 5% Ficoll ® PM 70.
Error bars indicate mean ± SEM; *p < 0.05; **p < 0.01.

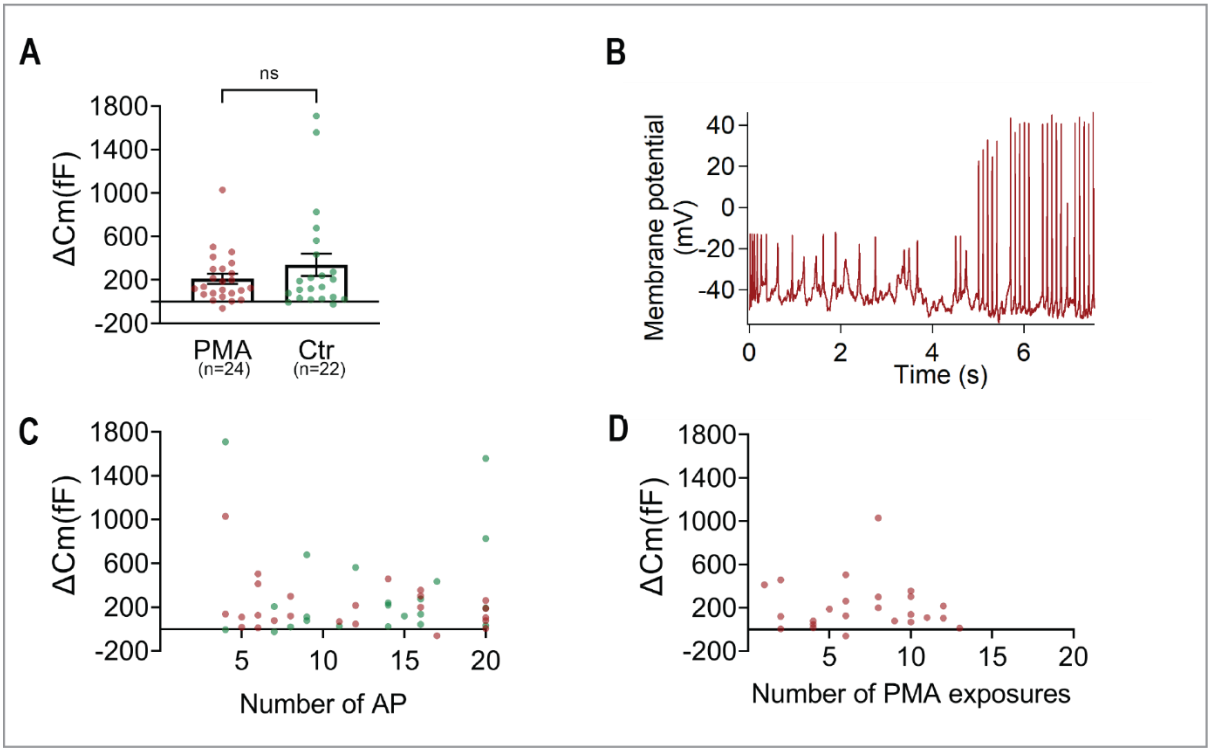

Figure 3. 13 **No significant difference between treated and not treated cells with 100 nM PMA upon four-burst at 10 Hz with electric field stimulation with 10 V.** (A) Change in cell capacitance between the 100 nM PMA and control condition. (B) Induced action potentials after the stimulation and PMA treatment. (C) No correlation between capacitance change and number of APs in the PMA (red) and control group (green). (D) No correlation between capacitance change and number of PMA exposures.

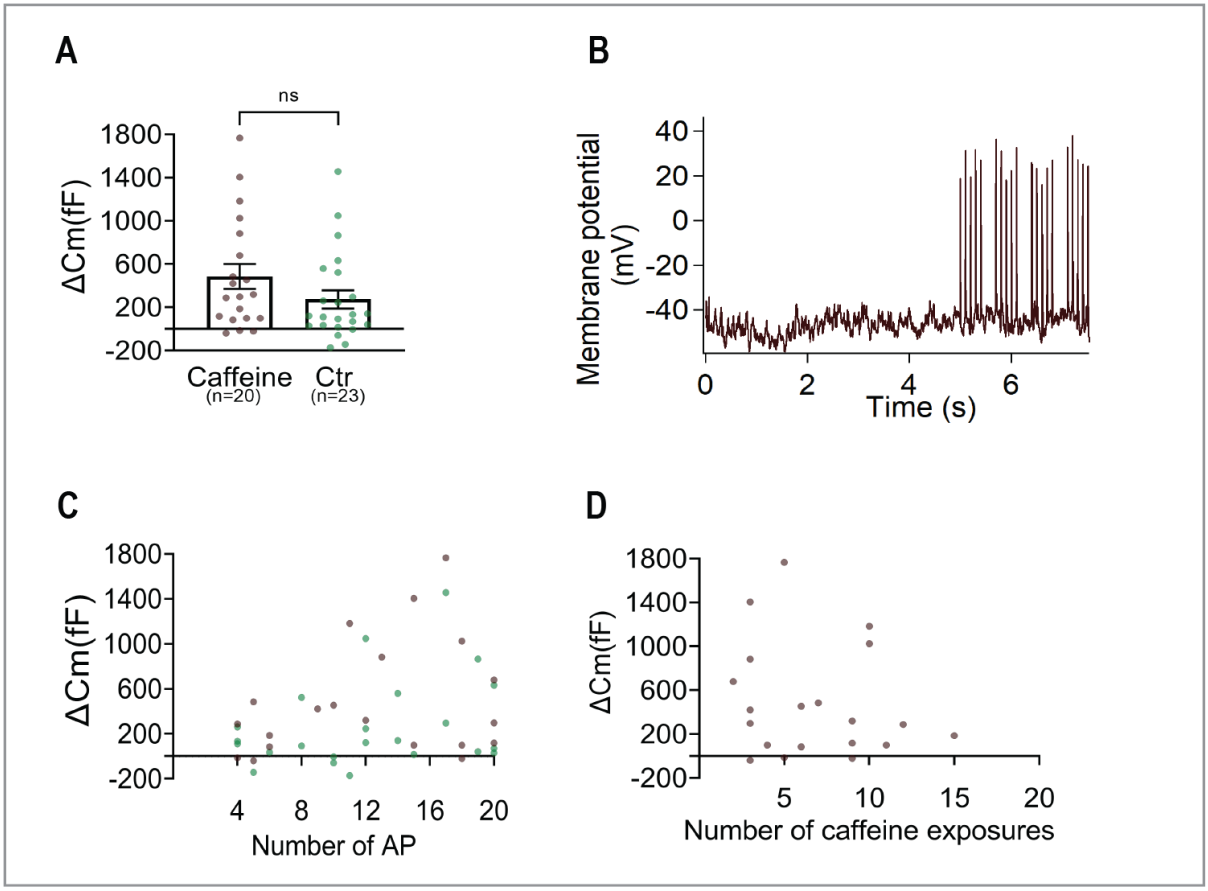

Figure 3. 14 **No significant difference between treated and not treated cells with 5 mM caffeine upon four-burst at 10 Hz with electric field stimulation with 10 V.** (A) Change in cell capacitance between the 5 mM caffeine and control condition. (B) Induced action potentials after the stimulation and caffeine treatment. (C) No correlation between capacitance change and number of APs in the caffeine (brown) and control group (green). (D) No correlation between capacitance change and number of caffeine exposures.

3.5. Voltage ramp stimulation of chromaffin cells

Using membrane capacitance measurements, we tested the effect of voltage ramp stimulation on DCV release. To increase the precision and consistency of the stimulation paradigm and address the current-clamp to voltage-clamp transition issue, we used ramp protocols. This method can provide a better understanding of the capacitance change and assure that the cell is consistently stimulated, which electrical field stimulation might not always ensure. In addition, voltage ramp stimulation allows for more controlled stimulation of individual cells than field stimulation and circumvents the time delay problem for analyzing capacitance change immediately after the stimulation. Different frequencies and a different number of stimuli were tested (4 Hz with 5 and 10 stimuli; 10 Hz with 5, 10, and 20 stimuli; 5 Burst at 10 Hz; 20 Hz with 5 and 10 stimuli). Average capacitance traces after voltage ramp stimulation are shown in Figure 3.15. By changing the number of stimuli (AP-like ramps) in the train, we determined the correlation between secretion and the number of AP-like ramps in a stimulus train. The amount of secretion was increased with the number of ramps in the train. However, no further increase in cell capacitance was detected when the AP frequency was increased from 4 to 20 Hz (Fig.

3.15 Q). We noticed a similar outcome with electric field stimulation, with no significant effect with stimulation at higher frequencies (Fig. 3.11). Stimulation with five-burst at 10 Hz (5 x 5 AP-like ramps) caused a robust increase in membrane capacitance (Fig. 3.15 L, R). To track endocytosis after stimulation, we extended the capacitance recordings to 30 s and performed recordings at near physiological temperature (33°C-34°C). Since the five-burst protocol seemed to give the most significant capacitance change, we decided to use this stimulation pattern for HPF. Due to software limitations at the Leica HPF device, we subsequently shortened the protocol to four bursts after confirming that four-burst at 10 Hz (4 x 5 AP-like ramps) also caused a sufficient capacitance change (Fig. 3.16.). Again, the solution containing 5% Ficoll ® PM 70 was tested. The decreasing post-stimulus Cm trace reflects endocytosis (Fig. 3.16).

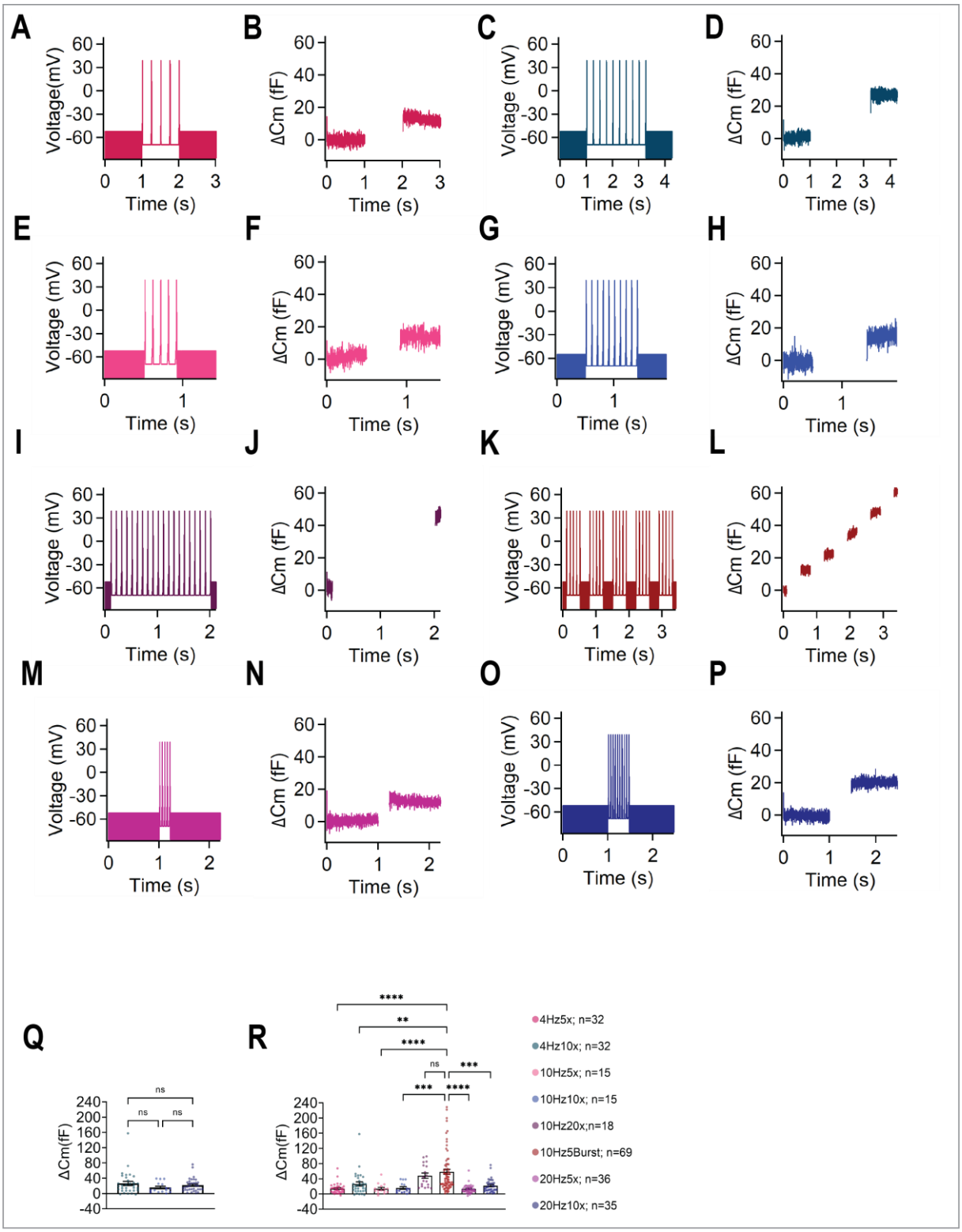

Figure 3. 15 **Establishing voltage ramp stimulation patterns for chromaffin cells.** (A) Voltage ramp stimulation at 4 Hz 5 x AP-like ramps and (B) average capacitance trace (n=32). (C) Voltage ramp stimulation at 4 Hz 10 x AP-like ramps and (D) average capacitance trace (n=32). (E) Voltage ramp stimulation at 10 Hz 5 x AP-like ramps and (F) average capacitance trace (n=15). (G) Voltage ramp stimulation at 10 Hz 10 x AP-like ramps (H) and average capacitance trace (n=15). (I) Voltage ramp stimulation at 10 Hz 20 x AP-like ramps and (J) average capacitance trace (n=18). (K) Voltage ramp stimulation with 5 x 5 AP-like ramps at 10 Hz and (L) average capacitance trace (n=69). (M) Voltage ramp stimulation at 20 Hz 5 x AP-like ramps and (N) average capacitance trace (n=36). (O) Voltage ramp stimulation at 20 Hz 10 x AP-like ramps and (P) average capacitance trace (n=35). (Q) Capacitance change after

4 Hz 10 x, 10 Hz 10 x, and 20 Hz 10 x AP-like ramps stimulation. No further increase in cell capacitance with increased AP frequency. (R) Robust increase in membrane capacitance after 5 x 5 AP-like ramps at 10 Hz.
Error bars indicate mean ± SEM; *p < 0.05; ***p < 0.001; ****p < 0.0001.

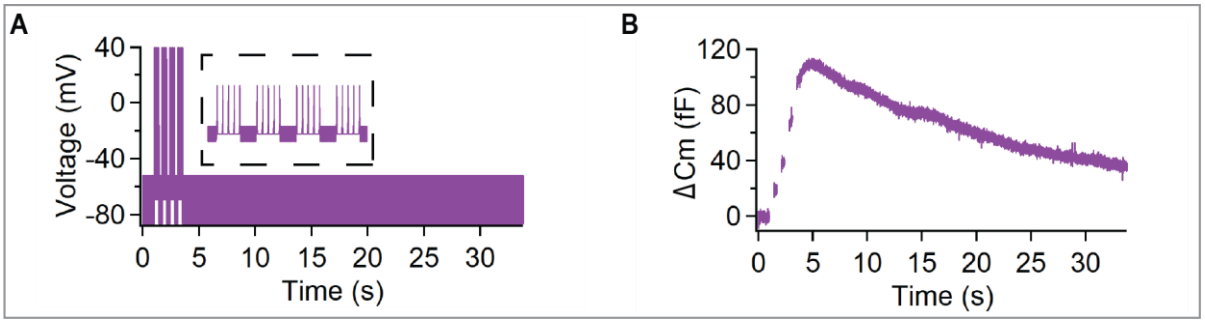

Figure 3. 16 **Robust increase in membrane capacitance after four-burst at 10Hz.** (A) Example four-burst at 10Hz stimulation with 30 s extension. The inset in the voltage-ramp stimulation panel shows an enlargement of the four-burst. (B) Average capacitance traces (n=60) during the four-burst at 10Hz in the presence of Ficoll ® PM 70.

3.6. Voltage ramp stimulation of chromaffin cells with four-burst of five stimuli at 10 Hz in the presence of PMA

Stimulation with voltage ramps that mimic AP waveform (AP-like ramps) provides better control for stimulating indivdual cells and also circumvents the temporal delay introduced by switching between voltage and current clamp. Since the application of PMA did not show the expected effect in electric field stimulation, we wanted to confirm that the application time is sufficient, so we tested PMA application in combination with voltage ramp stimulation. The cells were exposed for the 30 s to 100 nM PMA prior to four-burst at 10 Hz. Phorbol ester has previously been shown to enhance neuronal transmitter release (Pocotte et al., 1985; Rhee et al., 2002; Lou et al., 2008) and depolarization-induced exocytosis in chromaffin cells (Gillis et al., 1996). Our data with four-burst voltage ramp stimulation are consistent with the earlier findings. The application of PMA caused a significant change in capacitance compared to the control condition (Fig. 3.17 A, B, D), confirming that our application time was sufficient. The lack of PMA effect seen in field stimulation experiments may therfore be due to the presumably greater variability and lack of control over membrane potential inherent in the field stimulation paradigm. As with electric field stimulation, with voltage ramp stimulation, there is also no correlation between the change in capacitance and the number of PMA exposures (Fig. 3.17 C).

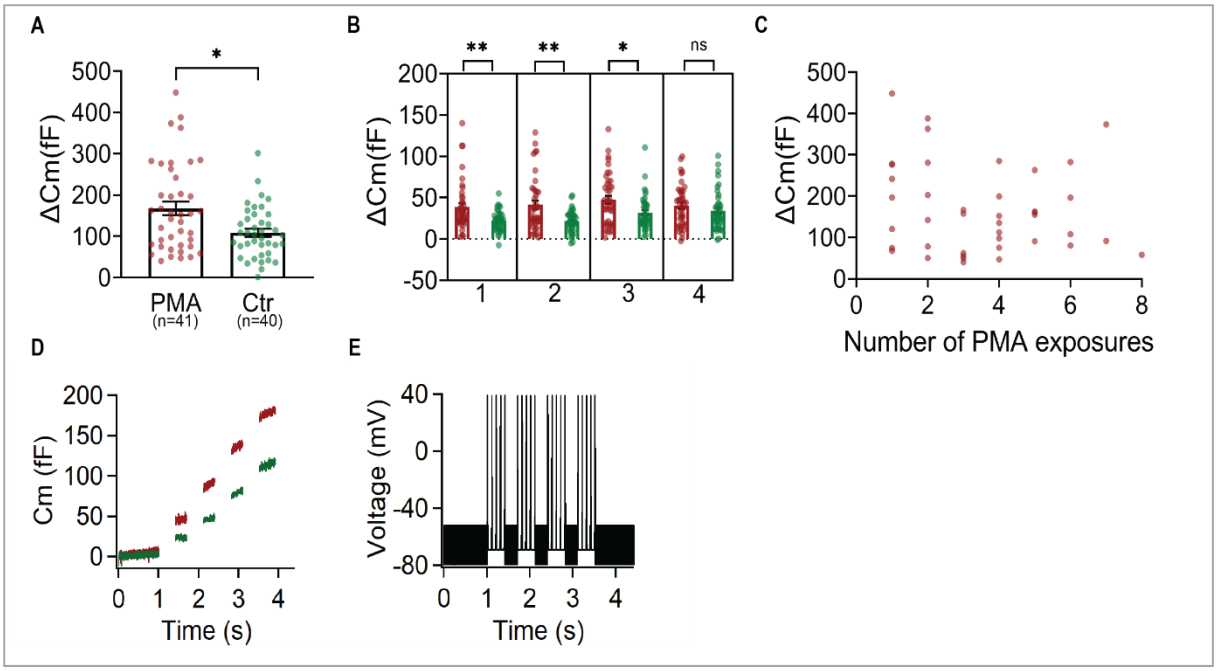

Figure 3. 17 **The phorbol ester PMA induces an increase in four-burst voltage ramp-evoked exocytosis in the chromaffin cell.** (A) ΔCm after the four-burst ramp stimulation. (B) ΔCm elicited by individual bursts. (C) No correlation between capacitance change and the number of PMA exposures. (D) Average capacitance traces with (red) and without (green) PMA during stimulation. (E) Example four short-burst at 10Hz stimulation.
Error bars indicate mean ± SEM; *p < 0.05; **p < 0.01.

3.7. Ultrastructural organization of cultured mouse chromaffin cells

According to the electrophysiological results of this research, Ficoll® PM 70 can be used for HPF and electrophysiological experiments, which led to the adoption of Ficoll® PM 70 in subsequent studies. Therefore, a solution of 5% Ficoll® PM 70 was chosen for the study because it prevented cell loss and reliably preserved cellular ultrastructure.

High-pressure frozen and freeze-substituted cultured chromaffin cells produced exceptional ultrastructural preservation utilizing the experimental strategy adopted in the current investigation. In well-preserved samples, observations from EM images revealed the presence of DCVs, the endoplasmic reticulum, Golgi membranes, endosomes, mitochondria, multi-vesicular bodies, vesicle contet release and endocytic events. Clathrin molecules covering endocytic events confirmed that the applied freeze substitution process preserved cytoskeletal components in cells frozen with our method. In addition, rapid HPF fixation of cultured chromaffin cells could capture dynamic cellular events in four conditions from two cultures: 1) electrical field stimulation with PMA treatment (Fig. 3.18 A-F); 2) PMA treatment (Fig. 3.18 G-L); 3) electric field stimulation with DMSO treatment (Fig. 3.18 M-R), and 4) no stimulation with DMSO treatment (vehicle control) (Fig. 3.18 S-X). The electric field (10 V cm^{-1}) stimulation protocol tested comprised the delivery of four 10 Hz trains, where each train comprised 5 x 1 ms light pulses, the interval between trains was 300 ms. Cells were frozen immediately after delivery of the last light pulse. Liquid media used for HPF was extracellular solution

supplemented with 5% Ficoll® PM 70 and treated with either 100 nM PMA (diluted in DMSO), or DMSO alone (vehicle control). Final concentration of DMSO in PMA- and DMSO-only conditions was 0.05 vol/vol %.

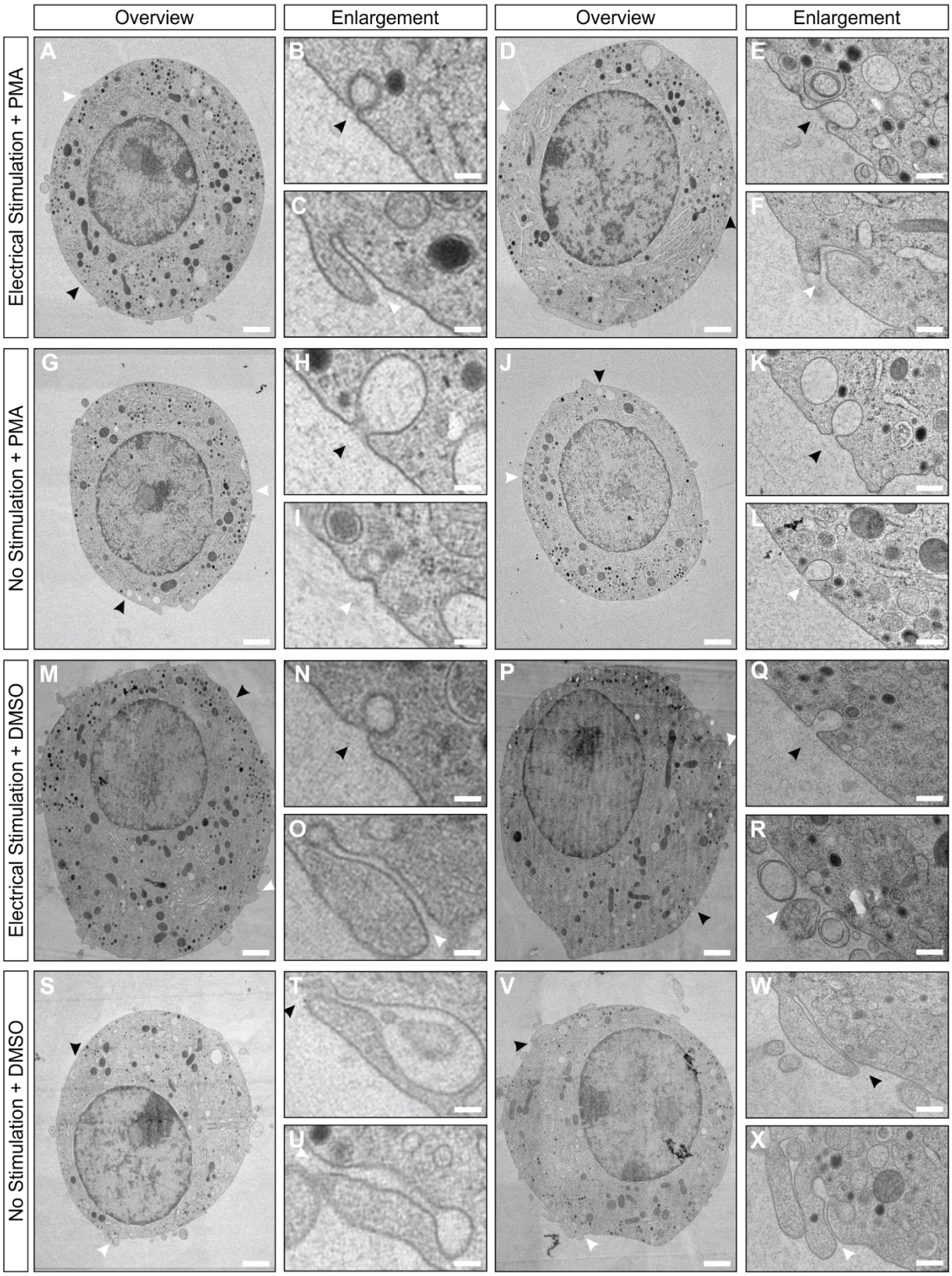

Figure 3. 18 **Ultrastructural organization of cultured mouse chromaffin cells.** (A-F) Transmission electron micrographs of cultured chromaffin cells and prominent membrane invaginations captured after electric field stimulation and PMA treatment. (G-L) Transmission

electron micrographs of cultured chromaffin cells and prominent membrane invaginations captured after PMA treatment. (M-R) Transmission electron micrographs of cultured chromaffin cells and prominent membrane invaginations captured after electric field stimulation and DMSO treatment. (S-X) Transmission electron micrographs of cultured chromaffin cells and prominent membrane invaginations captured with no stimulation and DMSO (control). (C, F, O, U, W, X) Tubular structures depicted in different conditions. (B, N) Well-preserved clathrin-coated membrane Ω-shaped profiles. (E, H, K, L, Q, R, T) Prominent non-coated Ω-shaped events. (I) Small endocytic event.
Scale bars: (A, G ,M, S, D, J, P, V), 1 μm; (B, C, H, I, N, O, T, U) 100 nm, (E, F, K, L, Q, R, W, X), 250 nm.

3.8. Mapping the spatial organization of membrane invaginations in mouse chromaffin cell cultures

Recent studies (Zhao et al., 2016; Shin et al., 2018) demonstrated DCV fusion pore dynamics in neuroendocrine chromaffin cells, paving the way for the detection of endocytic membrane dynamics. Endocytic membrane dynamics were newly demonstrated in live neuroendocrine chromaffin cells (Shin et al., 2021).

In our study, we observed robust signs of membrane invaginations, which showed a range of various shapes and dimensions, ranging from small to large and bulk-like. We focused on analyzing invaginations that were part of the cell membrane and those that exhibited a clathrin coat. Most exhibited a prominent electron-dense coat, verifying that clathrin coats are preserved and noticeable with our experimental setup. Employing electric field stimulation in combination with PMA treatment enabled us to visualize not only clathrin-coated membrane retrieval, but also for the first-time prominent vesicle content release (Fig. 3.19). Our experimental approach showed remarkable ultrastructural preservation. Thus, stimulation conducted in this study induced complete vesicle merging with the plasma membrane, which may indicate that the main exocytosis-endocytosis type triggered with electric field stimulation in combination with PMA may be full-collapse mode (Zenisek et al., 2002; Llobet et al., 2003; Fulop T. et al., 2005). Additionally, we classified the invaginations into four categories based on their shape and coating, including Ω-shaped events with a captured vesicle content release (Fig 3.20 A), Ω-shaped coated events (Fig 3.20 B), Ω-shaped non-coated large events (Fig 3.20 C), and tubular structures (Fig. 3.20 D).

We highlight the importance of understanding endocytic membrane dynamics in neuroendocrine chromaffin cells and the value of advanced imaging techniques for investigating these processes. Our findings add to this body of knowledge and provide insight into the various forms membrane invaginations can take in these cells.

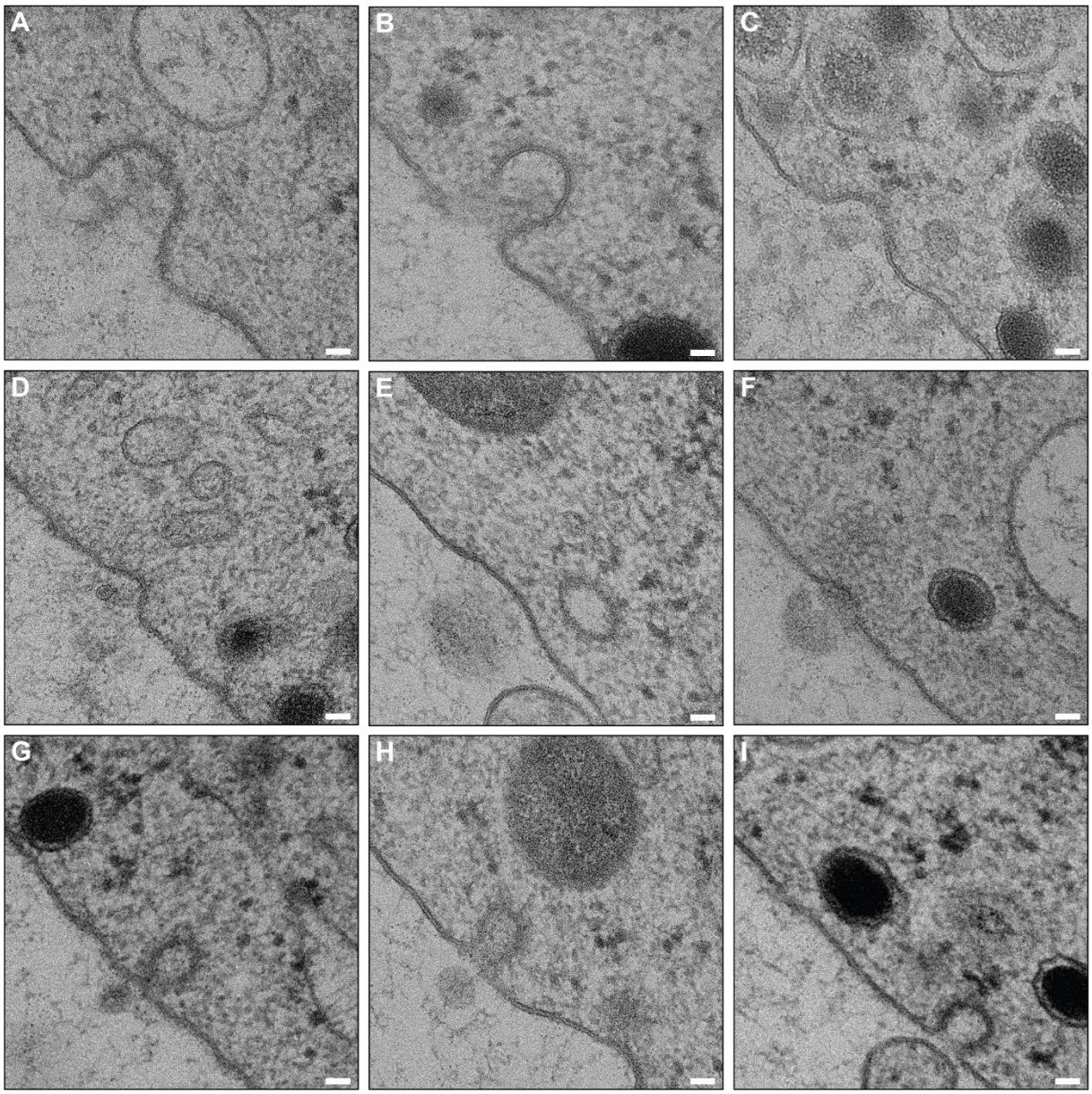

Figure 3. 19 **Transmission electron micrographs of prominent vesicle content release and clathrin-coated membrane retrieval captured after electric field stimulation and PMA treatment.** (A-D) Ω-shaped profiles filled with vesicle content. (E,F) Full-collapse fusion. (G-I) Clatrhin-coated membrane retrieval.
Scale bars: (A-I), 100 nm.

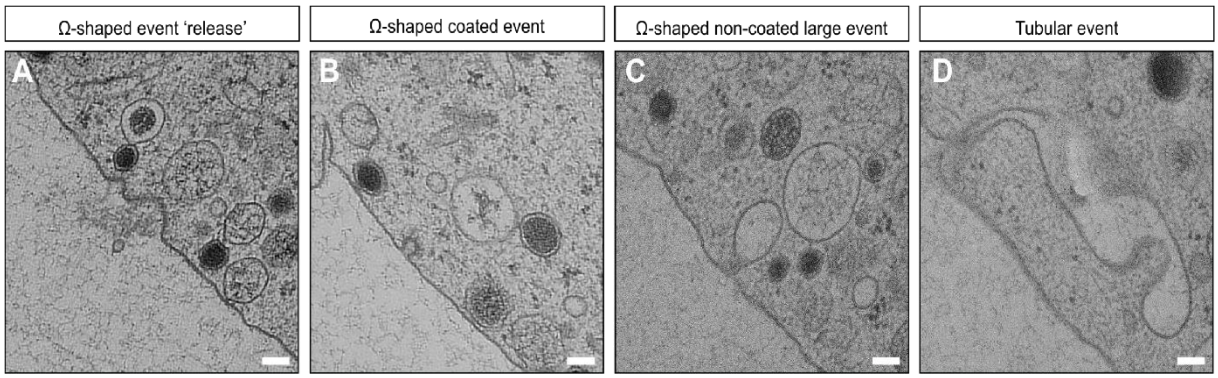

Figure 3. 20 **Transmission electron micrographs of membrane invagination categories captured after electric field stimulation and PMA treatment**. (A) Ω-shaped event depicting

the release of vesicle content. (B) Ω-shaped coated event. (C) Ω-shaped non-coated event. (D) Tubular structure. Scale bars: (A-D), 100 nm.

3.9. 2D-EM analysis of chromaffin cell morphology

Ultrastructural parameters of wild-type chromaffin cells were analyzed in electron micrographs from 60 nm ultrathin sections. Cells from two separate cultures were analyzed to rule out any prominent differences in cell morphology that might be due to culture related variation. We measured the entire cell perimeter and the length of membrane invaginations. The number and length of all events were normalized to the cell's perimeter. Quantifying the events contiguous with the membrane, we observed a significant decrease in the number of all events in cells stimulated with electric field stimulation and DMSO treatment (Fig. 3.21 A). We also noticed a reduction in all event lengths in cells exposed to electric field stimulation and DMSO compared to other conditions (Fig. 3.21 B). We first subdivided events into Ω-shaped and tubular events (Fig 3.21 C-F). We then detected differences in Ω-shaped events in cells stimulated with electric field stimulation and DMSO treatment compared to PMA-only cells (Fig. 3.21 C). No significant difference was seen in the length of Ω-shaped events between conditions (Fig. 3.21 D). Additionally, we saw a significant decrease in the number of tubular events in cells stimulated with electric field stimulation and DMSO (Fig. 3.21 E) and a reduction in tubular event lengths in cells exposed to electric field stimulation and DMSO compared to other conditions (Fig. 3.21 F). A possible explanation for this finding may be that electric field stimulation with four-burst (with total stimulation time 2520 ms) is too intense and prolonged, and bulk endocytosis may occur more rapidly than we were able to observe, or our stimulation pattern may trigger another endocytic mode. Then, we went on and subdivided Ω-shaped events into Ω-shaped events with the release of vesicle content, Ω-shaped coated events, and Ω-shaped non-coated large events (Fig. 3.19). We found a significantly smaller number of Ω-shaped coated events in cells stimulated with electric filed stimulation and DMSO treatment compared to PMA-only cells (Fig 3.22 A). According to current research, exposure to PMA may activate slower endocytosis processes such as clathrin-mediated endocytosis (Mykoniatis et al., 2010; Wu & Wu 2007). On the other hand, a strong electric field may cause the full collapse mode, in which the vesicles entirely collapse into the plasma membrane, and the Ω-shaped profiles are lost (Zenisek et al., 2002; Llobet et al., 2003; Fulop et al., 2005). However, no significant difference was detected in the number of vesicle content release and Ω-shaped non-coated large events between conditions (Fig 3.22 B, C). A possible explanation is that these events are rare and challenging to capture, considering the total number of DCVs calculated to fuse per cell from capacitance analyses and the fact that the EM analysis of cells in ultrathin sections surveys only a small fraction (Fig. 3.24 F, G) of the total cell surface.

We furthermore quantified individual event length per condition without normalization to the cell perimeter. To not overlook any events, the first bin was set to 100 nm (Fig 3.23 A-E). In

each group the most frequently observed events were ≈ 200-300 nm Ω-shaped coated events. Events of ≈ 100-500 nm mainly represent Ω-shaped coated events, and events of ≈ 600-3100 nm represent Ω-shaped non-coated large and elongated tubular events. The exact number of events is listed in Table 4. A cumulative plot of the data also revealed a tendency toward a reduced number of events in cells after electric field stimulation and DMSO represented (Fig 3.23 E). However, we did not observe a significant difference in individual event lengths between conditions (Fig 3.23 F).

We also measured the perimeter of the cells and did not see any notable difference in cell perimeter between conditions (Fig. 3.24 A-E). Knowing the cell perimeter, we estimated the average cell surface area (in μm^2) using the $4\pi r^2$ equation. Next, the average cell surface area (in pF) per condition was calculated assuming 1 $\mu F/cm^2$ (Man et al., 2015). Again, we did not notice a major difference in cell surface areas between conditions (Fig. 3.24 F). Finally, the average cell surface area of the 60 nm section (in pF) was also estimated with no significant difference between conditions (Fig. 3.24 G).

The percentage of cells with and without events per condition was also calculated. From all cells exposed to electric field stimulation and PMA, 74.6% had events, and 25.4% did not have events; from all cells exposed to PMA, 86.0% had events, and 14.0% did not have events; from all cells exposed to electric field stimulation and DMSO 55.0% had events, and 45.0% did not have events; for the non-stimulated and DMSO cells 83.1% had events, and 16.9% had no events. Thus, chromaffin cells that were exposed to electric field stimulation and DMSO tended to have a smaller number of events.

One of the hypotheses is that the four-burst electric field stimulation was quite intense, causing all or most of the release-ready vesicles to be released. With the lack of the Ω-shaped profiles, our stimulation may activate an exocytotic form of total collapse in which vesicles collapse entirely into the plasma membrane surface. Our observations (Fig.3.19 E, F) suggest that vesicle content release may match the previously described full-collapse event (Harata et al., 2006; Ceridono et al., 2011). The second explanation is that the chromaffin cells might not respond equally well to four bursts of electric field stimulation in all stimulated samples, which prevented events from forming. One of the explanations for detecting Ω-shaped profiles in non-stimulated and DMSO treated cells could mean that these profiles are formed before stimulation, which mediate different endocytic modes or will serve as a base for compound fusion and multivesicular release (Shin et al., 2021; Ge et al., 2022). Furthermore, these events, especially the ones involving small clathrin-coated structures, may also indicate a type of endocytosis that is constitutively active, even in the absence of any external stimulation.

Condition	Ω-shaped small events	Ω-shaped non-coated large and tubular events
Electrical stimulation + PMA	5 events of ≈ 100 nm, 92 events of ≈ 200 nm, 60 events of ≈ 300 nm, 15 events of ≈ 400 nm, 10 events of ≈ 500 nm.	8 events of ≈ 600 nm, 7 events of ≈ 700 nm, 6 events of ≈ 800 nm, 2 events of ≈ 900 nm, 6 events of ≈ 1000 nm, 3 events of ≈ 1100, 2 events of ≈ 1200 nm, 1 event of ≈ 1300 nm, 2 events of ≈ 1500 nm, 2 events of ≈ 1800 nm, 1 event of ≈ 1900 nm, 1 event of ≈ 2000 nm, 1 event of ≈ 2100 nm, 2 events of ≈ 2200 nm.
No stimulation + PMA	11 events of ≈ 100 nm, 83 events of ≈ 200 nm, 55 events of ≈ 300 nm, 22 events of ≈ 400 nm, 7 events of ≈ 500 nm.	8 events of ≈ 600 nm, 3 events of ≈ 700 nm , 4 events of ≈ 800 nm, 4 events of ≈ 900 nm, 4 events of ≈ 1000 nm, 3 events of ≈ 1100, 5 events of ≈ 1200 nm, 2 events of ≈ 1300 nm, 4 events of ≈ 1400 nm, 1 event of ≈ 1500 nm, 1 event of ≈ 1700 nm, 1 event of ≈ 1900 nm, 1 event of ≈ 2100 nm, 3 events of ≈ 2200 nm, 1 event of ≈ 2800 nm.
Electrical stimulation + DMSO	2 events of ≈ 100 nm, 40 events of ≈ 200 nm, 54 events of ≈ 300 nm, 19 events of ≈ 400 nm, 5 events of ≈ 500 nm.	6 events of ≈ 600 nm, 2 events of ≈ 700 nm, 3 events of ≈ 800 nm, 1 event of ≈ 900 nm, 1 event of ≈ 1000 nm, 2 events of ≈ 1100, 2 events of ≈ 1400 nm, 1 event of ≈ 1500 nm, 1 event of ≈ 1700 nm.
No stimulation + DMSO	3 events of ≈ 100 nm, 57 events of ≈ 200 nm, 48 events of ≈ 300 nm, 18 events of ≈ 400 nm, 7 events of ≈ 500 nm.	5 events of ≈ 600 nm, 4 events of ≈ 700 nm , 4 events of ≈ 800 nm, 3 events of ≈ 900 nm, 4 events of ≈ 1000 nm, 1 event of ≈ 1100, 1 event of ≈ 1200 nm, 2 events of ≈ 1300 nm, 2 events of ≈ 1500 nm, 1 event of ≈ 1600 nm, 2 events of ≈ 1700 nm, 1 event of ≈ 1900 nm, 1 event of ≈ 2100 nm, 1 event of ≈ 2300 nm, 2 events of ≈ 2600 nm, 1 event of ≈ 3100 nm.

Table 4. **Quantification of individual event length per condition.** The most frequently observed events were 200-300 nm Ω-shaped coated events.

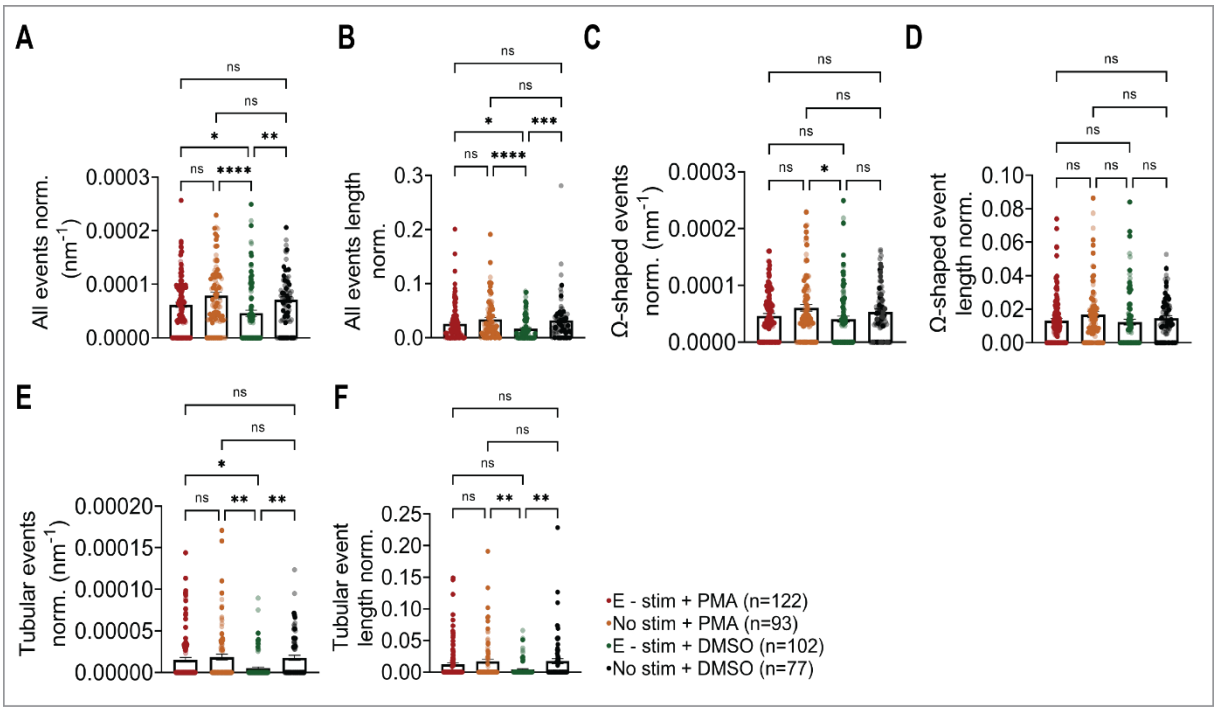

Figure 3. 21 **2D ultrastructural analysis of membrane invaginations in cultured chromaffin cells**. (A) A significant decrease in the number of all events in cells stimulated with electric field stimulation and DMSO (green). Normalization was calculated by dividing the number of all events by the cell perimeter (nm). (B) A reduction in all event lengths in cells exposed to E-stim and DMSO. Normalization was calculated by dividing the length of all events (nm) by the cell perimeter (nm). (C) Increased number of Ω-shaped PMA-only cells (orange) compared to cells exposed to E- stim and DMSO (green). Normalization was calculated by dividing the number of all Ω-shaped events by the cell perimeter (nm). (D) No major difference in the length of Ω-shaped events between conditions. Normalization was calculated by dividing the length of all Ω-shaped events (nm) by the cell perimeter (nm). (E) A significant decrease in the number of tubular events in cells stimulated with E- stim and DMSO. Normalization was calculated by dividing the number of all tubular events by the cell perimeter (nm). (F) A significant reduction in tubular event lengths in cells exposed to E- stim and DMSO. Normalization was calculated by dividing the length of all tubular events (nm) by the cell perimeter (nm).
The number of cultures: N=2; dark circles represent the first culture, and transparent circles represent the second culture. E-stim + PMA (red); No stim + PMA (orange); E-stim + DMSO (green); No stim + DMSO (black).
Error bars indicate mean ± SEM; *p < 0.05; **p < 0.01; ***p < 0.001; ****p < 0.0001.

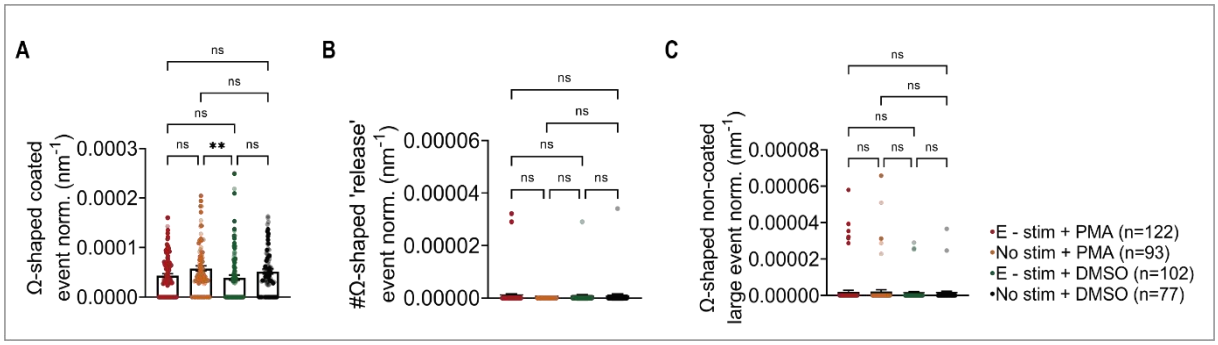

Figure 3. 22 **2D ultrastructural analysis of Ω-shaped profiles in cultured chromaffin cells**. (A) Reduced number of Ω-shaped coated events in cells stimulated with electric field stimulation and DMSO (green) compared to PMA-only cells (orange). Normalization was calculated by dividing the number of all Ω-shaped coated events by the cell perimeter (nm). (B) No significant difference in the number of Ω-shaped events depicting vesicle content

release. Normalization was calculated by dividing the number of all Ω-shaped 'release ' events by the cell perimeter (nm). (C) No major difference in the number of Ω-shaped non-coated large events between conditions. Normalization was calculated by dividing the number of all Ω-shaped non-coated large events by the cell perimeter (nm).
The number of cultures: N=2; dark circles represent the first culture, and transparent circles represent the second culture. E-stim + PMA (red); No stim + PMA (orange); E-stim + DMSO (green);No stim + DMSO (black).
Error bars indicate mean ± SEM; **p < 0.01.

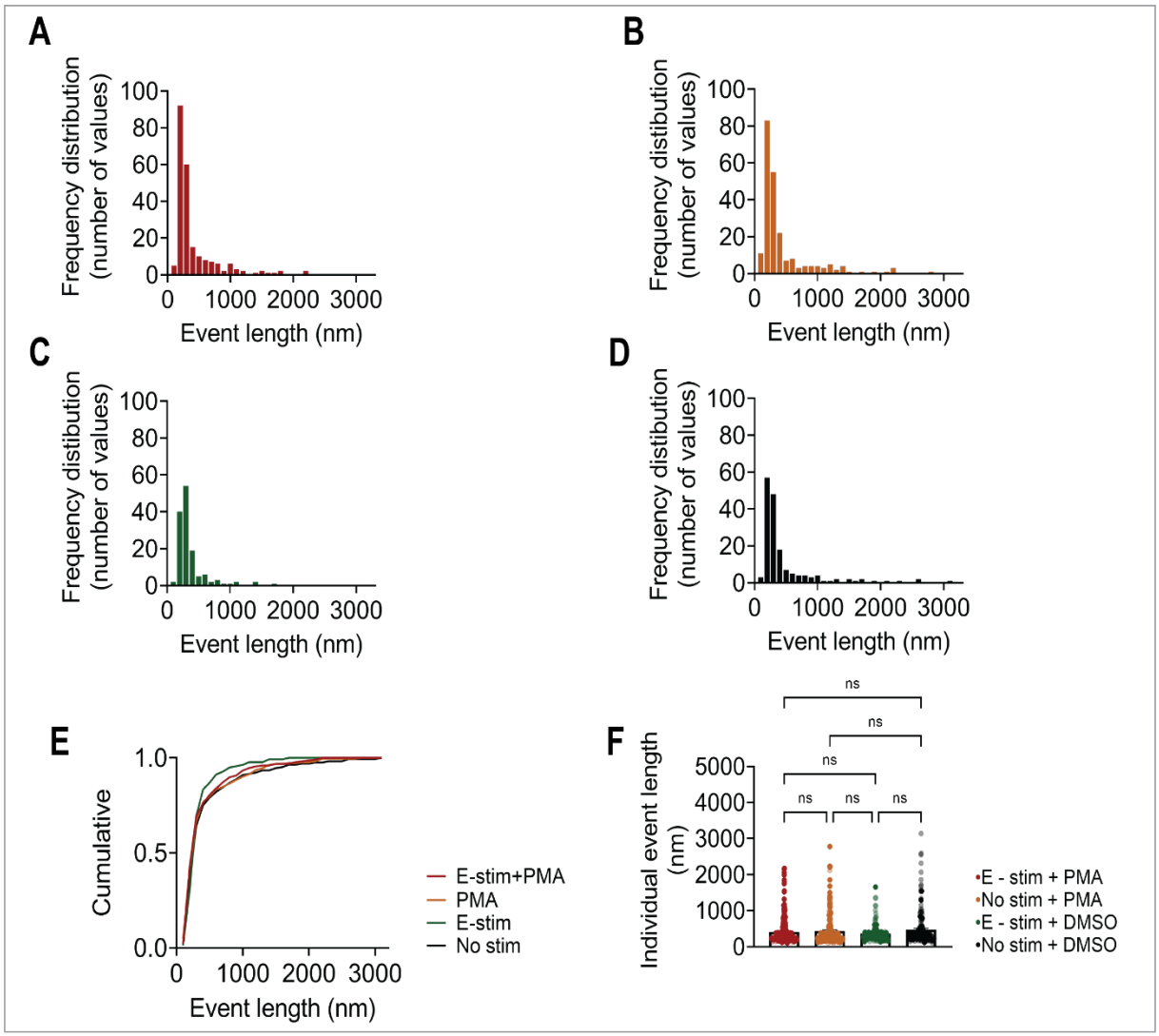

Figure 3. 23 **2D ultrastructural analysis of all events after four different conditions**. (A) Size distribution of all events from cells exposed to electric field stimulation and PMA. The most commonly seen events represent 200-300 nm Ω-shaped coated events. The histogram shows the absolute event number. (B) Size distribution of events from cells exposed to PMA, with the highest number of events representing Ω-shaped coated 200-300 nm events. (C) Size distribution of events from cells exposed to electric field stimulation and DMSO. The highest number of events represents Ω-shaped coated events of 200-300 nm. (D) Size distribution of events from non-stimulated and DMSO cells. The highest number of events represent Ω-shaped coated 200-300 nm events. (E) Cumulative distribution of events from 100 - 3100 nm. The curve (green) is shifted left, showing a tendency toward a reduced number of cell events after electric field stimulation and DMSO. (F) No difference in individual event length between conditions. E-stim + PMA (red); No stim + PMA (orange); E-stim + DMSO (green); No stim + DMSO (black).
Bin size (A,B,C,D,E); 100 nm.

The number of cultures: N=2; dark circles represent the first culture, and transparent circles represent the second culture.

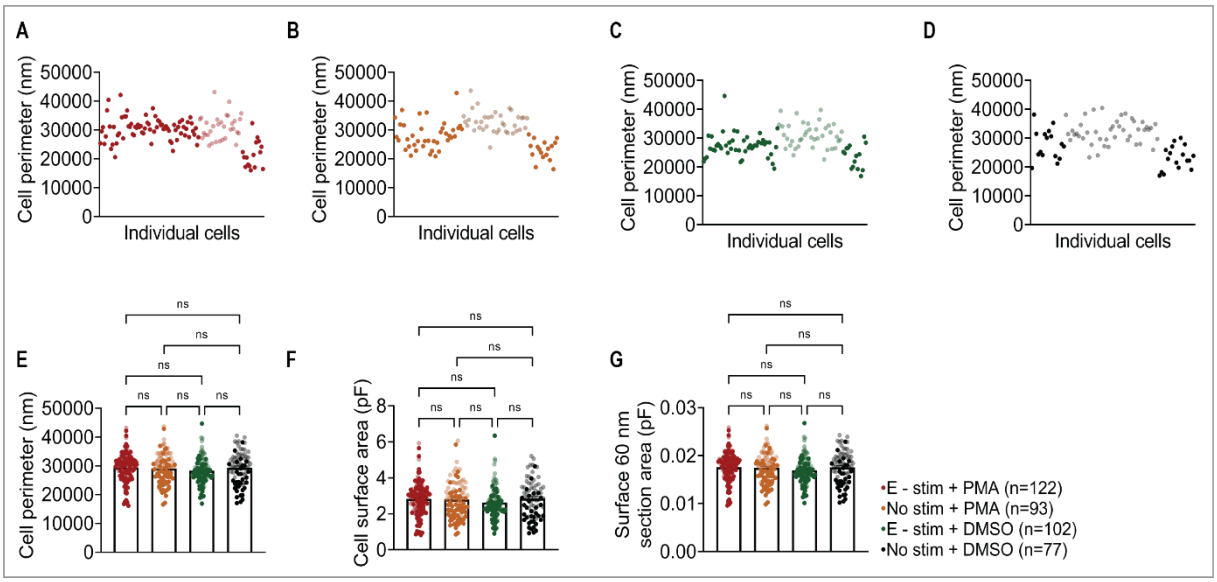

Figure 3. 24 **2D ultrastructural analysis of the cell perimeter and cell surface area in four different conditions.** (A) The perimeter of the cells exposed to electric field stimulation and PMA. (B) The perimeter of the cells exposed to PMA. (C) The perimeter of the cells exposed to electric field stimulation and DMSO. (D) The perimeter of the non-stimulated and DMSO cells. (E) No major difference between the perimeters of the cells between conditions. (F) Calculated cell surface areas (in pF) between conditions. (G) Calculated cell surface areas of the 60 nm section (in pF).
The number of cultures: N=2; dark circles represent the first culture, and lighter circles represent the second culture. E-stim + PMA (red); No stim + PMA (orange); E-stim + DMSO (green); No stim + DMSO (black).

4. Discussion

How processes of exocytosis and endocytosis are molecularly controlled under healthy and pathological states is a vital concern in contemporary cell biology. To resolve vesicle trafficking events on a millisecond time scale and to analyse the relationships between vesicles and the plasma membrane of excitable cells as well as the location of membrane recycling events about vesicle fusion sites, corresponding methodologies must have high temporal precision.

The scientific society now has access to "Zap-and-freeze" and "Flash-and-freeze" EM which allow electrical and optogenetic stimulation of neurons to be coupled with quick HPF cryo-fixation for EM (Watanabe et al., 2013; Imig et al., 2020; Kusick et al., 2020). These techniques were shown to be exceptionally effective for functional imaging. However, the "Zap-and-freeze" method has not been implemented in adrenal chromaffin cells, representing an effective and suitable model system for investigating exocytosis and endocytosis.

In essence, electrophysiological, ultrastructural, and molecular analyses of cultured chromaffin cells require a functional and adaptable experimental system. Therefore, to collect functional and ultrastructural data, we optimized a methodological approach that combines electrophysiology and "Zap-and-freeze" sample cryofixation combined with EM.

The present study shows that both optogenetic stimulation and electric field stimulation can be used to induce DCV release in cultured chromaffin cells. We decided to focus on electric field stimulation and employed field stimulation as well as voltage ramps mimicking action potentials to establish the stimulation pattern to be used prior to HPF. Capacitance recordings were used as a measure of DCV exocytosis. Amperometry was used to confirm that Ficoll® PM 70, which had to be added for HPF experiments to prevent cell loss during sample processing, did not affect catecholamine release and fusion pore dynamics.

Two-dimensional electron micrographs illustrated the appearance of potential endosome-like structures, large Ω -profiles, and release from secretory vesicles. Clathrin coats were conserved with our experimental workflow since most cells exhibited prominent coated endocytic structures. Our results indicate that our experimental method and subsequent EM analysis of cultured chromaffin cells enable visualization of large endosome-like intermediates, exocytic and endocytic events.

4.1. Optogenetic stimulation induced DCV release in mouse chromaffin cells

Previous studies illustrated how optogenetic tools could be employed to determine the functional architecture of dissociated β-cells (Westacott et al., 2017). Additionally, it has been demonstrated that optogenetic stimulation in PC12 cells induces dopamine release in a cell-

specific and time-precise manner (Chiu et al., 2014). However, no previous data explored the release of catecholamines from adrenal chromaffin cells employing the optogenetic technique.

Our study shows that ChR2-EYFP optogenetic activation can cause DCV release in chromaffin cells. Chromaffin cells expressing ChR2-EYFP were recorded in the current clamp configuration during optogenetic stimulation with a blue LED. In addition, cell capacitance was also recorded before and after the stimulation to monitor DCV fusion with the cell membrane in voltage clamp configuration. Our results showed that optogenetic stimulation induced APs at 4 Hz and 10 Hz in chromaffin cells expressing ChR2-EYFP using conventional WCPC and PWCPC. Surprisingly, we did not observe any difference in capacitance change induced by 4 Hz and 10 Hz stimulation. One possible reason is that the cells we tested had variable responses to the optogenetic stimulation, which could have masked any differences between the two frequencies. A potential solution to address this issue is using a larger number of cells. Another possibility is that the cells are reaching maximal levels of capacitance change at both frequencies, making it difficult to observe differences between them. Performing additional experiments, such as amperometry or calcium imaging, may determine the underlying cause of the lack of difference in capacitance change between the two frequencies. Additionally, not all cells responded to the stimulation. It was demonstrated that cells with a more positive membrane potential tended to be unresponsive to stimulation.

Overall, our study highlights the potential of optogenetics as a valuable tool for learning more about the mechanisms that control DCV release in chromaffin cells. However, because the expression of ChR2-EYFP was only detected in a subset of cells and since not all cells responded to the stimulation, we decided against optogenetics for further HPF experiments and proceeded with electric field stimulation.

4.2. Establishing stimulation patterns with electric field stimulation

4.2.1. Electric field stimulation induced DCV release in mouse chromaffin cells

When a neuron is located within an electric field, an electric current goes through the neuronal membrane, which causes the membrane's depolarization and/or hyperpolarization. Thus, electric field stimulation may cause cell excitation by depolarizing the cell, which generates action potentials by opening voltage-gated sodium and potassium channels (Hodgkin & Huxley, 1952). The impact of a 20 V/ cm electric field on the membrane potential variations was also demonstrated by changing the orientation of the electric field in dissociated bovine chromaffin cells (Hassan et al., 2002). Additionally, researchers revealed that a single unipolar pulse of 2 nanoseconds and 16 V/ cm evoked a transient increase in intracellular calcium levels due to activated voltage-gated calcium channels. However, the authors also showed that this cell response could be cancelled by a 2 nanoseconds bipolar pulse (Zaklit et al., 2021).

Our study conducted experiments to test the release of DCVs in chromaffin cells in response to various stimulations. In order to find the best stimulus strength and duration, we tested electric field stimulation. Using capacitance measurements, we examined the impact of various frequencies and stimulus intensities on DCV release. We discovered that a stimulus with a voltage of 40 V (at our stimulation chamber, width 0.65 cm) and a duration of 1 ms was effective in causing DCV release. In addition, we showed that field stimulation with 10, 20, and 30 stimuli delivered at 4 Hz caused a greater change in capacitance than control cells that were not stimulated. Interestingly, there was no statistical difference in the capacitance change induced by the different number of stimuli. Our premise is that the cells reached a saturation point in their response to stimuli, such that an additional number of stimuli did not lead to a significant change in capacitance. Increasing the sample size may enable us to clarify whether there is a significant difference between the number of stimuli. Furthermore, there was no major difference between the stimulated and unstimulated groups after stimulation with 10, 20, and 30 stimuli at 10 Hz. We hypothesized that, given that chromaffin cells often fire in bursts, the trains of stimuli might be too long for a 10 Hz frequency.

Our findings indicate that DCV release in chromaffin cells can be induced by electric field stimulation. To further determine the impact of various types of stimulation on DCV release, we continued with a discontinuous, burst-like stimulation pattern.

4.2.2. Electric field stimulation of chromaffin cells using stimulus bursts

Previous studies demonstrated that chromaffin cells show different patterns of electrical excitability, including a burst firing (Albiñana et al., 2015; Guarina et al., 2017; Martinez-Espinosa et al., 2014; Vandael et al., 2015). In addition, chromaffin cells possess various ion channels, such as voltage-gated Na^+ channels (Nav), voltage-gated Ca^{2+} channels (Cav), and K^+ channels (Kv), that modulate the cell's complex excitable activity. It has been demonstrated that the activity of Nav, Kv and Cav channels is highly regulated and plays an essential role in generating electrical activity observed in chromaffin cells (Lingle et al., 2018).

Considering the aforementioned studies on the intrinsic burst firing of chromaffin cells, we focused on testing the burst technique, which was the next stimulation pattern to be investigated in this study. The findings in our study imply that DCV release in chromaffin cells can be induced by four bursts of five stimuli delivered at 10 Hz. The rise in capacitance seen in both the standard extracellular solution and the solution containing 5% Ficoll ® PM 70 shows that the electric field stimulation with four bursts of five stimuli at 10 Hz is effective in causing robust vesicle release.

Additionally, since the strength of the electric field generated for the "Zap-and-freeze" method was 10 V/ cm^{-1} (Kusick et al., 2020), we tested stimulus strengths of 5-10 V at our stimulation

chamber (width 0.65 cm) to confirm that this was sufficient to evoke APs. Therefore, effective stimulus strength, time, and frequency with electric filed stimulation have been determined.

4.2.3. Electric field stimulation of chromaffin cells in combination with caffeine and phorbol-esters

In an effort to maximize DCV exocytosis, we tested both caffeine and phorbol esters in combination with electric field stimulation, to see if we could further enhance the response to stimulation.

An earlier study (Ohta et al., 2001) found that caffeine increased the release of catecholamines from voltage-clamped guinea pig adrenal chromaffin cells by causing the release of Ca^{2+} from internal stores in these cells. Therefore, these results showed evidence of Ca^{2+}-induced Ca^{2+} release (CICR) involvement in chromaffin cells (Alonso et al., 1999). CICR is a feedback mechanism that triggers the release of further calcium ions, resulting in a rapid increase in cytosolic calcium concentration and, ultimately, neurotransmitter secretion. However, in contrast to these findings, Ricardo Rigual et al. (2002) showed that in mouse chromaffin cells CICR is not functional. We investigated the effect of four-burst stimulation on cell capacitance in the presence of 5 mM caffeine, but no significant changes were observed in the capacitance of treated and non-treated cells. Our study simultaneously stimulated the cells with an electric field and caffeine. The electrical field stimulation may be concealing the effect of caffeine. Overall, while caffeine is known to stimulate the release of catecholamines from adrenal chromaffin cells in many studies, some studies have found no effect of caffeine on these cells. These discrepancies may be due to differences in experimental conditions, or the specific species studied.

Phorbol esters have previously been shown to enhance neuronal transmitter release (Pocotte et al., 1985; Rhee et al., 2002; Lou et al., 2008) and depolarization-induced exocytosis in chromaffin cells (Gillis et al., 1996; Houy et al., 2022). Therefore, our study assessed whether there is a more significant increase in cell capacitance upon four-burst stimulation with an additional brief application of 100 nM PMA. The study's results showed that the combination of PMA and four-burst field stimulation did not result in a significant increase in cell capacitance. We suggest two possible reasons for this outcome. Firstly, the field stimulation may have been strong enough to release a maximal number of vesicles, meaning that the addition of PMA did not result in any further release. Alternatively, since combining field stimulation with capacitance recordings requires switching back and forth between voltage and current clamp recordings, which introduces greater experimental variability than simple voltage clamp recordings, this could potentially obscure the effect of PMA.

However, our voltage ramp recordings done in the presence of PMA (see below, 4.3.2) suggest that phorbol esters can enhance transmitter release and exocytosis in adrenal chromaffin cells. Ramp stimulation allowed for more regulated stimulation of cultured chromaffin cells and overcame the time delay problem associated with evaluating capacitance change immediately after stimulation. Thus, the current study emphasizes the significance of considering the experimental conditions and parameters when investigating the effects of such compounds.

4.3. The effect of voltage ramp stimulation on DCV release in mouse chromaffin cells

4.3.1. Correlation between the number and frequency of AP-like ramps and DCV exocytosis

Earlier studies on the relationship between electrically induced secretion and stimulation have been conducted under voltage clamp conditions using artificial AP template voltage ramps (Duan et al., 2003). This method provided precise temporal resolution.

To assess the precision of the stimulation paradigm optimized with electric field stimulation, we used ramp protocols, which provided better control of the stimulation and circumvented the time delay problem of analyzing capacitance changes immediately after stimulation. The effects of voltage ramp stimulation on DCV release were studied using membrane capacitance recordings. To determine the correlation between secretion and the number of AP-like ramps, we tested different frequencies and the number of AP-like ramps in a stimulus train. We found that the amount of DCV exocytosis increased with the number of ramps in the train, but no further increase was detected when the AP frequency was increased from 4 to 20 Hz. A similar outcome was observed with electric field stimulation, with no significant effect at higher frequencies. This result is aligned with a previous study, where no further increase in secretion was observable with frequencies higher than 7 Hz (Duan et al., 2003). The study suggested the possible reason for this is the saturation of intracellular $Ca^{2+,}$ equivalent to the view that AP-induced secretion is entirely Ca^{2+}-dependent in chromaffin cells (Augustine & Neher, 1992; Zhang & Zhou, 2002). Stimulation with five short bursts at 10 Hz caused a robust increase in membrane capacitance.

Thus, our research is consistent with the previous study and indicates that voltage ramp stimulation is a useful technique for quantifying DCV release, and that the DCV exocytosis is significantly influenced by the number of ramps in a stimulus train. The results further imply that burst stimulation is a potent inducer of significant changes in membrane capacitance.

4.3.2. The PMA effect on DCV exocytosis using voltage-ramp stimulation

We tested PMA application simultaneously with voltage ramp stimulation because the application of PMA did not have the anticipated effect with electric field stimulation. This method allowed us to validate that the PMA application time was enough. The cells were exposed for the 30 s to 100 nM PMA prior to four-burst at 10 Hz. The application of PMA caused a significantly greater change in capacitance than the control condition, confirming that our application time was sufficient. Thus, we applied PMA treatment in HPF experiments.

Earlier studies using membrane capacitance measurements (Gillis et al., 1996) demonstrated that brief treatment with PMA increases exocytosis. The authors suggested that PKC influences a late step in secretion but not the Ca^{2+} sensitivity of the final step. Additionally, recent studies in mouse adrenal chromaffin cells (Houy et al., 2022) investigated the interaction of PMA with Munc13-1 and Munc13-2. This study suggests that the two different types of Munc13 proteins have differential roles in regulating the effects of PMA on exocytosis, concluding that phorbol ester, Munc13-2, and Syt7 promote DCV priming, a critical step in exocytosis.

Our data with four-burst voltage ramp stimulation is consistent with the earlier findings. Comparing the control condition with the application of PMA revealed a considerable enhancement of DCV exocytosis by PMA. Hence, the absence of the PMA effect observed in field stimulation tests may be attributable to the paradigm's lack of control over membrane potential and experimental variability. Therefore, we decided to use PMA for HPF experiments.

4.4. Preserved morphology of mouse cultured chromaffin cells

4.4.1. "Zap-and-freeze" method

Earlier studies on chromaffin cells (Plattner et al., 1997; Koval et al., 2001) investigated the morphology of these cells in unstimulated conditions. Additionally, there are only very few studies (Shin et al., 2021; Ratai et al., 2019; de Wit, 2009) that have managed to analyze cultured chromaffin cells by HPF because they are very challenging to retain throughout the sample preparation procedure. This is why recent approaches (Shin et al., 2021) froze centrifuged and pelleted cells. Most other studies have used aldehydes for sample fixation. Therefore, the present study aimed to investigate the "Zap-and-freeze" method followed by HPF and AFS on cultured chromaffin cells.

Using HPF and AFS to fix the sample, the sample's morphology is maintained in a near-native condition, underscoring the reliability of the method (Imig & Cooper., 2017; Siksou et al., 2009; Fernández-Busnadiego et al., 2011; Frotscher, 2007). Cryoprotectants are compounds that are frequently used during sample fixation (Pegg, 1972; Osetsky et al., 2011). Since the present

study aimed to conduct WCPC and HPF tests under the same conditions, we refrained from utilizing cryoprotectants to freeze cultured chromaffin cells. However, sample loss occurred, so Ficoll® PM 70 was tried as a substitute matrix to prevent cell loss. After confirming that Ficoll® PM 70 did not affect DCV exocytosis, a 5% solution of Ficoll® PM 70 was used because it did not promote cell death and generated good ultrastructural preservation of the cells. By applying our experimental approach, cultured chromaffin cells showed extraordinary ultrastructural preservation. Furthermore, cells frozen under physiological conditions retain their cytoskeletal components using our freeze substitution procedure. The study's findings show Ficoll® PM 70's value in improving the freezing quality in biological samples for ultrastructural preservation and the efficacy of utilizing Ficoll® PM 70 as a substitute matrix to avoid cell loss in the absence of a cryoprotectant.

The cells were fixed using HPF fixation, freeze-substitution, and EPON embedding, and then 2D electron micrographs were analyzed. Considering the total number of DCVs calculated to fuse per cell from capacitance analyses and the fact that the EM analysis of cells in ultrathin sections surveys only a small fraction (approx. 1% in Fig. 3.24 G) of the total cell surface, our experimental workflow provided not only excellent sample preservation but also the capture of rare dynamic cellular events.

4.4.2. Electron microscopic observation of membrane invaginations in cultured chromaffin cells

In this research, we tested four conditions: 1) electric field stimulation with PMA treatment; 2) PMA treatment; 3) electric field stimulation with DMSO treatment, and 4) no stimulation with DMSO treatment (vehicle control). Surprisingly, after quantifying the events contiguous with the membrane, we observed a significant reduction in the number of events in cells stimulated with electric field stimulation. Thus, the results of an experiment conducted on adrenal chromaffin cells demonstrated that electric field stimulation with DMSO leads to a significant decrease in the number of events compared to cells in other conditions. One explanation is that the four-burst field stimulation was too strong for the chromaffin cells, which resulted in the release of all release-ready vesicles and we were not able to capture these events. Our stimulation may activate an exo-endocytotic mode of complete collapse, where vesicles entirely collapse into the plasma membrane surface, leading to the loss of the Ω-shaped profile. This theory is supported by our data (Fig. 3.19) showing that vesicle content release may resemble the complete collapse event previously illustrated (Harata et al., 2006; Ceridono et al., 2011). The second possible explanation is that electric field stimulation may not have been equally effective for all stimulated samples.

In the present study large Ω-profiles, vesicle release and endosome-like structures were visible in 2D electron micrographs. Since most cells had apparent coated endocytic structures,

clathrin coating was maintained throughout our experimental protocol. Originally, it was thought that tubular membrane invaginations, sometimes referred to as bulk endocytosis, resulted from bulk endocytosis, phagocytosis, or compound exocytosis (Saheki & De Camilli, 2012; Wu et al., 2014; Kononenko & Haucke, 2015). Similarly, according to our findings, endosome-like intermediates can be seen when using our experimental setup.

We analyzed all membrane invaginations visible in 2D electron micrographs in cultured chromaffin cells. In all conditions, we observed strong evidence of membrane invaginations, which showed a variety of different shapes and dimensions. Therefore, we classified membrane invaginations into four categories: 1) Ω-shaped coated events, representing events with preserved clathrin-coat, 2) Ω-shaped events 'release', depicts the events with a captured vesicle content release, 3) Ω-shaped non-coated large events, and 4) tubular structures.

The most prominent events in all conditions were Ω-shaped coated events and tubular structures, which indicates that these events are inherent to the cells and their occurrence is not significantly affected by the applied treatments. In contrast, the release and Ω-shaped non-coated large events were infrequent and mostly captured after electric field stimulation combined with the PMA treatment. This data suggests that these events are less common and require specific conditions for their occurrence. Noticing Ω-shaped profiles in non-stimulated-DMSO-treated cells can also mean that these profiles are formed before stimulation and may serve as a base for compound fusion and multivesicular release from a single release site (Shin et al., 2021; Ge et al., 2022). To fuse, vesicles must move to and dock to the release sites of the plasma membrane, where vesicular V-SNARE and plasma membrane T-SNARE binding will occur (Jahn & Fasshauer, 2012; Kaeser & Regehr, 2014). However, a recent study demonstrated a new mechanism for the fast assembly of release sites at newly formed Ω-shaped profiles (Ge et al., 2022). Release machinery assembly may take time (Gandasi & Barg, 2014). Therefore, a quick assembly at preformed Ω-shaped profiles may enable vesicles to avoid using energy to travel to the flat plasma membrane release sites.

Tubular events could represent: (i) bulk endocytosis intermediates, or (ii) compound fusion intermediates. In the latter case, we would, however, expect to detect electron-dense DCV content within the tubular structures, which was not observed. Therefore, tubular structures may represent fragments of plasma membrane elongated and internalized by bulk endocytosis (Takei et al., 1996). In contrast to other endocytic modes, bulk endocytosis retrieves plasma membranes for more than one vesicle (Takei et al., 1996; Gad et al., 1998). It has also been shown that bulk endocytosis was a quick process initiated by intense stimulation (Clayton et al., 2008). Surprisingly, we observed a significant difference in the number of tubular events between cells stimulated with electric field stimulation with DMSO treatment and other groups. The cells stimulated with electric field stimulation with DMSO showed a significantly smaller

number of tubular events compared to other groups. An explanation for this finding is that electric field stimulation with four bursts may trigger another endocytic mode.

Additionally, we found that PMA-only treated cells had significantly more visible small Ω-shaped coated events than cells stimulated with electric field stimulation with DMSO. In various cell types, CME retrieves plasma membrane by forming membrane invaginations coated with clathrin (Pearse et al., 2000; Royle & Lagnado, 2003). It was found that slow membrane retrieval occurs through CME (Wu & Wu, 2007). These findings suggested that CME is a slow mechanism and that another process, which does not include clathrin, is responsible for quickly retrieving the plasma membrane. The KR endocytotic mode was considered to allow fast recycling of the plasma membrane, where a vesicle transiently touches the plasma membrane to release the content without entirely collapsing into the surface (Fesce et al., 1994). However, some findings (Zenisek et al., 2002; Llobet et al., 2003) demonstrated that vesicles collapsed fully into the surface in response to stimuli and that excess membrane was retrieved with a time constant of 1 s, indicating rapid endocytosis. Additionally, experiments on chromaffin cells demonstrated that under basal conditions, chromaffin cells demonstrate quick and effective local vesicle recycling. In contrast, the release of catecholamine and neuropeptide occurs in full collapse mode, which copes with the demands of the sympathetic "fight-or-flight" state (Fulop et al., 2005). These findings show that the transition between transient and full fusion in neuroendocrine chromaffin cells is a crucial physiological control. Our data demonstrates that PMA-only treatment induces a specific cellular response leading to Ω-shaped coated events, in contrast to electric field-DMSO treatment. The present study suggests that exposure to PMA leads to the activation of slower types of endocytosis, such as clathrin-mediated endocytosis (Mykoniatis et al., 2010). In contrast, strong stimulation with an electric field may trigger the full collapse mode, where vesicles completely collapse into the surface of the plasma membrane, which results in the loss of Ω-shaped profiles.

Our finding suggests that the mechanism by which cells respond to different stimuli can vary. It emphasizes the importance of comprehending the specific cellular responses induced by different treatments or stimuli. Additionally, we were able to capture a very prominent content release from secretory vesicles, showing the vesicle's total collapse into the plasma membrane—showing full collapse as a dominant mode of release and demonstrating that our experimental workflow was able to visualize rapid biological events in chromaffin cells.

4.4.3. Dominant mode of vesicle fusion and membrane retrieval

Recent EM studies (Shin et al., 2021; Ge et al., 2022) demonstrated that besides Ω-shaped, various additional shapes of membrane invagination, such as Λ-shaped, O-shaped, and 8-shaped profiles (which may represent compound fusion) could be captured. In the present

study, seeing Ω-shapes in unstimulated cells may match previous studies, meaning that they are formed before stimulation and may serve as a base for compound fusion. Additionally, events we observed (particularly the small clathrin-coated events) may also represent a constitutively active form of endocytosis that operates without stimulation. However, we did not notice transitional shapes or hemifusion intermediates.

Furthermore, Shin et al. (2021) found two main modes of endocytosis: preformed-Ω-profile closure and KR. Preformed-Ω-profile closure involves the formation of a deep invagination in the plasma membrane, which eventually closes off and forms a vesicle internalized into the cell. KR, conversely, involves a brief fusion of the vesicle with the plasma membrane, allowing for rapid cargo retrieval without significant changes to the membrane surface. In contrast, our study showed that the dominant mode after four-burst electric field stimulation with PMA might be full fusion, where the vesicle collapses entirely into the membrane surface to release the content (Fig. 3.19). The discrepancy between the two investigations could be due to various factors, such as the experimental conditions.

Moreover, using PMA in the present study may have also influenced the mode of endocytosis observed. Therefore, employing PMA may have stimulated a different mode of endocytosis than what Shin et al. (2021) observed in their study.

Overall, the present work shows that electric field stimulation and PMA administration can influence the occurrence of particular membrane events in cells and emphasizes the significance of considering the effects of experimental conditions on cellular processes.

5. Conclusion and outlook

In the present study, we combined electrophysiological and ultrastructural analysis to generate functional and morphological aspects of adrenal chromaffin cells.

The investigation used electrophysiology and EM to examine the effects of different stimuli on chromaffin cells, which are responsible for releasing catecholamines in response to stress or other stimuli. We investigated the suitability of optogenetic stimulation and field stimulation to evoke DCV exocytosis in chromaffin cells, using capacitance recordings to measure exocytosis. The study found that Ficoll® PM 70 did not change the properties of catecholamine release and can be used in further experiments. This study contributes to understanding the mechanisms behind DCV release in chromaffin cells and suggests that optogenetic and electric field stimulation applications can be utilized for further studies.

This research enabled us to freeze cultured chromaffin cells and acquire excellent preservation of the samples. According to our findings, our experimental procedure and subsequent 2D-EM analysis of cultured chromaffin cells allow the visualization of not only clathrin-coated membrane retrieval but also, for the first-time prominent vesicle content release. Moreover, our data seems to indicate full collapse as a dominant mode of release. The appearance of large Ω - shaped profiles and endosome-like structures were depicted in 2D electron micrographs. The next step in this study will be quantifying the vesicles near the plasma membrane per condition, which will give us insight into the number of docked and released vesicles in different conditions. However, one drawback of the 2D analysis is that measuring individual events' precise dimensions is impossible. Therefore, another step for this study is to perform 3D scanning transmission electron microscopy (STEM) tomography from 500 nm-thick sections. The three-dimensional analysis will reveal the form and full extent of individual membrane invaginations, giving us a better insight into ultrastructural characteristics of exo- and endocytic events in cultured chromaffin cells under different conditions.

Our research can be applied to studies that examine the exact mechanism of function of proteins crucial for exocytosis and endocytosis. For example, it is indeed interesting that in synapses in Munc13 ½ DKO, the vesicles are not released (Augustin et al., 1999; Richmond et al., 1999; Rosenmund et al., 2002). Ultrastructural analysis demonstrated, that in these animals, vesicles do not dock at active zones (Imig et al., 2014; Siksou et al., 2009; Weimer et al., 2006). However, in chromaffin cells, some release could still been detected (Man et al., 2015), but ultrastructural data of comparable quality of stimulated chromaffin cells of Munc13 ½ DKO animals have yet to be generated. Also, BAIAP3 was not shown to have an effect on exocytosis but is thought to be involved in DCV recycling (Wojcik et al., 2013; Man et al., 2015; Zhang et al., 2017; Sørensen, 2017). Therefore, to further investigate the function of Munc13

proteins in DCV biology, our established "Zap-and-freeze" method to stimulate and freeze cultured chromaffin cells can be utilized.

6. Bibliography

Alabi, A. A., & Tsien, R. W. (2013). Perspectives on kiss-and-run: role in exocytosis, endocytosis, and neurotransmission. Annual review of physiology, 75, 393–422. https://doi.org/10.1146/annurev-physiol-020911-153305

Albillos, A., Dernick, G., Horstmann, H., Almers, W., Alvarez de Toledo, G., & Lindau, M. (1997). The exocytotic event in chromaffin cells revealed by patch amperometry. Nature, 389(6650), 509–512. https://doi.org/10.1038/39081

Albiñana, E., Segura-Chama, P., Baraibar, A. M., Hernández-Cruz, A., & Hernández-Guijo, J. M. (2015). Different contributions of calcium channel subtypes to electrical excitability of chromaffin cells in rat adrenal slices. Journal of neurochemistry, 133(4), 511–521. https://doi.org/10.1111/jnc.13055

Almers, W., & Tse, F. W. (1990). Transmitter release from synapses: does a preassembled fusion pore initiate exocytosis? Neuron, 4(6), 813–818. https://doi.org/10.1016/0896-6273(90)90134-2

Alonso, M. T., Barrero, M. J., Michelena, P., Carnicero, E., Cuchillo, I., García, A. G., García-Sancho, J., Montero, M., & Alvarez, J. (1999). Ca2+-induced Ca2+ release in chromaffin cells seen from inside the ER with targeted aequorin. The Journal of cell biology, 144(2), 241–254. https://doi.org/10.1083/jcb.144.2.241

Anderson R. G. (1998). The caveolae membrane system. Annual review of biochemistry, 67, 199–225. https://doi.org/10.1146/annurev.biochem.67.1.199

Araç, D., Chen, X., Khant, H. A., Ubach, J., Ludtke, S. J., Kikkawa, M., Johnson, A. E., Chiu, W., Südhof, T. C., & Rizo, J. (2006). Close membrane-membrane proximity induced by Ca(2+)-dependent multivalent binding of synaptotagmin-1 to phospholipids. Nature structural & molecular biology, 13(3), 209–217. https://doi.org/10.1038/nsmb1056

Archer, D. A., Graham, M. E., & Burgoyne, R. D. (2002). Complexin regulates the closure of the fusion pore during regulated vesicle exocytosis. The Journal of biological chemistry, 277(21), 18249–18252. https://doi.org/10.1074/jbc.C200166200

Arpino, G., Somasundaram, A., Shin, W., Ge, L., Villareal, S., Chan, C. Y., Ashery, U., Shupliakov, O., Taraska, J. W., & Wu, L. G. (2022). Clathrin-mediated endocytosis cooperates with bulk endocytosis to generate vesicles. iScience, 25(2), 103809. https://doi.org/10.1016/j.isci.2022.103809

Artalejo, C. R., Henley, J. R., McNiven, M. A., & Palfrey, H. C. (1995). Rapid endocytosis coupled to exocytosis in adrenal chromaffin cells involves Ca2+, GTP, and dynamin but not clathrin. Proceedings of the National Academy of Sciences of the United States of America, 92(18), 8328–8332. https://doi.org/10.1073/pnas.92.18.8328

Ashery, U., Varoqueaux, F., Voets, T., Betz, A., Thakur, P., Koch, H., Neher, E., Brose, N., & Rettig, J. (2000). Munc13-1 acts as a priming factor for large dense-core vesicles in bovine chromaffin cells. The EMBO journal, 19(14), 3586–3596. https://doi.org/10.1093/emboj/19.14.3586

Augustin, I., Rosenmund, C., Südhof, T. C., & Brose, N. (1999). Munc13-1 is essential for fusion competence of glutamatergic synaptic vesicles. Nature, 400(6743), 457–461. https://doi.org/10.1038/22768

Augustine, G. J., & Neher, E. (1992). Calcium requirements for secretion in bovine chromaffin cells. The Journal of physiology, 450, 247–271. https://doi.org/10.1113/jphysiol.1992.sp019126

Ayesha N. Shajahan, Chinnaswamy Tiruppathi, Alan V. Smrcka, Asrar B. Malik, Richard D. Minshall, (2004) Gβγ Activation of Src Induces Caveolae-mediated Endocytosis in Endothelial Cells*, Journal of Biological Chemistry, Volume 279, Issue 46, 2004, Pages 48055-48062, ISSN 0021-9258, https://doi.org/10.1074/jbc.M405837200.

Bader, M. F., Holz, R. W., Kumakura, K., & Vitale, N. (2002). Exocytosis: the chromaffin cell as a model system. Annals of the New York Academy of Sciences, 971, 178–183. https://doi.org/10.1111/j.1749-6632.2002.tb04461.x

Bagalkot, T. R., Leblanc, N., & Craviso, G. L. (2019). Stimulation or Cancellation of Ca2+ Influx by Bipolar Nanosecond Pulsed Electric Fields in Adrenal Chromaffin Cells Can Be Achieved by Tuning Pulse Waveform. Scientific reports, 9(1), 11545. https://doi.org/10.1038/s41598-019-47929-4

Barbara MF Pearse, Corinne J Smith, David J Owen, Clathrin coat construction in endocytosis, Current Opinion in Structural Biology, Volume 10, Issue 2, 2000, Pages 220-228, ISSN 0959-440X, https://doi.org/10.1016/S0959-440X(00)00071-3.

Berberian, K., Torres, A. J., Fang, Q., Kisler, K., & Lindau, M. (2009). F-actin and myosin II accelerate catecholamine release from chromaffin granules. The Journal of neuroscience: the official journal of the Society for Neuroscience, 29(3), 863–870. https://doi.org/10.1523/JNEUROSCI.2818-08.2009

Berndt, A., Schoenenberger, P., Mattis, J., Tye, K. M., Deisseroth, K., Hegemann, P., & Oertner, T. G. (2011). High-efficiency channelrhodopsins for fast neuronal stimulation at low light levels. Proceedings of the National Academy of Sciences of the United States of America, 108(18), 7595–7600. https://doi.org/10.1073/pnas.1017210108

Bittner, M. A., & Holz, R. W. (1992). Kinetic analysis of secretion from permeabilized adrenal chromaffin cells reveals distinct components. The Journal of biological chemistry, 267(23), 16219–16225. https://pubmed.ncbi.nlm.nih.gov/1644807/

Bittner, M. A., Aikman, R. L., & Holz, R. W. (2013). A nibbling mechanism for clathrin-mediated retrieval of secretory granule membrane after exocytosis. The Journal of biological chemistry, 288(13), 9177–9188. https://doi.org/10.1074/jbc.M113.450361

Blackmer, T., Larsen, E., Bartleson, C. et al. G protein βγ directly regulates SNARE protein fusion machinery for secretory granule exocytosis. Nat Neurosci 8, 421–425 (2005). https://doi.org/10.1038/nn1423

Borisovska, M., Zhao, Y., Tsytsyura, Y., Glyvuk, N., Takamori, S., Matti, U., Rettig, J., Südhof, T., & Bruns, D. (2005). v-SNAREs control exocytosis of vesicles from priming to fusion. The EMBO journal, 24(12), 2114–2126. https://doi.org/10.1038/sj.emboj.7600696

Boucrot, E., Ferreira, A. P., Almeida-Souza, L., Debard, S., Vallis, Y., Howard, G., Bertot, L., Sauvonnet, N., & McMahon, H. T. (2015). Endophilin marks and controls a clathrin-independent endocytic pathway. Nature, 517(7535), 460–465. https://doi.org/10.1038/nature14067

Boucrot, E., Pick, A., Çamdere, G., Liska, N., Evergren, E., McMahon, H. T., & Kozlov, M. M. (2012). Membrane fission is promoted by insertion of amphipathic helices and is restricted by crescent BAR domains. Cell, 149(1), 124–136. https://doi.org/10.1016/j.cell.2012.01.047

Gu, F., Crump, C. M., & Thomas, G. (2001). Trans-Golgi network sorting. Cellular and molecular life sciences: CMLS, 58(8), 1067–1084. https://doi.org/10.1007/PL00000922

Bretou, M., Anne, C., & Darchen, F. (2008). A fast mode of membrane fusion dependent on tight SNARE zippering. The Journal of neuroscience: the official journal of the Society for Neuroscience, 28(34), 8470–8476. https://doi.org/10.1523/JNEUROSCI.0860-08.2008

Breustedt, J., Gundlfinger, A., Varoqueaux, F., Reim, K., Brose, N., & Schmitz, D. (2010). Munc13-2 differentially affects hippocampal synaptic transmission and plasticity. Cerebral cortex (New York, N.Y.: 1991), 20(5), 1109–1120. https://doi.org/10.1093/cercor/bhp170

Brodsky, F. M., Chen, C. Y., Knuehl, C., Towler, M. C., & Wakeham, D. E. (2001). Biological basket weaving: formation and function of clathrin-coated vesicles. Annual review of cell and developmental biology, 17, 517–568. https://doi.org/10.1146/annurev.cellbio.17.1.517

Brose, N., Rosenmund, C., & Rettig, J. (2000). Regulation of transmitter release by Unc-13 and its homologues. Current opinion in neurobiology, 10(3), 303–311. https://doi.org/10.1016/s0959-4388(00)00105-7

Burkhardt, P., Hattendorf, D. A., Weis, W. I., & Fasshauer, D. (2008). Munc18a controls SNARE assembly through its interaction with the syntaxin N-peptide. The EMBO journal, 27(7), 923–933. https://doi.org/10.1038/emboj.2008.37

Cai, H., Reim, K., Varoqueaux, F., Tapechum, S., Hill, K., Sørensen, J. B., Brose, N., & Chow, R. H. (2008). Complexin II plays a positive role in Ca2+-triggered exocytosis by facilitating vesicle priming. Proceedings of the National Academy of Sciences of the United States of America, 105(49), 19538–19543. https://doi.org/10.1073/pnas.0810232105

Carbone, E., Borges, R., Eiden, L. E., García, A. G., & Hernández-Cruz, A. (2019). Chromaffin Cells of the Adrenal Medulla: Physiology, Pharmacology, and Disease. Comprehensive Physiology, 9(4), 1443–1502. https://doi.org/10.1002/cphy.c190003

Carmichael, S. W., & Winkler, H. (1985). The Adrenal Chromaffin Cell. Scientific American, 253(2), 40–49. http://www.jstor.org/stable/24967764

Ceridono, M., Ory, S., Momboisse, F., Chasserot-Golaz, S., Houy, S., Calco, V., Haeberlé, A. M., Demais, V., Bailly, Y., Bader, M. F., & Gasman, S. (2011). Selective recapture of secretory granule components after full collapse exocytosis in neuroendocrine chromaffin cells. Traffic (Copenhagen, Denmark), 12(1), 72–88. https://doi.org/10.1111/j.1600-0854.2010.01125.x

Chen, Z., Cooper, B., Kalla, S., Varoqueaux, F., & Young, S. M., Jr (2013). The Munc13 proteins differentially regulate readily releasable pool dynamics and calcium-dependent recovery at a central synapse. The Journal of neuroscience: the official journal of the Society for Neuroscience, 33(19), 8336–8351. https://doi.org/10.1523/JNEUROSCI.5128-12.2013

Cheung, G., & Cousin, M. A. (2013). Synaptic vesicle generation from activity-dependent bulk endosomes requires calcium and calcineurin. The Journal of neuroscience: the official journal of the Society for Neuroscience, 33(8), 3370–3379. https://doi.org/10.1523/JNEUROSCI.4697-12.2013

Chiu, W. T., Lin, C. M., Tsai, T. C., Wu, C. W., Tsai, C. L., Lin, S. H., & Chen, J. J. (2014). Real-time electrochemical recording of dopamine release under optogenetic stimulation. PloS one, 9(2), e89293. https://doi.org/10.1371/journal.pone.0089293

Chow, R. H., von Rüden, L., & Neher, E. (1992). Delay in vesicle fusion revealed by electrochemical monitoring of single secretory events in adrenal chromaffin cells. Nature, 356(6364), 60–63. https://doi.org/10.1038/356060a0

Chung, S. H., Takai, Y., & Holz, R. W. (1995). Evidence that the Rab3a-binding protein, rabphilin3a, enhances regulated secretion. Studies in adrenal chromaffin cells. The Journal of biological chemistry, 270(28), 16714–16718. https://doi.org/10.1074/jbc.270.28.16714

Clayton, E. L., Evans, G. J., & Cousin, M. A. (2008). Bulk synaptic vesicle endocytosis is rapidly triggered during strong stimulation. The Journal of neuroscience: the official journal of the Society for Neuroscience, 28(26), 6627–6632. https://doi.org/10.1523/JNEUROSCI.1445-08.2008

Collins, B. M., McCoy, A. J., Kent, H. M., Evans, P. R., & Owen, D. J. (2002). Molecular architecture and functional model of the endocytic AP2 complex. Cell, 109(4), 523–535. https://doi.org/10.1016/s0092-8674(02)00735-3

Conibear, E., Tam, Y.Y.C. (2009). The Endocytic Pathway. In: Trafficking Inside Cells. Molecular Biology Intelligence Unit. Springer, New York, NY. https://doi.org/10.1007/978-0-387-93877-6_4

Conner, S. D., & Schmid, S. L. (2003). Regulated portals of entry into the cell. Nature, 422(6927), 37–44. https://doi.org/10.1038/nature01451

Coupland R. E. (1965). (Electron microscopic observations on the structure of the rat adrenal medulla. I. The ulstrastructure and organization of the chromaffin cells in the normal adrenal medulla. Journal of anatomy, 99(Pt 2), 231–254. https://pubmed.ncbi.nlm.nih.gov/14330730/

Cremona, O., Di Paolo, G., Wenk, M. R., Lüthi, A., Kim, W. T., Takei, K., Daniell, L., Nemoto, Y., Shears, S. B., Flavell, R. A., McCormick, D. A., & De Camilli, P. (1999). Essential role of phosphoinositide metabolism in synaptic vesicle recycling. Cell, 99(2), 179–188. https://doi.org/10.1016/s0092-8674(00)81649-9

Dahl, R., & Staehelin, L. A. (1989). High-pressure freezing for the preservation of biological structure: theory and practice. Journal of electron microscopy technique, 13(3), 165–174. https://doi.org/10.1002/jemt.1060130305

De Camilli, P., & Jahn, R. (1990). Pathways to regulated exocytosis in neurons. Annual review of physiology, 52, 625–645. https://doi.org/10.1146/annurev.ph.52.030190.003205

De Camilli, P., & Takei, K. (1996). Molecular mechanisms in synaptic vesicle endocytosis and recycling. Neuron, 16(3), 481–486. https://doi.org/10.1016/s0896-6273(00)80068-9

de Diego, A. M. G., Ortega-Cruz, D., & García, A. G. (2020). Disruption of Exocytosis in Sympathoadrenal Chromaffin Cells from Mouse Models of Neurodegenerative Diseases. International journal of molecular sciences, 21(6), 1946. https://doi.org/10.3390/ijms21061946

De Robertis, E.D., & Sabatini, D. D. (1960). Submicroscopic analysis of the secretory process in the adrenal medulla. Federation proceedings, 19(Suppl 5), 70–78. https://pubmed.ncbi.nlm.nih.gov/13720813/

de Wit, H., Cornelisse, L. N., Toonen, R. F., & Verhage, M. (2006). Docking of secretory vesicles is syntaxin dependent. PloS one, 1(1), e126. https://doi.org/10.1371/journal.pone.0000126

de Wit, H., Walter, A. M., Milosevic, I., Gulyás-Kovács, A., Riedel, D., Sørensen, J. B., & Verhage, M. (2009). Synaptotagmin-1 docks secretory vesicles to syntaxin-1/SNAP-25 acceptor complexes. Cell, 138(5), 935–946. https://doi.org/10.1016/j.cell.2009.07.027

Dembla, E., & Becherer, U. (2021). Biogenesis of large dense core vesicles in mouse chromaffin cells. Traffic (Copenhagen, Denmark), 22(3), 78–93. https://doi.org/10.1111/tra.12783

Díaz-Flores, L., Gutiérrez, R., Varela, H., Valladares, F., Alvarez-Argüelles, H., & Borges, R. (2008). Histogenesis and morphofunctional characteristics of chromaffin cells. Acta physiologica (Oxford, England), 192(2), 145–163. https://doi.org/10.1111/j.1748-1716.2007.01811.x

Diril, M. K., Wienisch, M., Jung, N., Klingauf, J., & Haucke, V. (2006). Stonin 2 is an AP-2-dependent endocytic sorting adaptor for synaptotagmin internalization and recycling. Developmental cell, 10(2), 233–244. https://doi.org/10.1016/j.devcel.2005.12.011

Dittman, J. S., & Regehr, W. G. (1998). Calcium dependence and recovery kinetics of presynaptic depression at the climbing fiber to Purkinje cell synapse. The Journal of neuroscience: the official journal of the Society for Neuroscience, 18(16), 6147–6162. https://doi.org/10.1523/JNEUROSCI.18-16-06147.1998

Duan, K., Yu, X., Zhang, C., & Zhou, Z. (2003). Control of secretion by temporal patterns of action potentials in adrenal chromaffin cells. The Journal of neuroscience: the official journal of the Society for Neuroscience, 23(35), 11235–11243. https://doi.org/10.1523/JNEUROSCI.23-35-11235.2003

Dulubova, I., Khvotchev, M., Liu, S., Huryeva, I., Südhof, T. C., & Rizo, J. (2007). Munc18-1 binds directly to the neuronal SNARE complex. Proceedings of the National Academy of Sciences of the United States of America, 104(8), 2697–2702. https://doi.org/10.1073/pnas.0611318104

Dulubova, I., Sugita, S., Hill, S., Hosaka, M., Fernandez, I., Südhof, T. C., & Rizo, J. (1999). A conformational switch in syntaxin during exocytosis: role of munc18. The EMBO journal, 18(16), 4372–4382. https://doi.org/10.1093/emboj/18.16.4372

Echarri, A., Muriel, O., Pavón, D. M., Azegrouz, H., Escolar, F., Terrón, M. C., Sanchez-Cabo, F., Martínez, F., Montoya, M. C., Llorca, O., & Del Pozo, M. A. (2012). Caveolar domain organization and trafficking is regulated by Abl kinases and mDia1. Journal of cell science, 125(Pt 13), 3097–3113. https://doi.org/10.1242/jcs.090134

Edeling, M. A., Smith, C., & Owen, D. (2006). Life of a clathrin coat: insights from clathrin and AP structures. Nature reviews. Molecular cell biology, 7(1), 32–44. https://doi.org/10.1038/nrm1786

Eranko, O., & Hanninen, L. (1960). Electron microscopic observations on the adrenal medulla of the rat. Acta pathologica et microbiologica Scandinavica, 50, 126–132. https://pubmed.ncbi.nlm.nih.gov/13697038/

Falcone, S., Cocucci, E., Podini, P., Kirchhausen, T., Clementi, E., & Meldolesi, J. (2006). Macropinocytosis: regulated coordination of endocytic and exocytic membrane traffic events. Journal of cell science, 119(Pt 22), 4758–4769. https://doi.org/10.1242/jcs.03238

Ferguson, S. M., & De Camilli, P. (2012). Dynamin, a membrane-remodelling GTPase. Nature reviews. Molecular cell biology, 13(2), 75–88. https://doi.org/10.1038/nrm3266

Ferguson, S. M., Brasnjo, G., Hayashi, M., Wölfel, M., Collesi, C., Giovedi, S., Raimondi, A., Gong, L. W., Ariel, P., Paradise, S., O'toole, E., Flavell, R., Cremona, O., Miesenböck, G., Ryan, T. A., & De Camilli, P. (2007). A selective activity-dependent requirement for dynamin 1 in synaptic vesicle endocytosis. Science (New York, N.Y.), 316(5824), 570–574. https://doi.org/10.1126/science.1140621

Fernández-Busnadiego, R., Schrod, N., Kochovski, Z., Asano, S., Vanhecke, D., Baumeister, W., & Lucic, V. (2011). Insights into the molecular organization of the neuron by cryo-electron

tomography. Journal of electron microscopy, 60 Suppl 1, S137–S148. https://doi.org/10.1093/jmicro/dfr018

Fesce, R., Grohovaz, F., Valtorta, F., & Meldolesi, J. (1994). Neurotransmitter release: fusion or 'kiss-and-run'?. Trends in cell biology, 4(1), 1–4. https://doi.org/10.1016/0962-8924(94)90025-6

Flannagan, R. S., Jaumouillé, V., & Grinstein, S. (2012). The cell biology of phagocytosis. Annual review of pathology, 7, 61–98. https://doi.org/10.1146/annurev-pathol-011811-132445

Ford, M. G., Mills, I. G., Peter, B. J., Vallis, Y., Praefcke, G. J., Evans, P. R., & McMahon, H. T. (2002). Curvature of clathrin-coated pits driven by epsin. Nature, 419(6905), 361–366. https://doi.org/10.1038/nature01020

Ford, M. G., Pearse, B. M., Higgins, M. K., Vallis, Y., Owen, D. J., Gibson, A., Hopkins, C. R., Evans, P. R., & McMahon, H. T. (2001). Simultaneous binding of PtdIns(4,5)P2 and clathrin by AP180 in the nucleation of clathrin lattices on membranes. Science (New York, N.Y.), 291(5506), 1051–1055. https://doi.org/10.1126/science.291.5506.1051

Frotscher, M., Zhao, S., Graber, W., Drakew, A., & Studer, D. (2007). New ways of looking at synapses. Histochemistry and cell biology, 128(2), 91–96. https://doi.org/10.1007/s00418-007-0305-7

Fulop, T., Radabaugh, S., & Smith, C. (2005). Activity-dependent differential transmitter release in mouse adrenal chromaffin cells. The Journal of neuroscience: the official journal of the Society for Neuroscience, 25(32), 7324–7332. https://doi.org/10.1523/JNEUROSCI.2042-05.2005

Furuya, S., Edwards, C., & Ornberg, R. L. (1989). Exocytosis of bovine chromaffin granules in Ficoll captured by rapid freezing. Journal of electron microscopy, 38(2), 143–147. https://pubmed.ncbi.nlm.nih.gov/2769145/

Gaffaney, J. D., Dunning, F. M., Wang, Z., Hui, E., & Chapman, E. R. (2008). Synaptotagmin C2B domain regulates Ca2+-triggered fusion in vitro: critical residues revealed by scanning alanine mutagenesis. The Journal of biological chemistry, 283(46), 31763–31775. https://doi.org/10.1074/jbc.M803355200

Gandasi, N., Barg, S. Contact-induced clustering of syntaxin and munc18 docks secretory granules at the exocytosis site. Nat Commun 5, 3914 (2014). https://doi.org/10.1038/ncomms4914

Ge, L., Shin, W., Arpino, G., Wei, L., Chan, C. Y., Bleck, C. K. E., Zhao, W., & Wu, L. G. (2022). Sequential compound fusion and kiss-and-run mediate exo- and endocytosis in excitable cells. Science advances, 8(24), eabm6049. https://doi.org/10.1126/sciadv.abm6049

Gerachshenko, T., Blackmer, T., Yoon, E. J., Bartleson, C., Hamm, H. E., & Alford, S. (2005). Gbetagamma acts at the C terminus of SNAP-25 to mediate presynaptic inhibition. Nature neuroscience, 8(5), 597–605. https://doi.org/10.1038/nn1439

Gerber, S. H., Rah, J. C., Min, S. W., Liu, X., de Wit, H., Dulubova, I., Meyer, A. C., Rizo, J., Arancillo, M., Hammer, R. E., Verhage, M., Rosenmund, C., & Südhof, T. C. (2008). Conformational switch of syntaxin-1 controls synaptic vesicle fusion. Science (New York, N.Y.), 321(5895), 1507–1510. https://doi.org/10.1126/science.1163174

Gillespie J. I. (1979). The effect of repetitive stimulation on the passive electrical properties of the presynaptic terminal of the squid giant synapse. Proceedings of the Royal Society of London. Series B, Biological sciences, 206(1164), 293–306. https://doi.org/10.1098/rspb.1979.0106

Gingrich, K. J., & Byrne, J. H. (1985). Simulation of synaptic depression, posttetanic potentiation, and presynaptic facilitation of synaptic potentials from sensory neurons mediating gill-withdrawal reflex in Aplysia. Journal of neurophysiology, 53(3), 652–669. https://doi.org/10.1152/jn.1985.53.3.652

Gomis, A., Burrone, J., & Lagnado, L. (1999). Two actions of calcium regulate the supply of releasable vesicles at the ribbon synapse of retinal bipolar cells. The Journal of neuroscience: the official journal of the Society for Neuroscience, 19(15), 6309–6317. https://doi.org/10.1523/JNEUROSCI.19-15-06309.1999

Gonon, F., Msghina, M., & Stjärne, L. (1993). Kinetics of noradrenaline released by sympathetic nerves. Neuroscience, 56(3), 535–538. https://doi.org/10.1016/0306-4522(93)90354-i

González-Hernández, J. A., Bornstein, S. R., Ehrhart-Bornstein, M., Geschwend, J. E., Adler, G., & Scherbaum, W. A. (1994). Macrophages within the human adrenal gland. Cell and tissue research, 278(2), 201–205. https://doi.org/10.1007/BF00414161

Gowrisankaran, S., Houy, S., Del Castillo, J. G. P., Steubler, V., Gelker, M., Kroll, J., Pinheiro, P. S., Schwitters, D., Halbsgut, N., Pechstein, A., van Weering, J. R. T., Maritzen, T., Haucke, V., Raimundo, N., Sørensen, J. B., & Milosevic, I. (2020). Endophilin-A coordinates priming and fusion of neurosecretory vesicles via intersectin. Nature communications, 11(1), 1266. https://doi.org/10.1038/s41467-020-14993-8

Guan, R., Dai, H., Harrison, S. C., & Kirchhausen, T. (2010). Structure of the PTEN-like region of auxilin, a detector of clathrin-coated vesicle budding. Structure (London, England: 1993), 18(9), 1191–1198. https://doi.org/10.1016/j.str.2010.06.016

Guarina, L., Vandael, D. H., Carabelli, V., & Carbone, E. (2017). Low pHo boosts burst firing and catecholamine release by blocking TASK-1 and BK channels while preserving Cav1 channels in mouse chromaffin cells. The Journal of physiology, 595(8), 2587–2609. https://doi.org/10.1113/JP273735

Gulyás-Kovács, A., de Wit, H., Milosevic, I., Kochubey, O., Toonen, R., Klingauf, J., Verhage, M., & Sørensen, J. B. (2007). Munc18-1: sequential interactions with the fusion machinery stimulate vesicle docking and priming. The Journal of neuroscience: the official journal of the Society for Neuroscience, 27(32), 8676–8686. https://doi.org/10.1523/JNEUROSCI.0658-07.2007

Hammarlund, M., Palfreyman, M. T., Watanabe, S., Olsen, S., & Jorgensen, E. M. (2007). Open syntaxin docks synaptic vesicles. PLoS biology, 5(8), e198. https://doi.org/10.1371/journal.pbio.0050198

Harata, N. C., Aravanis, A. M., & Tsien, R. W. (2006). Kiss-and-run and full-collapse fusion as modes of exo-endocytosis in neurosecretion. Journal of neurochemistry, 97(6), 1546–1570. https://doi.org/10.1111/j.1471-4159.2006.03987.x

Hayashi, M., Raimondi, A., O'Toole, E., Paradise, S., Collesi, C., Cremona, O., Ferguson, S. M., & De Camilli, P. (2008). Cell- and stimulus-dependent heterogeneity of synaptic vesicle endocytic recycling mechanisms revealed by studies of dynamin 1-null neurons. Proceedings

of the National Academy of Sciences of the United States of America, 105(6), 2175–2180. https://doi.org/10.1073/pnas.0712171105

Helge Gad, Peter Löw, Elena Zotova, Lennart Brodin, Oleg Shupliakov, (1998). Dissociation between Ca2+-Triggered Synaptic Vesicle Exocytosis and Clathrin-Mediated Endocytosis at a Central Synapse, Neuron, Volume 21, Issue 3, 1998, Pages 607-616, ISSN 0896-6273, https://doi.org/10.1016/S0896-6273(00)80570-X.

Henley, J. R., Krueger, E. W., Oswald, B. J., & McNiven, M. A. (1998). Dynamin-mediated internalization of caveolae. The Journal of cell biology, 141(1), 85–99. https://doi.org/10.1083/jcb.141.1.85

Henne, W. M., Boucrot, E., Meinecke, M., Evergren, E., Vallis, Y., Mittal, R., & McMahon, H. T. (2010). FCHo proteins are nucleators of clathrin-mediated endocytosis. Science (New York, N.Y.), 328(5983), 1281–1284. https://doi.org/10.1126/science.1188462

Hinshaw J. E. (2000). Dynamin and its role in membrane fission. Annual review of cell and developmental biology, 16, 483–519. https://doi.org/10.1146/annurev.cellbio.16.1.483

Hiroyuki Kabayama, Takeshi Nakamura, Makoto Takeuchi, Hirohide Iwasaki, Masahiko Taniguchi, Naoko Tokushige, Katsuhiko Mikoshiba, (2009). Ca2+ induces macropinocytosis via F-actin depolymerization during growth cone collapse, Molecular and Cellular Neuroscience, Volume 40, Issue 1, 2009, Pages 27-38, ISSN 1044-7431, https://doi.org/10.1016/j.mcn.2008.08.009.

Hodgkin, A. L., & Huxley, A. F. (1952). A quantitative description of membrane current and its application to conduction and excitation in nerve. The Journal of physiology, 117(4), 500–544. https://doi.org/10.1113/jphysiol.1952.sp004764

Holroyd, P., Lang, T., Wenzel, D., De Camilli, P., & Jahn, R. (2002). Imaging direct, dynamin-dependent recapture of fusing secretory granules on plasma membrane lawns from PC12 cells. Proceedings of the National Academy of Sciences of the United States of America, 99(26), 16806–16811. https://doi.org/10.1073/pnas.222677399

https://www.heka.com/

Imig, C., & Cooper, B. H. (2017). 3D Analysis of Synaptic Ultrastructure in Organotypic Hippocampal Slice Culture by High-Pressure Freezing and Electron Tomography. Methods in molecular biology (Clifton, N.J.), 1538, 215–231. https://doi.org/10.1007/978-1-4939-6688-2_15

Imig, C., López-Murcia, F. J., Maus, L., García-Plaza, I. H., Mortensen, L. S., Schwark, M., Schwarze, V., Angibaud, J., Nägerl, U. V., Taschenberger, H., Brose, N., & Cooper, B. H. (2020). Ultrastructural Imaging of Activity-Dependent Synaptic Membrane-Trafficking Events in Cultured Brain Slices. Neuron, 108(5), 843–860.e8. https://doi.org/10.1016/j.neuron.2020.09.004

Imig, C., Min, S. W., Krinner, S., Arancillo, M., Rosenmund, C., Südhof, T. C., Rhee, J., Brose, N., & Cooper, B. H. (2014). The morphological and molecular nature of synaptic vesicle priming at presynaptic active zones. Neuron, 84(2), 416–431. https://doi.org/10.1016/j.neuron.2014.10.009

Ishibashi, H., Moorhouse, A.J., Nabekura, J. (2012). Perforated Whole-Cell Patch-Clamp Technique: A User's Guide. In: Okada, Y. (eds) Patch Clamp Techniques. Springer Protocols Handbooks. Springer, Tokyo. https://doi.org/10.1007/978-4-431-53993-3_4

Itoh, T., & De Camilli, P. (2006). BAR, F-BAR (EFC) and ENTH/ANTH domains in the regulation of membrane-cytosol interfaces and membrane curvature. Biochimica et biophysica acta, 1761(8), 897–912. https://doi.org/10.1016/j.bbalip.2006.06.015

Jack T.H. Wang, Rohan D. Teasdale, David Liebl, (2014). Macropinosome quantitation assay, MethodsX, Volume 1, 2014, Pages 36-41, ISSN 2215-0161, https://doi.org/10.1016/j.mex.2014.05.002.

Jaffe, L. A., Hagiwara, S., & Kado, R. T. (1978). The time course of cortical vesicle fusion in sea urchin eggs observed as membrane capacitance changes. Developmental biology, 67(1), 243–248. https://doi.org/10.1016/0012-1606(78)90314-7

Jahn, R., & Fasshauer, D. (2012). Molecular machines governing exocytosis of synaptic vesicles. Nature, 490(7419), 201–207. https://doi.org/10.1038/nature11320

James Rae, Kim Cooper, Peter Gates, Mitchell Watsky, (1991). Low access resistance perforated patch recordings using amphotericin B, Journal of Neuroscience Methods, Volume 37, Issue 1, 1991, Pages 15-26, ISSN 0165-0270, https://doi.org/10.1016/0165-0270(91)90017-T.

Josette Zaklit, Gale L. Craviso, Normand Leblanc, P. Thomas Vernier, Esin B. Sözer, 2-ns Electrostimulation of Ca2+ Influx into Chromaffin Cells: Rapid Modulation by Field Reversal, Biophysical Journal, Volume 120, Issue 3, 2021, Pages 556-567, ISSN 0006-3495, https://doi.org/10.1016/j.bpj.2020.12.017.

Kaeser, P. S., & Regehr, W. G. (2014). Molecular mechanisms for synchronous, asynchronous, and spontaneous neurotransmitter release. Annual review of physiology, 76, 333–363. https://doi.org/10.1146/annurev-physiol-021113-170338

Kesavan, J., Borisovska, M., & Bruns, D. (2007). v-SNARE actions during Ca(2+)-triggered exocytosis. Cell, 131(2), 351–363. https://doi.org/10.1016/j.cell.2007.09.025

Kevin D. Gillis, Rotraut Mößner, Erwin Neher, (1996). Protein Kinase C Enhances Exocytosis from Chromaffin Cells by Increasing the Size of the Readily Releasable Pool of Secretory Granules, Neuron, Volume 16, Issue 6, 1996, Pages 1209-1220, ISSN 0896-6273, https://doi.org/10.1016/S0896-6273(00)80147-6.

Khvotchev, M., Dulubova, I., Sun, J., Dai, H., Rizo, J., & Südhof, T. C. (2007). Dual modes of Munc18-1/SNARE interactions are coupled by functionally critical binding to syntaxin-1 N terminus. The Journal of neuroscience: the official journal of the Society for Neuroscience, 27(45), 12147–12155. https://doi.org/10.1523/JNEUROSCI.3655-07.2007

Kim, T., Gondré-Lewis, M. C., Arnaoutova, I., & Loh, Y. P. (2006). Dense-core secretory granule biogenesis. Physiology (Bethesda, Md.), 21, 124–133. https://doi.org/10.1152/physiol.00043.2005

Kirchhausen T. (2000). Clathrin. Annual review of biochemistry, 69, 699–727. https://doi.org/10.1146/annurev.biochem.69.1.699

Kobayashi, S., & Coupland, R. E. (1993). Morphological aspects of chromaffin tissue: the differential fixation of adrenaline and noradrenaline. Journal of anatomy, 183 (Pt 2) (Pt 2), 223–235, https://www.ncbi.nlm.nih.gov/pmc/articles/PMC1259904/

Koch, H., Hofmann, K., & Brose, N. (2000). Definition of Munc13-homology-domains and characterization of a novel ubiquitously expressed Munc13 isoform. The Biochemical journal, 349(Pt 1), 247–253. https://doi.org/10.1042/0264-6021:3490247

Koh, T. W., & Bellen, H. J. (2003). Synaptotagmin I, a Ca2+ sensor for neurotransmitter release. Trends in neurosciences, 26(8), 413–422. https://doi.org/10.1016/S0166-2236(03)00195-4

Kononenko, N. L., & Haucke, V. (2015). Molecular mechanisms of presynaptic membrane retrieval and synaptic vesicle reformation. Neuron, 85(3), 484–496. https://doi.org/10.1016/j.neuron.2014.12.016

Koval, L. M., Yavorskaya, E. N., & Lukyanetz, E. A. (2001). Electron microscopic evidence for multiple types of secretory vesicles in bovine chromaffin cells. General and comparative endocrinology, 121(3), 261–277. https://doi.org/10.1006/gcen.2000.7592

Kremer, J. R., Mastronarde, D. N., & McIntosh, J. R. (1996). Computer visualization of three-dimensional image data using IMOD. Journal of structural biology, 116(1), 71–76. https://doi.org/10.1006/jsbi.1996.0013

Kusick, G.F., Chin, M., Raychaudhuri, S. et al. (2020). Synaptic vesicles transiently dock to refill release sites. Nat Neurosci 23, 1329–1338 (2020). https://doi.org/10.1038/s41593-020-00716-1

Kwun Nok M Man, Cordelia Imig, Alexander M Walter, Paulo S Pinheiro, David R Stevens, Jens Rettig, Jakob B Sørensen, Benjamin H Cooper, Nils Brose, Sonja M Wojcik (2015) Identification of a Munc13-sensitive step in chromaffin cell large dense-core vesicle exocytosis eLife 4:e10635 https://doi.org/10.7554/eLife.10635

Lever J.D. (1955). Electron microscopic observations on the normal and denervated adrenal medulla of the rat. Endocrinology, 57(5), 621–635. https://doi.org/10.1210/endo-57-5-621

Lin, X. P., Mintern, J. D., & Gleeson, P. A. (2020). Macropinocytosis in Different Cell Types: Similarities and Differences. Membranes, 10(8), 177. https://doi.org/10.3390/membranes10080177

Lindau, M., Neher, E. Patch-clamp techniques for time-resolved capacitance measurements in single cells. Pflugers Arch. 411, 137–146 (1988). https://doi.org/10.1007/BF00582306

Lingle, C. J., Martinez-Espinosa, P. L., Guarina, L., & Carbone, E. (2018). Roles of Na+, Ca2+, and K+ channels in the generation of repetitive firing and rhythmic bursting in adrenal chromaffin cells. Pflugers Archiv : European journal of physiology, 470(1), 39–52. https://doi.org/10.1007/s00424-017-2048-1

Liu, Y., Schirra, C., Edelmann, L., Matti, U., Rhee, J., Hof, D., Bruns, D., Brose, N., Rieger, H., Stevens, D. R., & Rettig, J. (2010). Two distinct secretory vesicle-priming steps in adrenal chromaffin cells. The Journal of cell biology, 190(6), 1067–1077. https://doi.org/10.1083/jcb.201001164

Liu, Y., Schirra, C., Stevens, D. R., Matti, U., Speidel, D., Hof, D., Bruns, D., Brose, N., & Rettig, J. (2008). CAPS facilitates filling of the rapidly releasable pool of large dense-core vesicles. The Journal of neuroscience: the official journal of the Society for Neuroscience, 28(21), 5594–5601. https://doi.org/10.1523/JNEUROSCI.5672-07.2008

Llobet, A., Beaumont, V., & Lagnado, L. (2003). Real-time measurement of exocytosis and endocytosis using interference of light. Neuron, 40(6), 1075–1086. https://doi.org/10.1016/s0896-6273(03)00765-7

Lou, X., Korogod, N., Brose, N., & Schneggenburger, R. (2008). Phorbol esters modulate spontaneous and Ca2+-evoked transmitter release via acting on both Munc13 and protein

kinase C. The Journal of neuroscience: the official journal of the Society for Neuroscience, 28(33), 8257–8267. https://doi.org/10.1523/JNEUROSCI.0550-08.2008

Luft J. H. (1961). Improvements in epoxy resin embedding methods. The Journal of biophysical and biochemical cytology, 9(2), 409–414. https://doi.org/10.1083/jcb.9.2.409

Lynch, K. J., Skalli, O., & Sabri, F. (2018). Growing Neural PC-12 Cell on Crosslinked Silica Aerogels Increases Neurite Extension in the Presence of an Electric Field. Journal of functional biomaterials, 9(2), 30. https://doi.org/10.3390/jfb9020030

Lynch, K. L., Gerona, R. R., Larsen, E. C., Marcia, R. F., Mitchell, J. C., & Martin, T. F. (2007). Synaptotagmin C2A loop 2 mediates Ca2+-dependent SNARE interactions essential for Ca2+-triggered vesicle exocytosis. Molecular biology of the cell, 18(12), 4957–4968. https://doi.org/10.1091/mbc.e07-04-0368

Madisen, L., Mao, T., Koch, H., Zhuo, J. M., Berenyi, A., Fujisawa, S., Hsu, Y. W., Garcia, A. J., 3rd, Gu, X., Zanella, S., Kidney, J., Gu, H., Mao, Y., Hooks, B. M., Boyden, E. S., Buzsáki, G., Ramirez, J. M., Jones, A. R., Svoboda, K., Han, X., … Zeng, H. (2012). A toolbox of Cre-dependent optogenetic transgenic mice for light-induced activation and silencing. Nature neuroscience, 15(5), 793–802. https://doi.org/10.1038/nn.3078

Maria Eleni Kastriti, Polina Kameneva, Igor Adameyko, (2020). Stem cells, evolutionary aspects and pathology of the adrenal medulla: A new developmental paradigm, Molecular and Cellular Endocrinology, Volume 518, 2020,110998, ISSN 0303-7207, https://doi.org/10.1016/j.mce.2020.110998.

Marsh, M., & McMahon, H. T. (1999). The structural era of endocytosis. Science (New York, N.Y.), 285(5425), 215–220. https://doi.org/10.1126/science.285.5425.215

Martinez-Espinosa, P. L., Yang, C., Gonzalez-Perez, V., Xia, X. M., & Lingle, C. J. (2014). Knockout of the BK β2 subunit abolishes inactivation of BK currents in mouse adrenal chromaffin cells and results in slow-wave burst activity. The Journal of general physiology, 144(4), 275–295. https://doi.org/10.1085/jgp.201411253

Maus, L., Lee, C., Altas, B., Sertel, S. M., Weyand, K., Rizzoli, S. O., Rhee, J., Brose, N., Imig, C., & Cooper, B. H. (2020). Ultrastructural Correlates of Presynaptic Functional Heterogeneity in Hippocampal Synapses. Cell reports, 30(11), 3632–3643.e8. https://doi.org/10.1016/j.celrep.2020.02.083

Maycox, P. R., Link, E., Reetz, A., Morris, S. A., & Jahn, R. (1992). Clathrin-coated vesicles in nervous tissue are involved primarily in synaptic vesicle recycling. The Journal of cell biology, 118(6), 1379–1388. https://doi.org/10.1083/jcb.118.6.1379

Mercer, J., & Helenius, A. (2012). Gulping rather than sipping: macropinocytosis as a way of virus entry. Current opinion in microbiology, 15(4), 490–499. https://doi.org/10.1016/j.mib.2012.05.016

Merighi A. (2018). Costorage of High Molecular Weight Neurotransmitters in Large Dense Core Vesicles of Mammalian Neurons. Frontiers in cellular neuroscience, 12, 272. https://doi.org/10.3389/fncel.2018.00272

Milosevic I. (2018). Revisiting the Role of Clathrin-Mediated Endoytosis in Synaptic Vesicle Recycling. Frontiers in cellular neuroscience, 12, 27. https://doi.org/10.3389/fncel.2018.00027

Moor, H. (1987). Theory and Practice of High Pressure Freezing. In: Steinbrecht, R.A., Zierold, K. (eds) Cryotechniques in Biological Electron Microscopy. Springer, Berlin, Heidelberg. https://doi.org/10.1007/978-3-642-72815-0_8

Mosharov, E. V., & Sulzer, D. (2005). Analysis of exocytotic events recorded by amperometry. Nature methods, 2(9), 651–658. https://doi.org/10.1038/nmeth782

Mykoniatis, A., Shen, L., Fedor-Chaiken, M., Tang, J., Tang, X., Worrell, R. T., Delpire, E., Turner, J. R., Matlin, K. S., Bouyer, P., & Matthews, J. B. (2010). Phorbol 12-myristate 13-acetate-induced endocytosis of the Na-K-2Cl cotransporter in MDCK cells is associated with a clathrin-dependent pathway. American journal of physiology. Cell physiology, 298(1), C85–C97. https://doi.org/10.1152/ajpcell.00118.2009

N. Hassan, I. Chatterjee, N. G. Publicover and G. L. Craviso, "Mapping membrane-potential perturbations of chromaffin cells exposed to electric fields," in IEEE Transactions on Plasma Science, vol. 30, no. 4, pp. 1516-1524, Aug. 2002, DOI:10.1109/TPS.2002.804210

Nagy, G., Kim, J. H., Pang, Z. P., Matti, U., Rettig, J., Südhof, T. C., & Sørensen, J. B. (2006). Different effects on fast exocytosis induced by synaptotagmin 1 and 2 isoforms and abundance but not by phosphorylation. The Journal of neuroscience: the official journal of the Society for Neuroscience, 26(2), 632–643. https://doi.org/10.1523/JNEUROSCI.2589-05.2006

Neher E. (1998). Vesicle pools and Ca2+ microdomains: new tools for understanding their roles in neurotransmitter release. Neuron, 20(3), 389–399. https://doi.org/10.1016/s0896-6273(00)80983-6

Neher, E., & Marty, A. (1982). Discrete changes of cell membrane capacitance observed under conditions of enhanced secretion in bovine adrenal chromaffin cells. Proceedings of the National Academy of Sciences of the United States of America, 79(21), 6712–6716. https://doi.org/10.1073/pnas.79.21.6712

Neher, E., & Penner, R. (1994). Mice sans synaptotagmin. Nature, 372(6504), 316–317. https://doi.org/10.1038/372316a0

Oh, P., McIntosh, D. P., & Schnitzer, J. E. (1998). Dynamin at the neck of caveolae mediates their budding to form transport vesicles by GTP-driven fission from the plasma membrane of endothelium. The Journal of cell biology, 141(1), 101–114. https://doi.org/10.1083/jcb.141.1.101

Ohta, T., Wakade, A. R., Nakazato, Y., & Ito, S. (2001). Ca(2+)-dependent K(+) current and exocytosis in responses to caffeine and muscarine in voltage-clamped guinea-pig adrenal chromaffin cells. Journal of neurochemistry, 78(6), 1243–1255. https://doi.org/10.1046/j.1471-4159.2001.00502.x

Oliver, J. D., 3rd, Anderson, S., Troy, J. L., Brenner, B. M., & Deen, W. H. (1992). Determination of glomerular size-selectivity in the normal rat with Ficoll. Journal of the American Society of Nephrology: JASN, 3(2), 214–228. https://doi.org/10.1681/ASN.V32214

Osetsky A. I. (2011). Thermodynamic aspects of cluster crystallization in cryoprotective solutions. Cryo letters, 32(3), 216–224. https://pubmed.ncbi.nlm.nih.gov/21766151/

Owen, D. J., Collins, B. M., & Evans, P. R. (2004). Adaptors for clathrin coats: structure and function. Annual review of cell and developmental biology, 20, 153–191. https://doi.org/10.1146/annurev.cellbio.20.010403.104543

Paillart, C., Li, J., Matthews, G., & Sterling, P. (2003). Endocytosis and vesicle recycling at a ribbon synapse. The Journal of neuroscience: the official journal of the Society for Neuroscience, 23(10), 4092–4099. https://doi.org/10.1523/JNEUROSCI.23-10-04092.2003

Parsons, T. D., Coorssen, J. R., Horstmann, H., & Almers, W. (1995). Docked granules, the exocytic burst, and the need for ATP hydrolysis in endocrine cells. Neuron, 15(5), 1085–1096. https://doi.org/10.1016/0896-6273(95)90097-7

Pegg D. E. (1972). Perfusion of rabbit kidneys with cryoprotective agents. Cryobiology, 9(5), 411–419. https://doi.org/10.1016/0011-2240(72)90158-7

Pelkmans, L., & Helenius, A. (2002). Endocytosis via caveolae. Traffic (Copenhagen, Denmark), 3(5), 311–320. https://doi.org/10.1034/j.1600-0854.2002.30501.x

Pelkmans, L., Kartenbeck, J., & Helenius, A. (2001). Caveolar endocytosis of simian virus 40 reveals a new two-step vesicular-transport pathway to the ER. Nature cell biology, 3(5), 473–483. https://doi.org/10.1038/35074539

Plattner, H., Artalejo, A. R., & Neher, E. (1997). Ultrastructural organization of bovine chromaffin cell cortex-analysis by cryofixation and morphometry of aspects pertinent to exocytosis. The Journal of cell biology, 139(7), 1709–1717. https://doi.org/10.1083/jcb.139.7.1709

Pocotte, S. L., Frye, R. A., Senter, R. A., TerBush, D. R., Lee, S. A., & Holz, R. W. (1985). Effects of phorbol ester on catecholamine secretion and protein phosphorylation in adrenal medullary cell cultures. Proceedings of the National Academy of Sciences of the United States of America, 82(3), 930–934. https://doi.org/10.1073/pnas.82.3.930

Ratai, O., Schirra, C., Rajabov, E., Brunk, I., Ahnert-Hilger, G., Chitirala, P., Becherer, U., Stevens, D. R., & Rettig, J. (2019). An Alternative Exon of CAPS2 Influences Catecholamine Loading into LDCVs of Chromaffin Cells. The Journal of neuroscience: the official journal of the Society for Neuroscience, 39(1), 18–27. https://doi.org/10.1523/JNEUROSCI.2040-18.2018

Razani, B., Combs, T. P., Wang, X. B., Frank, P. G., Park, D. S., Russell, R. G., Li, M., Tang, B., Jelicks, L. A., Scherer, P. E., & Lisanti, M. P. (2002). Caveolin-1-deficient mice are lean, resistant to diet-induced obesity, and show hypertriglyceridemia with adipocyte abnormalities. The Journal of biological chemistry, 277(10), 8635–8647. https://doi.org/10.1074/jbc.M110970200

Renard, H. F., Simunovic, M., Lemière, J., Boucrot, E., Garcia-Castillo, M. D., Arumugam, S., Chambon, V., Lamaze, C., Wunder, C., Kenworthy, A. K., Schmidt, A. A., McMahon, H. T., Sykes, C., Bassereau, P., & Johannes, L. (2015). Endophilin-A2 functions in membrane scission in clathrin-independent endocytosis. Nature, 517(7535), 493–496. https://doi.org/10.1038/nature14064

Rettig, J., & Neher, E. (2002). Emerging roles of presynaptic proteins in Ca++-triggered exocytosis. Science (New York, N.Y.), 298(5594), 781–785. https://doi.org/10.1126/science.1075375

Rhee, J. S., Betz, A., Pyott, S., Reim, K., Varoqueaux, F., Augustin, I., Hesse, D., Südhof, T. C., Takahashi, M., Rosenmund, C., & Brose, N. (2002). Beta phorbol ester- and diacylglycerol-induced augmentation of transmitter release is mediated by Munc13s and not by PKCs. Cell, 108(1), 121–133. https://doi.org/10.1016/s0092-8674(01)00635-3

Richmond, J. E., Davis, W. S., & Jorgensen, E. M. (1999). UNC-13 is required for synaptic vesicle fusion in C. elegans. Nature neuroscience, 2(11), 959–964. https://doi.org/10.1038/14755

Rigual, R., Montero, M., Rico, A. J., Prieto-Lloret, J., Alonso, M. T., & Alvarez, J. (2002). Modulation of secretion by the endoplasmic reticulum in mouse chromaffin cells. The European journal of neuroscience, 16(9), 1690–1696. https://doi.org/10.1046/j.1460-9568.11-2.02244.x

Robert H Chow, Jürgen Klingauf, Christian Heinemann, Robert S Zucker, Erwin Neher. (1996). Mechanisms Determining the Time Course of Secretion in Neuroendocrine Cells, Neuron, Volume 16, Issue 2, 1996, Pages 369-376, ISSN 0896-6273, https://doi.org/10.1016/S0896-6273(00)80054-9.

Rosenmund, C., Sigler, A., Augustin, I., Reim, K., Brose, N., & Rhee, J. S. (2002). Differential control of vesicle priming and short-term plasticity by Munc13 isoforms. Neuron, 33(3), 411–424. https://doi.org/10.1016/s0896-6273(02)00568-8

Rostaing, P., Real, E., Siksou, L., Lechaire, J. P., Boudier, T., Boeckers, T. M., Gertler, F., Gundelfinger, E. D., Triller, A., & Marty, S. (2006). Analysis of synaptic ultrastructure without fixative using high-pressure freezing and tomography. The European journal of neuroscience, 24(12), 3463–3474. https://doi.org/10.1111/j.1460-9568.2006.05234.x

Rothberg, K. G., Heuser, J. E., Donzell, W. C., Ying, Y. S., Glenney, J. R., & Anderson, R. G. (1992). Caveolin, a protein component of caveolae membrane coats. Cell, 68(4), 673–682. https://doi.org/10.1016/0092-8674(92)90143-z

Royle, S. J., & Lagnado, L. (2003). Endocytosis at the synaptic terminal. The Journal of physiology, 553(Pt 2), 345–355. https://doi.org/10.1113/jphysiol.2003.049221

Saheki, Y., & De Camilli, P. (2012). Synaptic vesicle endocytosis. Cold Spring Harbor perspectives in biology, 4(9), a005645. https://doi.org/10.1101/cshperspect.a005645

Schober, A., Wolf, N., Huber, K., Hertel, R., Krieglstein, K., Minichiello, L., Kahane, N., Widenfalk, J., Kalcheim, C., Olson, L., Klein, R., Lewin, G. R., & Unsicker, K. (1998). TrkB and neurotrophin-4 are important for development and maintenance of sympathetic preganglionic neurons innervating the adrenal medulla. The Journal of neuroscience: the official journal of the Society for Neuroscience, 18(18), 7272–7284. https://doi.org/10.1523/JNEUROSCI.18-18-07272.1998

Schonn, J. S., Maximov, A., Lao, Y., Südhof, T. C., & Sørensen, J. B. (2008). Synaptotagmin-1 and -7 are functionally overlapping Ca2+ sensors for exocytosis in adrenal chromaffin cells. Proceedings of the National Academy of Sciences of the United States of America, 105(10), 3998–4003. https://doi.org/10.1073/pnas.0712373105

Schuske, K. R., Richmond, J. E., Matthies, D. S., Davis, W. S., Runz, S., Rube, D. A., van der Bliek, A. M., & Jorgensen, E. M. (2003). Endophilin is required for synaptic vesicle endocytosis by localizing synaptojanin. Neuron, 40(4), 749–762.https://doi.org/10.1016/s0896-6273(03)00667-6

Sébastien Houy, Joana S Martins, Noa Lipstein, Jakob Balslev Sørensen (2022) Phorbolester-activated Munc13-1 and ubMunc13-2 exert opposing effects on dense-core vesicle secretion eLife 11: e79433 https://doi.org/10.7554/eLife.79433

Segovia, M., Alés, E., Montes, M. A., Bonifas, I., Jemal, I., Lindau, M., Maximov, A., Südhof, T. C., & Alvarez de Toledo, G. (2010). Push-and-pull regulation of the fusion pore by synaptotagmin-7. Proceedings of the National Academy of Sciences of the United States of America, 107(44), 19032–19037. https://doi.org/10.1073/pnas.1014070107

Seto, E. S., Bellen, H. J., & Lloyd, T. E. (2002). When cell biology meets development: endocytic regulation of signaling pathways. Genes & development, 16(11), 1314–1336. https://doi.org/10.1101/gad.989602

Seward, E. P., Chernevskaya, N. I., & Nowycky, M. C. (1996). Ba2+ ions evoke two kinetically distinct patterns of exocytosis in chromaffin cells, but not in neurohypophysial nerve terminals. The Journal of neuroscience : the official journal of the Society for Neuroscience, 16(4), 1370–1379. https://doi.org/10.1523/JNEUROSCI.16-04-01370.1996

Shi, L., Shen, Q. T., Kiel, A., Wang, J., Wang, H. W., Melia, T. J., Rothman, J. E., & Pincet, F. (2012). SNARE proteins: one to fuse and three to keep the nascent fusion pore open. Science (New York, N.Y.), 335(6074), 1355–1359. https://doi.org/10.1126/science.1214984

Shin, W., Wei, L., Arpino, G., Ge, L., Guo, X., Chan, C. Y., Hamid, E., Shupliakov, O., Bleck, C. K. E., & Wu, L. G. (2021). Preformed Ω-profile closure and kiss-and-run mediate endocytosis and diverse endocytic modes in neuroendocrine chromaffin cells. Neuron, 109(19), 3119–3134.e5. https://doi.org/10.1016/j.neuron.2021.07.019

Siksou, L., Varoqueaux, F., Pascual, O., Triller, A., Brose, N., & Marty, S. (2009). A common molecular basis for membrane docking and functional priming of synaptic vesicles. The European journal of neuroscience, 30(1), 49–56. https://doi.org/10.1111/j.1460-9568.2009.06811.x

Sjostrand, F. S., & Wetzstein, R. (1956). Elektronenmikroskopische Untersuchung der phäochromen (chromaffinen) Granula in den Markzellen der Nebenniere [Electron microscopic research of the pheochrome (chromaffin) granula in the cells of adrenal medulla]. Experientia, 12(5), 196–199. https://doi.org/10.1007/BF02170794

Slepnev, V. I., & De Camilli, P. (2000). Accessory factors in clathrin-dependent synaptic vesicle endocytosis. Nature reviews. Neuroscience, 1(3), 161–172. https://doi.org/10.1038/35044540

Smith, C., & Neher, E. (1997). Multiple forms of endocytosis in bovine adrenal chromaffin cells. The Journal of cell biology, 139(4), 885–894. https://doi.org/10.1083/jcb.139.4.885

Song, B. D., & Schmid, S. L. (2003). A molecular motor or a regulator? Dynamin's in a class of its own. Biochemistry, 42(6), 1369–1376. https://doi.org/10.1021/bi027062h

Sørensen J. B. (2017). Ride the wave: Retrograde trafficking becomes Ca2+ dependent with BAIAP3. The Journal of cell biology, 216(7), 1887–1889. https://doi.org/10.1083/jcb.201706007

Sørensen, J. B., Nagy, G., Varoqueaux, F., Nehring, R. B., Brose, N., Wilson, M. C., & Neher, E. (2003). Differential control of the releasable vesicle pools by SNAP-25 splice variants and SNAP-23. Cell, 114(1), 75–86. https://doi.org/10.1016/s0092-8674(03)00477-x

Sørensen, J.B. Formation, stabilisation and fusion of the readily releasable pool of secretory vesicles. Pflugers Arch - Eur J Physiol 448, 347–362 (2004). https://doi.org/10.1007/s00424-004-1247-8

Speidel, D., Bruederle, C. E., Enk, C., Voets, T., Varoqueaux, F., Reim, K., Becherer, U., Fornai, F., Ruggieri, S., Holighaus, Y., Weihe, E., Bruns, D., Brose, N., & Rettig, J. (2005). CAPS1 regulates catecholamine loading of large dense-core vesicles. Neuron, 46(1), 75–88. https://doi.org/10.1016/j.neuron.2005.02.019

Stevens, C. F., & Wesseling, J. F. (1998). Activity-dependent modulation of the rate at which synaptic vesicles become available to undergo exocytosis. Neuron, 21(2), 415–424. https://doi.org/10.1016/s0896-6273(00)80550-4

Stevens, D. R., & Rettig, J. (2009). The Ca (2+)-dependent activator protein for secretion CAPS: do I dock or do I prime?. Molecular neurobiology, 39(1), 62–72. https://doi.org/10.1007/s12035-009-8052-5

Stevens, D. R., Schirra, C., Becherer, U., & Rettig, J. (2011). Vesicle pools: lessons from adrenal chromaffin cells. Frontiers in synaptic neuroscience, 3, 2. https://doi.org/10.3389/fnsyn.2011.00002

Stevens, C. F., & Williams, J. H. (2000). "Kiss and run" exocytosis at hippocampal synapses. Proceedings of the National Academy of Sciences of the United States of America, 97(23), 12828–12833. https://doi.org/10.1073/pnas.230438697

Steyer, J., Horstmann, H. & Almers, W. Transport, docking and exocytosis of single secretory granules in live chromaffin cells. Nature 388, 474–478 (1997). https://doi.org/10.1038/41329

Südhof T. C. (2004). The synaptic vesicle cycle. Annual review of neuroscience, 27, 509–547. https://doi.org/10.1146/annurev.neuro.26.041002.131412

Südhof T. C. (2013). Neurotransmitter release: the last millisecond in the life of a synaptic vesicle. Neuron, 80(3), 675–690. https://doi.org/10.1016/j.neuron.2013.10.022

Südhof, T. C., & Rothman, J. E. (2009). Membrane fusion: grappling with SNARE and SM proteins. Science (New York, N.Y.), 323(5913), 474–477. https://doi.org/10.1126/science.1161748

Takahashi, Y., Sipp, D., & Enomoto, H. (2013). Tissue interactions in neural crest cell development and disease. *Science (New York, N.Y.)*, *341*(6148), 860–863. https://doi.org/10.1126/science.1230717

Takei, K., Mundigl, O., Daniell, L., & De Camilli, P. (1996). The synaptic vesicle cycle: a single vesicle budding step involving clathrin and dynamin. The Journal of cell biology, 133(6), 1237–1250. https://doi.org/10.1083/jcb.133.6.1237

Tang, J., Maximov, A., Shin, O. H., Dai, H., Rizo, J., & Südhof, T. C. (2006). A complexin/synaptotagmin 1 switch controls fast synaptic vesicle exocytosis. Cell, 126(6), 1175–1187. https://doi.org/10.1016/j.cell.2006.08.030

Taraska, J. W., Perrais, D., Ohara-Imaizumi, M., Nagamatsu, S., & Almers, W. (2003). Secretory granules are recaptured largely intact after stimulated exocytosis in cultured endocrine cells. Proceedings of the National Academy of Sciences of the United States of America, 100(4), 2070–2075. https://doi.org/10.1073/pnas.0337526100

Tawfik, B., Martins, J. S., Houy, S., Imig, C., Pinheiro, P. S., Wojcik, S. M., Brose, N., Cooper, B. H., & Sørensen, J. B. (2021). Synaptotagmin-7 places dense-core vesicles at the cell membrane to promote Munc13-2- and Ca2+-dependent priming. eLife, 10, e64527. https://doi.org/10.7554/eLife.64527

Thomas Voets, Ruud F. Toonen, Elisabeth C. Brian, Heidi de Wit, Tobias Moser, Jens Rettig, Thomas C. Südhof, Erwin Neher, Matthijs Verhage, Munc18-1 Promotes Large Dense-Core Vesicle Docking, Neuron, Volume 31, Issue 4, (2001), Pages 581-592, ISSN 0896-6273, https://doi.org/10.1016/S0896-6273(01)00391-9.

Tian, J. H., Wu, Z. X., Unzicker, M., Lu, L., Cai, Q., Li, C., Schirra, C., Matti, U., Stevens, D., Deng, C., Rettig, J., & Sheng, Z. H. (2005). The role of Snapin in neurosecretion: snapin knock-out mice exhibit impaired calcium-dependent exocytosis of large dense-core vesicles in chromaffin cells. The Journal of neuroscience: the official journal of the Society for Neuroscience, 25(45), 10546–10555. https://doi.org/10.1523/JNEUROSCI.3275-05.2005

Trexler, A. J., Sochacki, K. A., & Taraska, J. W. (2016). Imaging the recruitment and loss of proteins and lipids at single sites of calcium-triggered exocytosis. Molecular biology of the cell, 27(15), 2423–2434. https://doi.org/10.1091/mbc.E16-01-0057

Tsuboi, T., McMahon, H. T., & Rutter, G. A. (2004). Mechanisms of dense core vesicle recapture following "kiss and run" ("cavicapture") exocytosis in insulin-secreting cells. The Journal of biological chemistry, 279(45), 47115–47124. https://doi.org/10.1074/jbc.M408179200

Unsicker, K., Huber, K., Schütz, G., & Kalcheim, C. (2005). The chromaffin cell and its development. Neurochemical research, 30(6-7), 921–925. https://doi.org/10.1007/s11064-005-6966-5

Uribe-Querol, E., & Rosales, C. (2020). Phagocytosis: Our Current Understanding of a Universal Biological Process. Frontiers in immunology, 11, 1066. https://doi.org/10.3389/fimmu.2020.01066

van Weering, J. R., Toonen, R. F., & Verhage, M. (2007). The role of Rab3a in secretory vesicle docking requires association/dissociation of guanidine phosphates and Munc18-1. PloS one, 2(7), e616. https://doi.org/10.1371/journal.pone.0000616

Vandael, D. H., Ottaviani, M. M., Legros, C., Lefort, C., Guérineau, N. C., Allio, A., Carabelli, V., & Carbone, E. (2015). Reduced availability of voltage-gated sodium channels by depolarization or blockade by tetrodotoxin boosts burst firing and catecholamine release in mouse chromaffin cells. The Journal of physiology, 593(4), 905–927. https://doi.org/10.1113/jphysiol.2014.283374

Varoqueaux, F., Sigler, A., Rhee, J. S., Brose, N., Enk, C., Reim, K., & Rosenmund, C. (2002). Total arrest of spontaneous and evoked synaptic transmission but normal synaptogenesis in the absence of Munc13-mediated vesicle priming. Proceedings of the National Academy of Sciences of the United States of America, 99(13), 9037–9042. https://doi.org/10.1073/pnas.122623799

Venturoli, D., & Rippe, B. (2005). Ficoll and dextran vs. globular proteins as probes for testing glomerular permselectivity: effects of molecular size, shape, charge, and deformability. American journal of physiology. Renal physiology, 288(4), F605–F613. https://doi.org/10.1152/ajprenal.00171.2004

Verhage, M., & Sørensen, J. B. (2008). Vesicle docking in regulated exocytosis. Traffic (Copenhagen, Denmark), 9(9), 1414–1424. https://doi.org/10.1111/j.1600-0854.2008.00759.x

Verstreken, P., Koh, T. W., Schulze, K. L., Zhai, R. G., Hiesinger, P. R., Zhou, Y., Mehta, S. Q., Cao, Y., Roos, J., & Bellen, H. J. (2003). Synaptojanin is recruited by endophilin to promote synaptic vesicle uncoating. Neuron, 40(4), 733–748. https://doi.org/10.1016/s0896-6273(03)00644-5

Voets, (2000). Dissection of Three Ca2+-Dependent Steps Leading to Secretion in Chromaffin Cells from Mouse Adrenal Slices, Neuron, Volume 28, Issue 2, 2000, Pages 537-545, ISSN 0896-6273, https://doi.org/10.1016/S0896-6273(00)00131-8.

Voets, T., Moser, T., Lund, P. E., Chow, R. H., Geppert, M., Südhof, T. C., & Neher, E. (2001). Intracellular calcium dependence of large dense-core vesicle exocytosis in the absence of synaptotagmin I. Proceedings of the National Academy of Sciences of the United States of America, 98(20), 11680–11685. https://doi.org/10.1073/pnas.201398798

Voets, T., Neher, E., & Moser, T. (1999). Mechanisms underlying phasic and sustained secretion in chromaffin cells from mouse adrenal slices. Neuron, 23(3), 607–615. https://doi.org/10.1016/s0896-6273(00)80812-0

Vogel, K.S. (1996). Origin of Adrenal Chromaffin Cells from the Neural Crest. In: Genetic Mechanisms in Multiple Endocrine Neoplasia Type 2. Medical Intelligence Unit. Springer, Berlin, Heidelberg. https://doi.org/10.1007/978-3-662-21948-5_5

von Gersdorff, H., & Matthews, G. (1994). Dynamics of synaptic vesicle fusion and membrane retrieval in synaptic terminals. Nature, 367(6465), 735–739. https://doi.org/10.1038/367735a0

von Rüden, L., & Neher, E. (1993). A Ca-dependent early step in the release of catecholamines from adrenal chromaffin cells. Science (New York, N.Y.), 262(5136), 1061–1065. https://doi.org/10.1126/science.8235626

Wang, C. T., Grishanin, R., Earles, C. A., Chang, P. Y., Martin, T. F., Chapman, E. R., & Jackson, M. B. (2001). Synaptotagmin modulation of fusion pore kinetics in regulated exocytosis of dense-core vesicles. Science (New York, N.Y.), 294(5544), 1111–1115. https://doi.org/10.1126/science.1064002

Watanabe S. (2016). Flash-and-Freeze: Coordinating Optogenetic Stimulation with Rapid Freezing to Visualize Membrane Dynamics at Synapses with Millisecond Resolution. Frontiers in synaptic neuroscience, 8, 24. https://doi.org/10.3389/fnsyn.2016.00024

Watanabe, S., & Boucrot, E. (2017). Fast and ultrafast endocytosis. Current opinion in cell biology, 47, 64–71. https://doi.org/10.1016/j.ceb.2017.02.013

Watanabe, S., Rost, B. R., Camacho-Pérez, M., Davis, M. W., Söhl-Kielczynski, B., Rosenmund, C., & Jorgensen, E. M. (2013). Ultrafast endocytosis at mouse hippocampal synapses. Nature, 504(7479), 242–247. https://doi.org/10.1038/nature12809

Watanabe, S., Trimbuch, T., Camacho-Pérez, M., Rost, B. R., Brokowski, B., Söhl-Kielczynski, B., Felies, A., Davis, M. W., Rosenmund, C., & Jorgensen, E. M. (2014). Clathrin regenerates synaptic vesicles from endosomes. Nature, 515(7526), 228–233. https://doi.org/10.1038/nature13846

Weimer, R. M., Gracheva, E. O., Meyrignac, O., Miller, K. G., Richmond, J. E., & Bessereau, J. L. (2006). UNC-13 and UNC-10/rim localize synaptic vesicles to specific membrane domains. The Journal of neuroscience: the official journal of the Society for Neuroscience, 26(31), 8040–8047. https://doi.org/10.1523/JNEUROSCI.2350-06.2006

Weimer, R. M., Richmond, J. E., Davis, W. S., Hadwiger, G., Nonet, M. L., & Jorgensen, E. M. (2003). Defects in synaptic vesicle docking in unc-18 mutants. Nature neuroscience, 6(10), 1023–1030. https://doi.org/10.1038/nn1118

Westacott, M. J., Ludin, N. W. F., & Benninger, R. K. P. (2017). Spatially Organized β-Cell Subpopulations Control Electrical Dynamics across Islets of Langerhans. Biophysical journal, 113(5), 1093–1108. https://doi.org/10.1016/j.bpj.2017.07.021

Wojcik, S. M., & Brose, N. (2007). Regulation of membrane fusion in synaptic excitation-secretion coupling: speed and accuracy matter. Neuron, 55(1), 11–24. https://doi.org/10.1016/j.neuron.2007.06.013

Wojcik, S. M., Tantra, M., Stepniak, B., Man, K. N., Müller-Ribbe, K., Begemann, M., Ju, A., Papiol, S., Ronnenberg, A., Gurvich, A., Shin, Y., Augustin, I., Brose, N., & Ehrenreich, H. (2013). Genetic markers of a Munc13 protein family member, BAIAP3, are gender specifically

associated with anxiety and benzodiazepine abuse in mice and humans. Molecular medicine (Cambridge, Mass.), 19(1), 135–148. https://doi.org/10.2119/molmed.2013.00033

Wonchul Shin, Gianvito Arpino, Sathish Thiyagarajan, Rui Su, Lihao Ge, Zachary McDargh, Xiaoli Guo, Lisi Wei, Oleg Shupliakov, Albert Jin, Ben O'Shaughnessy, Ling-Gang Wu, (2020). Vesicle Shrinking and Enlargement Play Opposing Roles in the Release of Exocytotic Contents, Cell Reports, Volume 30, Issue 2, 2020, Pages 421-431.e7, ISSN 2211-1247, https://doi.org/10.1016/j.celrep.2019.12.044.

Wonchul Shin, Lihao Ge, Gianvito Arpino, Seth A. Villarreal, Edaeni Hamid, Huisheng Liu, Wei-Dong Zhao, Peter J. Wen, Hsueh-Cheng Chiang, Ling-Gang Wu, (2018). Visualization of Membrane Pore in Live Cells Reveals a Dynamic-Pore Theory Governing Fusion and Endocytosis, Cell, Volume 173, Issue 4, 2018, Pages 934-945.e12, ISSN 0092-8674, https://doi.org/10.1016/j.cell.2018.02.062.

Wu, L. G., Ryan, T. A., & Lagnado, L. (2007). Modes of vesicle retrieval at ribbon synapses, calyx-type synapses, and small central synapses. The Journal of neuroscience: the official journal of the Society for Neuroscience, 27(44), 11793–11802. https://doi.org/10.1523/JNEUROSCI.3471-07.2007

Wu, W., & Wu, L. G. (2007). Rapid bulk endocytosis and its kinetics of fission pore closure at a central synapse. Proceedings of the National Academy of Sciences of the United States of America, 104(24), 10234–10239. https://doi.org/10.1073/pnas.0611512104

Wu, Y., Gu, Y., Morphew, M. K., Yao, J., Yeh, F. L., Dong, M., & Chapman, E. R. (2012). All three components of the neuronal SNARE complex contribute to secretory vesicle docking. The Journal of cell biology, 198(3), 323–330. https://doi.org/10.1083/jcb.201106158

Wu, Y., O'Toole, E. T., Girard, M., Ritter, B., Messa, M., Liu, X., McPherson, P. S., Ferguson, S. M., & De Camilli, P. (2014). A dynamin 1-, dynamin 3- and clathrin-independent pathway of synaptic vesicle recycling mediated by bulk endocytosis. eLife, 3, e01621. https://doi.org/10.7554/eLife.01621

Xing, Y., Böcking, T., Wolf, M., Grigorieff, N., Kirchhausen, T., & Harrison, S. C. (2010). Structure of clathrin coat with bound Hsc70 and auxilin: mechanism of Hsc70-facilitated disassembly. The EMBO journal, 29(3), 655–665. https://doi.org/10.1038/emboj.2009.383

Xue, M., Ma, C., Craig, T. K., Rosenmund, C., & Rizo, J. (2008). The Janus-faced nature of the C(2)B domain is fundamental for synaptotagmin-1 function. Nature structural & molecular biology, 15(11), 1160–1168. https://doi.org/10.1038/nsmb.1508

Y. Georgalis, M. Philipp, R. Aleksandrova, J.K. Krüger, (2012). Light scattering studies on Ficoll PM70 solutions reveal two distinct diffusive modes, Journal of Colloid and Interface Science, Volume 386, Issue 1, 2012, Pages 141-147, ISSN 0021-9797, https://doi.org/10.1016/j.jcis.2012.07.062

Yamada, E. (1955). The Fine Structure of the Renal Glomerulus of the Mouse. The Journal of Biophysical and Biochemical Cytology, 1(6), 551–566. http://www.jstor.org/stable/1602923

Zenisek, D., Steyer, J. A., Feldman, M. E., & Almers, W. (2002). A membrane marker leaves synaptic vesicles in milliseconds after exocytosis in retinal bipolar cells. Neuron, 35(6), 1085–1097. https://doi.org/10.1016/s0896-6273(02)00896-6

Zhang, C., & Zhou, Z. (2002). Ca (2+)-independent but voltage-dependent secretion in mammalian dorsal root ganglion neurons. Nature neuroscience, 5(5), 425–430. https://doi.org/10.1038/nn845

Zhang, X., Jiang, S., Mitok, K. A., Li, L., Attie, A. D., & Martin, T. F. J. (2017). BAIAP3, a C2 domain-containing Munc13 protein, controls the fate of dense-core vesicles in neuroendocrine cells. The Journal of cell biology, 216(7), 2151–2166. https://doi.org/10.1083/jcb.201702099

Zhao, W. D., Hamid, E., Shin, W., Wen, P. J., Krystofiak, E. S., Villarreal, S. A., Chiang, H. C., Kachar, B., & Wu, L. G. (2016). Hemi-fused structure mediates and controls fusion and fission in live cells. Nature, 534(7608), 548–552. https://doi.org/10.1038/nature18598

Zilly, F. E., Sørensen, J. B., Jahn, R., & Lang, T. (2006). Munc18-bound syntaxin readily forms SNARE complexes with synaptobrevin in native plasma membranes. PLoS biology, 4(10), e330. https://doi.org/10.1371/journal.pbio.0040330

Acknowledgments

I want to express my sincere gratitude to Dr. Sonja Wojcik for accepting me as her doctoral student. She patiently taught me all there is to know about culture systems, patch-clamp technique, and electrophysiology. She made my transfer into the lab as easy as it could. Her thoughtful encouragement and support enabled me to persevere during difficult circumstances. I could not have achieved as much without her guidance and supervision as I did.

Working and getting to know Prof. Dr. Nils Brose, an excellent director, was a great privilege. I owe him huge gratitude for allowing me to work in his outstanding laboratory.

Many thanks to my committee members, Prof. Dr. Thomas Dresbach and Prof. Dr. Tobias Moser, for their scientific feedback at committee meetings and for their support throughout these years.

Thank you to the additional members of my examination committee, Prof. Dr. Tiago Fleming Outeiro, Dr. Brett Carter, and Prof. Dr. Rubén Fernández-Busnadiego, for taking the time and being a part of my final doctoral examination.

I want to thank my collaborators. Dr. Benjamin H. Cooper, thank you for your enormous cooperation and help, especially with electron microscopy. This project was accomplished with his resourceful and trustworthy guidance. Kirsten Weyand and Valentin Schwarze, thank you for all the significant help with high-pressure freezing experiments, analyses, and constant discussion.

Thanks to Dr. Cordelia Imig and Dr. Ahmed Shaaban for the pleasant discussion about chromaffin cells, patch-clamp, and their encouragement.

Thank you to Astrid Zeuch and Sabine Beuermann for their technical support.

Big thanks to Dr. Holger Taschenberger for the conversations in the E-Phys part and the friendly advice.

I want to express my genuine gratitude to all the past and present doctoral students in the Brose department. Special thanks to Aisha, Dragana, Matea, Inés, Fidi, Mrinalini and Jutta for engaging in endless discussion about science and life.

Further, I would like to acknowledge the support of all members of the Brose department throughout my Ph.D. training.

Finally yet importantly, I want to thank my family and friends for their enormous daily support. I am incredibly grateful to my parents, who are always there for me, for their affection and devotion, for believing in me, and for encouraging me frequently. Also, huge thanks to my amazing cousins, who took good care of me in challenging situations. Thanks to my boyfriend Jamie, who helped me move forward and never give up. I thank Alek and Jana for their trustworthy, loyal, and long-lasting friendship.

I want to dedicate this work to my unforgettable, exceptional, and awesome brother - Srecko, who was by my side his entire life and loved me deeply and unconditionally.

List of publications

Rankov Petrovic B, Hrncic D, Mladenovic D, Simic T, Suvakov S, Jovanovic D, Puskas N, Zaletel I, Velimirovic M, **Cirkovic V**, Macut D, Stanojlovic O, Rasic-Markovic A. (2019). Prenatal Androgenization Induces Anxiety-Like Behavior in Female Rats, Associated with Reduction of Inhibitory Interneurons and Increased BDNF in Hippocampus and Cortex. Biomed Res Int. 2019 Jun 10; 2019:3426092. doi: 10.1155/2019/3426092.